

IN SITU SENSING OF LEAF CUTICULAR WAX, PECAN YIELD AND  
PECAN LEAF NITROGEN CONCENTRATION

By

JAMES A. HARDIN  
Bachelor of Science in Mechanical Engineering  
Michigan Technological University  
Houghton, Michigan  
1984

Submitted to the Faculty of the  
Graduate College of the  
Oklahoma State University  
in partial fulfillment of  
the requirements for  
the Degree of  
DOCTOR OF PHILOSOPHY  
July, 2012

IN SITU SENSING OF LEAF CUTICULAR WAX,  
PECAN YIELD AND PECAN LEAF NITROGEN  
CONCENTRATION

Dissertation Approved:

Dr. Carol Jones

---

Dissertation Adviser

Dr. Timothy Bowser

---

Dr. Paul Weckler

---

Dr. Niels Maness

---

Outside Committee Member

Dr. Sheryl A. Tucker

---

Dean of the Graduate College

## TABLE OF CONTENTS

Chapter	Page
I. INTRODUCTION.....	1
II. RAPID IN SITU QUANTIFICATION OF SPINACH CUTICULAR WAX USING FTIR-ATR AND DSC .....	3
Introduction.....	4
Existing cuticle wax measurement methods.....	8
Proposed cuticle wax measurement methods .....	9
Experimental objectives for rapid in situ measurement of leaf cuticular wax ..	16
Materials and methods .....	17
Plant materials .....	17
FTIR-ATR measurements .....	18
Chloroform extraction of CM waxes.....	21
High performance thin layer chromatography.....	21
Gas chromatography.....	22
Scanning electron microscopy (SEM).....	22
Transmission electron microscopy (TEM).....	23
Cuticular membrane isolation.....	23
Dried leaf cuticle measurement protocol.....	24
Statistical analysis.....	24
DSC measurements.....	25
Results and discussion .....	26
Leaf cuticular wax composition .....	26
Transmission electron Microscopy.....	28
FTIR-ATR spectra.....	30
Wax quantification on fresh leaves using FTIR-ATR.....	32
Wax quantification on dried spinach leaves using FTIR-ATR .....	40
Wax quantification using DSC .....	43
Conclusion .....	45
References.....	47
III. ESTIMATION OF PECAN YIELD USING TERRESTRIAL MICROWAVE SENSING.....	55
Introduction.....	56
Existing remote sensing technologies for estimating pecan yield in situ .....	57
Materials and Methods.....	62

Plant materials .....	62
Vector network analyzer measurements .....	63
Sample holder and measurement procedure .....	65
Data analysis .....	67
Results and discussion .....	67
Plant materials .....	67
VNA measurements .....	68
Implications for future investigations .....	83
Conclusions .....	84
References: .....	86
IV. IN SITU MEASUREMENT OF PECAN LEAF NITROGEN CONCENTRATION USING A CHLOROPHYLL METER AND VIS-NIR MULTISPECTRAL CAMERA	90
Introduction .....	91
Materials and methods .....	94
Site descriptions .....	94
Sampling protocol – SPAD meter .....	95
Sampling protocol and image processing – Vis-NIR multispectral camera .....	98
Statistical analysis .....	98
Results and discussion .....	98
Foliar nitrogen .....	98
SPAD meter .....	99
Vis-NIR multispectral camera .....	102
Conclusion .....	106
References .....	107
V. CONCLUSION .....	111
APPENDICES .....	115

## LIST OF TABLES

### CHAPTER II

Table 1. Growth chamber conditions for spinach specimens. ....	18
Table 2. Composition of cuticular waxes from fast growth and slow growth spinach leaves.....	27
Table 3. Principal component analysis results of training spectra of spinach. ....	33
Table 4. Comparison of best linear regression models based on $R^2_A$ for training, validation and field grown samples. ....	36
Table 5. Pearson correlation coefficients for selected predictor variables in important wax prediction models.....	39
Table 6. Root mean square error and mean difference between fresh and rehydrated spinach leaf cuticular wax load predicted by each of the 14 best performing models with 4 or 5 predictor frequencies. ....	42

### CHAPTER III

Table 7. Pecan canopy materials used in microwave experiments with associated moisture content .....	67
--	----

### CHAPTER IV

Table 8. Cultivar and nitrogen treatments for pecan trees in study. ....	95
Table 9. Duncan Tech MS3100 camera gain and exposure settings for collecting pecan images .....	96
Table 10. Equations for predicting foliar nitrogen concentration from SPAD readings on three cultivars of pecan. ....	100
Table 11. Histogram peak intensity of NIR image pixels from images of ‘Pawnee’ and ‘Kanza’ pecan trees taken in 2010. ....	103
Table 12. Regression relationships of leaf N concentration to NDVI, GNDVI and green reflectance from images of ‘Pawnee’ and ‘Kanza’ pecan trees taken in 2010. ....	105

## LIST OF FIGURES

### CHAPTER II

Figure 1. Generalized structure of the plant cuticle.....	6
Figure 2. System for ATR measurement of cuticle membrane overlaying polysaccharide rich layer. ....	12
Figure 3. Spinach leaf held against IRE with conformal elastomeric tip during FTIR-ATR spectral scan. ....	19
Figure 4. Diagram of spinach leaf sampling protocol for FTIR-ATR, GC and DSC sample set. ....	20
Figure 5. Diagram of spinach leaf sampling protocol for measurement of dried leaf cuticular waxes.....	20
Figure 6. HPTLC plates of chloroform extracted spinach cuticular wax. ....	26
Figure 7. Typical GC response of spinach leaf chloroform extract following derivatization.....	28
Figure 8. Representative transmission electron microscope images of spinach leaf epidermis.....	29
Figure 9. SEM images of FG (left images) and SG (right images) spinach leaf surface..	30
Figure 10. FTIR-ATR reflectance spectra of spinach.....	32
Figure 11. First four eigenvectors for 28 training spectra.. ....	34
Figure 12. Effect of predictor variable quantity on coefficient of variation for the best fitting linear models. ....	35
Figure 13. Typical FTIR-ATR spectra of fresh and wilted spinach leaves. ....	37
Figure 14. Comparison of cuticular wax measured by GC to predicted amount from FTIR-ATR.....	39
Figure 15. Typical leaf surface texture of fresh, dried at 50 °C for 24 h, and rehydrated spinach in water at 22 °C for 2 h.....	40
Figure 16. Comparison of wax predictions from model 11 on leaves in the fresh and rehydrated state .....	42
Figure 17. Representative differential scanning calorimetry thermalgram of spinach cuticular wax.....	43

Figure 18. Typical DSC thermalgram of leaf sample showing peak area measured between 40 and 73 °C. ....	44
Figure 19. Comparison of spinach cuticular wax determined by GC and DSC. ....	45

### CHAPTER III

Figure 20. Pecan canopy test stand showing antenna, specimen holder on support shelf, absorbent material on floor and VNA in background.....	64
Figure 21. Typical sample of leaves and branches and nuts being loaded into specimen holder for VNA measurements. ....	66
Figure 22. Sectioned ‘Maramec’ pecan nuts at each sampling date in 2010.....	68
Figure 23. VNA spectral response of representative canopy sample with 0 to 9 pecan nuts.....	69
Figure 24. Mean VNA spectral response for pecan leaves and branches and nuts .....	71
Figure 25. Effect of harvest date on mean VNA spectral response for nuts.....	72
Figure 26. Weighting of first five eigenvectors from partial least squares regression of canopy samples for nut mass at individual harvest dates and all dates pooled together. ..	73
Figure 27. Distribution of the ten most influential frequencies from each of the first five eigenvectors from partial least squares regression of canopy samples for nut mass at individual harvest dates and all dates pooled together.....	74
Figure 28. Variance accounted for by the first 10 eigenvectors from partial least squares regression of fresh leaf canopy samples for nut mass at individual harvest dates and all dates pooled together. ....	75
Figure 29. Variance accounted for by the first 10 eigenvectors from partial least squares regression of fresh and partially dried canopy samples for nut mass at individual harvest dates and all dates pooled together. ....	76
Figure 30. Coefficients of determination from linear regression of nut mass at each frequency from canopy samples for individual harvest dates and all dates pooled together. ....	77
Figure 31. Weighting of first five eigenvectors from partial least squares regression of baseline and canopy samples for total water mass at individual harvest dates and all dates pooled together.....	79
Figure 32. Weighting of first five eigenvectors from partial least squares regression of baseline and canopy samples for total dry mass at individual harvest dates and all dates pooled together.....	80

Figure 33. Variance accounted for by the first 10 eigenvectors from partial least squares regression of baseline and canopy samples for total water mass at individual harvest dates and all dates pooled together.....	81
Figure 34. Variance accounted for by the first 10 eigenvectors from partial least squares regression of baseline and canopy samples for total dry mass at individual harvest dates and all dates pooled together.....	81
Figure 35. Coefficients of determination and P-values from linear regression of total water mass at each frequency from baseline and canopy samples for individual harvest dates and all dates pooled together. ....	82
Figure 36. Coefficients of determination and P-values from linear regression of total dry mass at each frequency from baseline and canopy samples for individual harvest dates and all dates pooled together.....	83

#### CHAPTER IV

Figure 37. Representative NIR image composure of pecan tree obtained with multispectral camera. Reflectance standard is in lower left of image. Rectangle represents leaf area selected for analysis. ....	97
Figure 38. Mass fraction of nitrogen in dried pecan leaves during 2010 growing season for ‘Kanza’, ‘Maramec’ and ‘Pawnee’ trees.....	99
Figure 39. Correlation of foliar nitrogen concentration to SPAD response for ‘Kanza’, ‘Maramec’, and ‘Pawnee’ pecan trees by month in 2010.....	101
Figure 40. Intensity distribution of NIR, green and red pixels in leaf area image of representative pecan tree.....	103
Figure 41. Effect of NIR pixel threshold on leaf area image of a representative pecan tree. ....	104

## CHAPTER I

### INTRODUCTION

Development of sensor technologies for rapid in situ measurement of plant conditions can lead to efficiency and productivity improvements for producers, scientists, engineers and processors.

This dissertation presents research conducted on three distinct sensor applications that exploit the visible-near infrared, mid infrared, and microwave regions of the electromagnetic spectrum.

Chapter two reports on alternative methods to rapidly quantify cuticular waxes that occur on the aerial parts of plant leaves with minimal sample preparation. Current methods require solvent extraction of the waxes and quantification with gas chromatography. Fourier transform infrared spectroscopy with attenuated total reflectance shows promise as an alternative to current methods. The technique allows rapid in situ quantification of waxes and minimal sample preparation is required. Associated experiments using differential scanning calorimetry to quantify waxes on dried leaf sections did not yield useful predictions of wax quantity.

Chapters three and four investigate sensing technologies for enabling precision agriculture in pecan orchards. Precision agricultural practices, including in situ yield estimates and variable rate fertilizer applications, have been developed for a variety of field crops. The goal of precision agriculture is to optimize efficiency and productivity by sensing plant conditions and applying treatments at the correct level at an optimum spatial scale. Measurement of foliar nitrogen and

estimating nut yield are two essential tasks in current pecan management practices and represent opportunities for deployment of precision agriculture practices.

Foliar nitrogen concentration is used to assess tree health and nutritional needs. The current protocol for measuring foliar nitrogen in pecan trees is to hand harvest and dry leaf samples, which are then sent to a lab for chemical analysis. In addition to being a time and labor intensive endeavor, expense makes it prohibitive to sample every tree in the orchard. Chapter three reports the results of research using a hand held chlorophyll meter used to take field measurements of leaf nitrogen. In addition, a protocol to extract foliar nitrogen concentration from images taken from a high resolution visible and near infrared camera within the orchard was developed.

Accurate yield estimates of pecans throughout the growing season are important for optimizing production, managing alternate bearing behavior, and for marketing and business purposes. Yield estimates are currently obtained by scouting an orchard and counting nuts on a subsample of the trees. Estimates are inaccurate and due to the effort involved, yield data are generally not obtained on every tree. Chapter four documents empirical research on the backscatter response of microwaves to pecan tree canopy components: nuts, secondary branches, and leaves. Microwave energy can penetrate into the canopy of trees to interact with objects hidden from view. The objective of this investigation was to assess if short-range backscattered microwaves from the canopy of a pecan tree can be used to sense nut yield. Baseline results from this investigation will be used to develop future experiments to be conducted under field conditions. Furthermore, if successful in pecans, the technology has potential for extension to other orchard fruit and nut crops.

## CHAPTER II

### RAPID IN SITU QUANTIFICATION OF SPINACH CUTICULAR WAX USING FTIR-ATR AND DSC

**Abstract:** The ability to rapidly quantify and characterize the cuticular wax on agricultural crops in situ may have significance in crop production, storage and processing. Gas chromatography of solvent extracted waxes is the most common method of measurement. This paper reports on two potential, quantitative, in situ measurement techniques to measure cuticular waxes, tested on spinach leaves. The first technique used Fourier transform infrared spectroscopy with attenuated total internal reflectance optics (FTIR-ATR) to quantify cuticular waxes. FTIR-ATR spectra were subjected to principal component analysis (PCA) to identify potentially important wavelengths. Linear regression techniques using wavelengths identified by PCA and wax quantified by gas chromatography resulted in predictive models with  $R^2 > 0.86$  using as few as four predictor wavelengths. The models developed for fresh spinach were used to measure the waxes on rehydrated dried spinach. The mean difference in waxes measured on rehydrated dried leaves varied among the models from 18 to 129% of wax on fresh leaves. The second wax measurement technique attempted to directly quantify cuticle wax on leaves by using differential scanning calorimetry (DSC) to measure the heat of fusion of the cuticular wax on dried leaf discs. This method did not provide reliable predictions of wax loads on leaves.

## Introduction

The plant cuticle is a hydrophobic lipid polymer membrane that covers the aerial parts of all plants. Physical and chemical properties of the cuticle are important to many plant physiological processes such as transpiration, protection from solar radiation and desiccation, exclusion of pathogens and contaminants, and absorption of agricultural chemicals. The cuticle is also instrumental in the interaction of insects with the plant surface (Stork 1980). For these and other reasons, the cuticle is an area of active inquiry.

The plant cuticle membrane (CM) consists of three general layers (Jetter et al. 2000). The outermost layer is the epicuticular wax (EW) layer consisting of soluble cuticular lipids (SCL) of varying composition. SCL's can be dissolved and recovered (chloroform or chloroform/methanol are common solvents) from leaves leaving the rest of the cuticle intact. The next layer is the cuticle matrix (MX) which consists of cutin infused with SCLs. The MX can have cutin arranged in a lamellar structure or it can be amorphous with no regular organization. The EW plus MX are often called the cuticle proper. The innermost layer, under the MX and in contact with a layer of pectin outside the cell wall, is the cuticular layer. The cuticular layer is a transition zone between the cuticle proper and the cell wall, containing cutin and waxes plus embedded polysaccharides pectin, hemicelluloses, and cellulose (Lopez-Casado et al. 2007). The pectin layer is contiguous with the middle lamella. In many cases the CM can be enzymatically separated, intact, from host plant organs using pectinase which breaks down the polysaccharide layer between the CM and the cell wall of the epidermal cells (Orgell 1955).

Relative thickness, structural arrangement and chemical composition of the various layers of the cuticle vary widely among plant species, organs and throughout ontogeny (Bargel et al. 2006; Jeffree 1984; Kunst et al. 2005). SCLs in the MX and cuticular layer are termed intracuticular waxes (IW) while SCLs above the MX are called epicuticular waxes (EW). Mass fractions of

each component vary widely by plant location and species but SCL's are typically 20 to 60% of the CM mass. Interaction of the MX and SCL determines the ultimate chemical, structural and photo properties of the CM (Schreiber and Schönherr 2009). Research on cuticle wax accumulation has been shown to effect resistance to pathogens (Uppalapati et al. 2012), rate of water loss and drought resistance (Islam et al. 2009; Riederer and Schreiber 2001; Zhang et al. 2007). Studies of *Arabidopsis* have shown that C16 and C18 fatty acids within epidermal cells are the precursors of cuticular waxes. Fatty acids undergo elongation and then are converted into various wax components before transport across the cell wall into the cuticle. (Samuels et al. 2008).

Cuticular waxes are primarily composed of linear long-chain aliphatic compounds (e.g., fatty acids, aldehydes, alcohols, alkanes, secondary alcohols and esters) with chain lengths ranging from C20 to C70. Other components such as triterpenoids, flavonoids and phenylpropanoids are also present in some plants (Schreiber and Schönherr 2009). The MX consists primarily of cutin and polar polymers. Cutin is a biopolyester composed primarily of C16 and C18 acid and alcohol monomers. The CM components occur in varying proportions on different plant organs and the proportions change during ontogeny (Bargel et al. 2006).

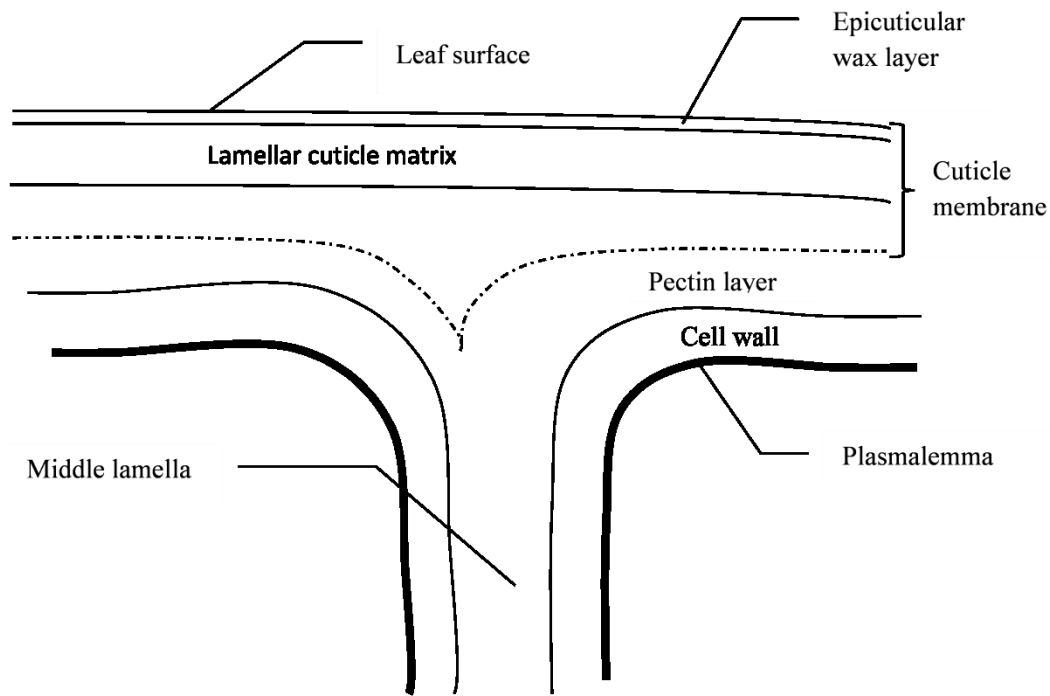


Figure 1. Generalized structure of the plant cuticle. Adapted from Jetter et al. (2000).

The outer structure of the cuticle is complex with some chemical classes located only in specific layers of the cuticle while others are distributed throughout (Jetter and Sodhi 2010). The crystalline structures found on the outermost layer of the cuticle derive their geometry from a primary wax constituent although other secondary components likely play a role. The crystalline structure forms when the concentration of the crystal forming constituent reaches a critical level. At concentrations less than the critical level, no crystals are formed. Many methods of chemical analysis of extracted waxes do not maintain the stratification of wax components thus the results in the literature should be viewed with that in mind (Jetter et al. 2000). Techniques to investigate the stratification of cuticular waxes include Raman spectroscopy, FTIR and various mechanical separation techniques (Buschhaus et al. 2007; Els et al. 2003; Jetter et al. 2000).

The thickness of the CM on mature leaves varies widely from 30nm to 30  $\mu\text{m}$ . Average thickness of the CM is on the order of 3  $\mu\text{m}$  (Jeffree 2006). Wax accumulation is known to be influenced by many factors including light and osmotic stress. Plants exposed to severe environments often

have thicker CM for greater protection from desiccation and solar damage (Samuels et al. 2008). Fast growing plants tend to have thinner CM's on leaves and stems. The CM on most fruits is thicker than other parts of the plant (Bauer et al. 2004; Peschel et al. 2007).

Spinach is a crop of interest in Oklahoma and there is current research at Oklahoma State University investigating microbial contamination of fresh market spinach. In a study investigating the composition of spinach cuticle by Holloway (1974), EW was removed by brief immersion of leaves in chloroform. Following that, CM disks were enzymatically isolated and the waxes and cutin analyzed. Holloway found  $7 \mu\text{g cm}^{-2}$  of intracuticular wax comprised mostly of primary alcohols (C24 to C30) and mono-basic acids (C16, C24 to C30) and  $10 \mu\text{g cm}^{-2}$  of cutin in isolated CM. Cutin analysis revealed a complex mixture primarily containing C16 and C18 epoxy compounds. TEM images of spinach cuticle reveal that the thickness of the spinach CM was 263nm, the cuticle proper 110 nm and the cuticular layer 160 nm. The MX is largely amorphous although a faint lamellar structure of cutin is found in some locations (Holloway 1974; Holloway et al. 1981; Jeffree 2006). In addition to the components identified by Holloway (1974) spinach waxes are likely to contain a mixture of long chain aliphatic components (alkanes, aldehydes, esters) and triterpenoids (Jenks et al. 1995; Peschel et al. 2007; Rashotte et al. 2004; Schreiber and Schönherr 2009).

Hydration of the cuticle changes its viscoelastic behavior. Generally the extent of elastic deformation increases at the expense of plastic deformation and hydration has been shown to slightly reduce the fracture strength of the cuticle (Edelmann et al. 2005; Petracek and Bukovac 1995). This suggests that the cuticle on dried leaves would be more likely to be permanently deformed but not more likely to break when subjected to mechanical stress than a hydrated cuticle. Strength and toughness of the cuticle change a relatively small amount after drying while the rest of the leaf undergoes profound reductions in these mechanical properties. The cuticle is a

thin membrane relative to the leaf thickness and its absolute strength is small. The cuticle may however, contribute enough strength to significantly reduce breakage during routine material handling and storage of dried leaf materials. Without the viscoelastic properties of the cuticle, brittle dried leaves would be subject to shattering due to mechanical stresses. Cuticular wax alone has low mechanical strength. Extracting waxes from isolated ripe tomato cuticles caused changes in mechanical properties similar to those induced by drying. Wax apparently acts as a filler and lubricant within the cutin matrix (Petracek and Bukovac 1995). Aliphatic cuticular lipids are relatively stable chemically with primary environmental reactions caused by photolysis and oxidizing agents such as ozone, hydroxyl and nitrate radicals, oxygen radicals (Calvert et al. 2008; Jetter et al. 1996; Percy et al. 2009).

#### Existing cuticle wax measurement methods

Several cuticular wax quantification methods are found in the literature. Solvent extracted waxes can be gravimetrically determined after evaporating the solvent. Techniques for analysis of solvent extracted waxes using gas chromatography (GC) have been widely documented. Measurements of the CM have been accomplished using transmission electron microscopy (TEM), however documented fixation protocols don't conserve surface wax structure and are not appropriate for measurement of EW waxes (Franke et al. 2005). Isolation of EW wax from leaves has been demonstrated by mechanical removal using cryo-adhesive and chemical adhesive techniques. Waxes are separated from the adhesive by solvent extraction for GC quantification (Riedel et al. 2003). The cuticle membrane can be separated from underlying leaf material by enzymatic digestion of the polysaccharide rich layer which anchors the cuticle to the epidermal cell wall. SCLs can be separated from cutin by solvent extraction. (Buschhaus et al. 2007). All of these methods require time consuming preparatory protocols and each has limitations on accuracy and selectivity. The objective of this research project was to investigate new

experimental methods to rapidly measure cuticle wax on leaves of plants in situ in a field environment.

### Proposed cuticle wax measurement methods

#### *Fourier transform infrared spectroscopy - Attenuated total reflectance*

Attenuated total reflectance (ATR) spectroscopy measures the energy profile of a reflected beam of light that intersects an edge of a refractive crystal at an angle greater than the critical angle where total internal reflection occurs. The evanescent wave produced under these conditions penetrates a short distance into a sample held in contact with the internal reflective element (IRE). The interaction of the evanescent wave with the sample can reveal information about the surface chemistry of the sample. The evanescent wave penetration depth is dependent on the refractive indices of the IRE and sample, angle of light w.r.t. the IRE and wavelength (eq. 1). Fourier transform infrared spectroscopy ATR (FTIR-ATR) is a common laboratory tool for analysis of surface chemistry of organic polymers. Greene and Bain (2005), Ribeiro da Luz (2006), and others have used the limited penetration depth of infrared evanescent waves to study cuticle surface and laminar structure, however no literature sources have been identified where the thickness of the cuticle was measured using this technique.

The electromagnetic field intensity of the evanescent wave falls off exponentially with distance  $z$  from the IRE-sample interface according to the relation:  $E=E_0e^{-z/d_p}$ . Evanescent wave penetration depth,  $d_p$ , in a non-attenuating sample is:

$$d_p = \frac{\lambda/n_1}{2\pi\sqrt{\sin^2\theta - (n_2/n_1)^2}} \quad (1)$$

The refractive indices of the IRE and sample are  $n_1$  and  $n_2$  respectively. The angle of incident light is  $\theta$  and  $\lambda$  is the wavelength of incident light in free space. The penetration depth is defined

as point where the intensity of the evanescent wave falls to  $1/e$  the intensity at the surface. When the sample is layered, such as in the case of a cuticle with an underlying polysaccharide layer binding the CM to epidermal cell walls, an estimate of the CM thickness is possible by ATR if the CM thickness is in the same order of magnitude as  $d_p$  (Muller and Abraham-Fuchs 1993). If refractive indices of each layer are known, reflectivity of incident light can be calculated by methods of Muller and Abraham-Fuchs (1993). Refractive indices of waxes vary according to their composition but 1.46 to 1.51 is typical for alkane rich hydrocarbons in the C16 to C30 range found in waxes and cutin of the CM. Diamond and ZnSe have refractive indices of 2.4, germanium is 4.0 at  $1000\text{ cm}^{-1}$ . This suggests that CM on the order of  $1\text{ }\mu\text{m}$  thick could be probed over the mid IR spectral analysis range of  $2.5$  to  $25\text{ }\mu\text{m}$  with a diamond IRE.

Several absorption bands are of interest for FTIR-ATR of plant cuticles. Cuticle lipids are predominately long chain aliphatic molecules dominated by  $-\text{CH}_2-$  monomers which adsorb strongly at  $2915$  and  $2850\text{ cm}^{-1}$  (C-C stretching) and  $1462\text{ cm}^{-1}$  (C-C deformation). Water absorbs strongly in the  $3300$  (O-H stretching),  $2125$  and  $1633\text{ cm}^{-1}$  (O-H absorption) bands. Cell wall polysaccharides exhibit characteristic differences concentrated in the  $1200$  to  $900\text{ cm}^{-1}$  region. This absorption region is dominated by ring vibrations overlapped with stretching vibrations of C-OH side groups and the C-O-C glycosidic bond vibration (Kacuráková et al. 2000). Cellulose and other cell wall polysaccharides absorb strongly at  $1446\text{ cm}^{-1}$  (C-H stretching),  $1055$  and  $1032\text{ cm}^{-1}$  from C-O and C-OH stretching vibrations. The ability of FTIR-ATR to differentiate between cell wall polysaccharides and cuticle components is likely to play an important role in measuring thickness due to the spatial arrangement of these elements in the plant epidermis.

The proximity of cellulose and pectin in the cell wall to the ATR IRE may be exploited to provide an indicator of cuticle thickness. The total thickness of cuticle proper, pectin layer and primary cell wall of epidermal cells of eight varieties of forage plants was  $2.62\text{ }\mu\text{m}$  ( $0.119\text{ s.e.}$ ) (Rezvani

and Wilman 1998). This is large in relation to  $d_p$  in most ATR configurations. Furthermore, it is likely that a combination of absorption bands, both direct and indirect, will need to be analyzed to quantify cuticle and wax thickness. Thinner cuticles will likely lead to greater attenuation from water, cellulose and pectin and lower attenuation from lipids. Subtle differences in leaf components will also confound the ability of FTIR-ATR to accurately measure cuticle thickness. Turakhozhaev (1997) found well-pronounced absorption bands in pectin extracted from apple in various ways at  $1749\text{ cm}^{-1}$ . Depending on the extraction method absorption bands were also found at  $1450, 1620, 3311, 3400, 3500, 3600$  and  $3263\text{ cm}^{-1}$ . Lu et al. (2008) successfully used FTIR-ATR analysis to identify different varieties of ground *Camellia* L. leaves. The absorption spectrum depends on the relative amount of specific chemical bonds in the sample and these slight differences were enough to discern different varieties. Dubis et al. (1999) noted that in situ FTIR-ATR analysis of cuticle waxes was more difficult on plants with thinner layers of wax because of interference from water contained in underlying polysaccharides associated with the cell wall. Wilson et al. (2000) found minor changes in intensity of polarized FTIR spectral peaks of cellulose and pectin when examining cell walls under mechanical and dehydration stress. It can be expected that some variation in infrared spectral response will be induced by changes in water content and by deformation caused by clamping a leaf sample against the optics of an ATR attachment.

The thickness of some thin membranes can be calculated by analyzing the attenuation of internally reflected light by the method outlined by Muller and Abraham-Fuchs (1993). If the leaf epidermis is modeled as optically homogeneous layers (Figure 3) and optical properties of each layer are distinct, the thickness of the cuticle could be calculated by solving equation (2) for perpendicularly polarized light by means of a non-linear optimization algorithm.

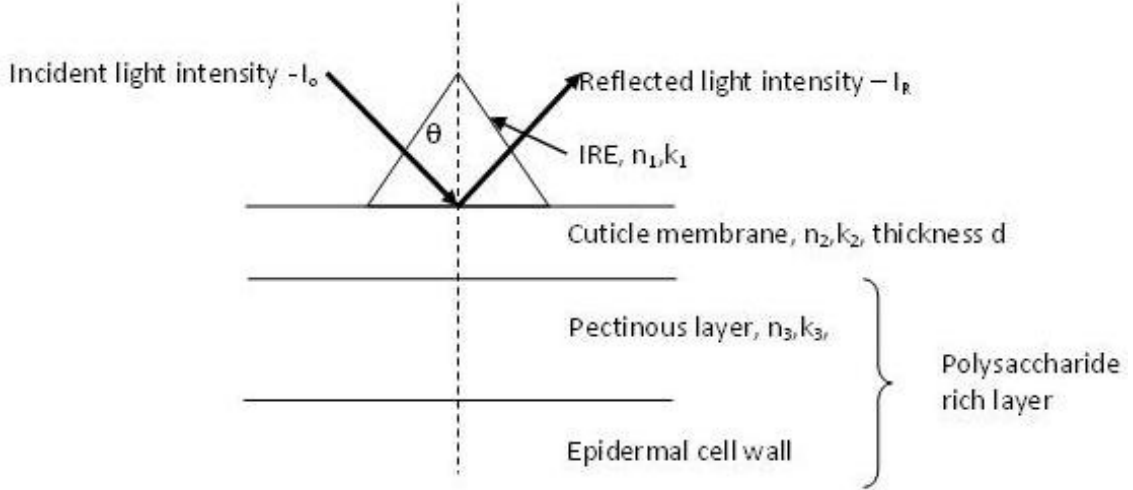


Figure 2. System for ATR measurement of cuticle membrane overlaying polysaccharide rich layer.  $k$ : absorption index of the layer,  $n$ : refractive index of the layer and  $d$ : the thickness of the CM.

$$R_{\perp} = I_{R\perp}/I_{o\perp} = \frac{\xi' - \eta'}{\xi' + \eta'}; \quad \xi' = A^2 + B^2 + a^2 + b^2 \quad \text{and} \quad \eta' = 2(AB + ab)$$

$$A = \cos\theta S \quad \text{and} \quad a = \cos\theta s; \quad B = \omega_2^- \bar{S} - \omega_2^+ \bar{s} \quad \text{and} \quad b = \omega_2^- \bar{s} + \omega_2^+ \bar{S}$$

$$S = \omega_2^- D^+ + \omega_3^- D^- + \vartheta(\omega_3^+ - \omega_2^+); \quad s = \omega_2^+ D^+ + \omega_3^+ D^- + \vartheta(\omega_2^- - \omega_3^-);$$

$$\bar{S} = \omega_2^- D^- + \omega_3^- D^+ + \vartheta(\omega_2^+ - \omega_3^+); \quad \bar{s} = \omega_2^+ D^- + \omega_3^+ D^+ + \vartheta(\omega_3^- - \omega_2^-)$$

$$D^{\pm} = 1 \pm D^2 \cos 2\varphi; \quad \vartheta = D^2 \sin 2\varphi; \quad D = e^{\left(\frac{-d}{d_p}\right)}; \quad \varphi = -\frac{2\pi}{\lambda} n_1 \omega_2^- d$$

$$\omega_2^{\pm} = \frac{1}{\sqrt{2}} \left( \sqrt{v_2^2 + \mu_2^2} \pm v_2 \right)^{1/2}; \quad \omega_3^{\pm} = \frac{1}{\sqrt{2}} \left( \sqrt{v_3^2 + \mu_3^2} \pm v_3 \right)^{1/2};$$

$$v_2 = \sin^2\theta - n_{21}^2(1 - \kappa_2^2); \quad v_3 = \sin^2\theta - n_{31}^2(1 - \kappa_3^2); \quad \mu_2 = 2n_{21}^2\kappa_2; \quad \mu_3 = 2n_{31}^2\kappa_3$$

$$n_{21} = \frac{n_2}{n_1}; \quad n_{31} = \frac{n_3}{n_1}; \quad \tilde{n}_2 = n_2(1 + i\kappa_2); \quad d'_p = \frac{\lambda}{2\pi n_1 \omega_2^+} \quad (2)$$

The stated assumptions of known, homogeneous optical properties are not found in real plant surfaces, thus a better approach to determining thickness would be to calibrate the ATR

measurements to cuticle thickness determined by other methods. Using similar reasoning Kane et al. (2009) used FTIR-ATR to measure the thickness of a thin film of coatings on ultrahigh molecular weight polyethylene substrate. The ether groups present in the cross-linked coating, but absent in the substrate, absorbed at  $1115\text{ cm}^{-1}$ . Their procedure used AFM thickness measurements to correlate the FTIR-ATR peak area absorbance readings at  $1115\text{ cm}^{-1}$  to coating thickness. Coating thicknesses measured ranged from 30 to 200 nm thick, less than one-third the 600 nm penetration depth of the evanescent wave in their configuration.

Yang et al. (2005) used substrate absorbance to measure the thickness of a thin polystyrene coating on a polypropylene substrate. Their technique required measuring the area of the methyl absorption band ( $1375\text{ cm}^{-1}$ ) in the bulk substrate at varying incidence angles above the critical angle and correlating the results to thickness. The measured systems of Kane et al. (2009) and Yang et al. (2005) consisted of distinct layers of pure, homogenous polymeric materials. In addition to the layers being more chemically homogeneous, the top layer was more consistent in thickness than a leaf CM and the substrate was orders of magnitude thicker than  $d_p$ .

Contact of the sample leaf with the IRE is critical to obtaining reliable CM thickness measurements. Stuchebryukov and Rudoy (1992) were able to show that the intermittent contact gap caused by a rough surface could be compensated for by incorporating a known surface roughness into calculations. This effectively added another layer to the three layer ATR equations noted above. This confounding effect may be eliminated by high contact forces to effectively eliminate the gap by deforming the leaf surface and forcing it to contact the IRE.

For infield measurements, portable and ruggedized FTIR-ATR instruments are currently available for scanning the thermal IR spectrum. A purpose-built ATR sensor that analyzes several IR frequencies specific to cuticular measurements would be a significant, but achievable,

engineering design challenge. Electronic emitters and/or receivers with sufficient spectral precision in the IR band will be required along with significant processing capabilities.

*Thermal measurement: Differential scanning calorimetry*

The thermal properties of cuticular waxes have been used to study cuticular characteristics. Scanning Thermal Microscopy (SThM) uses atomic force microscopy (AFM) techniques with thermal probes to detect thermal properties of surface components. Perkins et al. (2005) used SThM to study the effects of surfactants on cuticle wax of *Prunus laurocerasus* leaves. They found that SThM techniques allowed them to spatially map wax transition properties at a submicron scale across the leaf surface. Similar techniques might be applied to determine wax thickness. If the SThM tip is held at a temperature above the melting point of the cuticle wax during a scan, the energy needed to keep the tip at that temperature would be related to the amount of wax being melted and in turn its thickness. In this scenario, penetration depth of the tip would need to be limited to the wax layer by underlying structural elements in the leaf. Methods to do that are not readily apparent.

Directly measuring the wax content of a leaf section is in theory possible using differential scanning calorimetry (DSC) of leaf sections. Coret and Chamel (1994) used DSC on extracted 10-20 mg samples of box-tree (*Buxus sempervirens L.*) cuticle wax and found an enthalpy of fusion of 30 uJ/ug centered around a temperature of 50.8°C. If the phase transition temperatures of the waxes on a leaf can be separated from thermal transitions of other leaf components such as gelling of intracellular pectin, protein denaturing and water vaporization, DSC may be a technology for quantification of cuticular wax. The wide variety of cuticle components found on plants will likely result in a wide melting band. Increasing chain length, degree of saturation, and number of methylene units between methyl side groups generally increases melting temperature of the specific wax components (Gibbs and Pomonis 1995). Reconstituted wax of *Hedera helix*

and *Juglans regia* had a melting midpoint of 82 and 71 °C respectively and exhibited a melting range of 75-86 and 41-82 °C respectively when evaluated by FTIR with a temperature controlled cell holder. Whole leaves of *Hedera helix* and *Juglans regia* evaluated by the same equipment showed an increase in melting midpoint to 86 and 79 °C respectively and exhibited a melting range of 78-89 and 41-93 °C respectively (Merk et al. 1997). This change in melting behavior indicates that other leaf components are interfering with the heating profile of the waxes of those species in situ. Furthermore, current DSC technology would not likely be able to discern between adaxial and abaxial waxes. DSC is typically performed on homogenized samples in the lab. The specific heat of cutin and cuticular wax varies with temperature, moisture content and wax/cutin composition (Casado and Heredia 2001; Matas et al. 2004). Reynhardt and Riederer (1991) used DSC on insolated CM, cuticle wax and MX of *Citrus aurantium* leaves. The isolated wax produced endothermic peaks at 57 and 70°C. However these peaks were not evident in the thermalgram of the intact CM on leaves. *Citrus aurantium* has very low wax content, approximately 4% of the CM, which could explain the lack of sufficient profile of wax melting in isolated CM to determine wax quantity. This study does cast doubt on the viability of this technique to accurately measure wax thickness on leaves of plants, like citrus, that have low wax coverage.

The precision of analytical DSC equipment should be sufficient to discern transition temperatures of wax on many leaves. For example Ristic and Jenks (2002) found 10ug cm<sup>-2</sup> of wax, primarily C30 to 32, on two varieties of maize and Holloway (1974) found 7 ug cm<sup>-2</sup> of intracuticular wax on spinach leaves. This results in a wax thickness of approximately 25 to 50 nm on each surface of the leaf. With a melting point of 50°C and a heat of fusion of 30uJ/ug, a spinach leaf sample would require about 200 uJ cm<sup>-2</sup> for the phase transition of a 50 nm thick wax layer. Spinach cuticular wax is a tiny fraction of the total leaf mass - less than 0.1%. The wax mass fraction can be increased about 10 fold by drying leaves since they contain >90% water. If thermal phase

transitions of other leaf components do not mask the wax melting transition it is not unreasonable to expect that useful predictions of wax thickness could be discerned with laboratory grade DSC equipment. Pectin gels above the temperature of interest and should not be an interferent (Ye et al. 2008). Further information on the nature of the wax layers may be discerned by analyzing the profile of the heat flux curve. For example, if  $T_{\text{melt}}$  of epicuticular and intracuticular wax are different, the relative dwell times at each components melting temperature could provide insight into the amount of each component present in the tissue sample if enough precision in the measurements can be made.

There are two main types of DSCs available: heat flux and power compensated DSCs. Most current laboratory DSCs operate on the heat flux principle. Both types monitor a differential signal between an analytical and reference sample to determine the differential amount of heat flux that has been absorbed by the sample. Heat flux DSCs operate by maintaining a steady heat flux to the sample and reference sample in the furnace. Temperature of the two samples is precisely monitored over time by a network of thermocouples. For two similar samples, the differential temperature is due to a phase transition in one of the samples. Power compensated DSCs use a closely coupled control algorithm to vary the heat flux to each sample to maintain a constant temperature profile. The differential heat flux can be attributed to a phase change or reaction in one of the samples (Hohne et al. 2003).

#### Experimental objectives for rapid in situ measurement of leaf cuticular wax

A search of the literature reveals a dearth of rapid, in situ methods for quantitative measurement of cuticle thickness or cuticular waxes. The composition and spatial arrangement of the plant cuticle suggests that FTIR-ATR spectroscopy and DSC may hold promise as methods for rapid, in situ quantification of cuticular waxes. The objective of our experiments was to develop empirical methods to measure the amount of cuticular wax using FTIR-ATR and DSC on spinach

leaves. Successful demonstration of these new quantitative methods on spinach leaves would provide a reference for other researchers looking for rapid, non-extractive laboratory procedures to quantify cuticular wax in other plants.

## Materials and methods

### Plant materials

Fresh picked fully expanded spinach leaves (*Spinacia oleracea* L. cv. Silverwhale) in good condition suitable for fresh market sale, ranging in age from 42 to 63 days were used for these experiments. Plants were grown in pots in either a slow growth (SG) or a fast growth (FG) chamber that simulated early and late season field conditions (Table 1). Leaves from different growth conditions were selected so that a range of wax and CM thickness was available for model building and verification. Leaves from 28 plants were harvested for model building. A sample of leaves from 13 plants sown at a later date was used for model validation. A second validation sample of a different spinach cultivar (*Spinacia oleracea* L. cv. Tyee) grown outdoors in Bixby, Oklahoma was also tested. It was planted on March 30, 2011 and harvested 63 days later. An additional three plantings of Silverwhale spinach, spaced 10 days apart, were grown in a greenhouse for experiments to measure cuticular waxes on dried leaves using FTIR-ATR. These leaves were harvested 53 to 76 days after planting.

Leaves were stored in plastic bags at 4°C in a high relative humidity environment to slow desiccation and decomposition prior to testing (Kosma et al. 2009). Immediately before analysis leaves were gently agitated in distilled water for 30 s two times to remove surface particulates and water soluble contaminants from the leaf surface.

Chamber	Day length (h)	Day temp (°C)	Night temp (°C)	Time to maturity (days)
Slow growth	10	18	7	45-50
Fast growth	12	24	18	35-40

Table 1. Growth chamber conditions for spinach specimens.

Wax load and CM thickness are spatially non-uniform, generally varying from stem to tip and transversally across the leaf (Jeffree 2006). To account for this variation, solvent extracted GC samples, FTIR-ATR spectral scans and DSC sections were taken as close together on the leaf surface as possible to minimize variation (Figure 4 and Figure 5). The DSC protocol will analyze waxes on both sides of the leaf while FTIR-ATR and GC will be single sided measurements. Therefore, top and bottom GC wax measurements from the same leaf were pooled to compare to DSC results.

#### FTIR-ATR measurements

FTIR-ATR analysis was conducted on a Thermo Science Nicolet 6700 with a single reflection diamond IRE ATR attachment. The active sampling area of this device was approximately 1.5 mm in diameter. A hold down clamp with a conformable tip made from a rubber stopper (size 000) was used to maintain contact between the leaf sample and ATR IRE (Ivanova and Singh 2003). A uniform pressure of 0.1 MPa was maintained by first measuring the stress – strain relationship of the elastomeric tip and then compressing it a known distance with the screw clamp (Figure 3).

Separate FTIR-ATR sampling protocols were used on leaves depending on whether waxes would be analyzed by GC or in a dried condition. On leaves where cuticle waxes would be analyzed by GC, three spectra over the range of 650-4000  $\text{cm}^{-1}$  were collected from three different locations in a 10 mm diameter area to be extracted (Figure 4). For leaves that were to be dried, three measurements were taken on the fresh leaf adjacent to the section that was removed and dried.

Two more measurements were taken from the removed leaf section after it had been dried and rehydrated (Figure 5).

In addition, spectra of selected isolated leaf components (wax, cutin, cellulose and water) were collected using appropriate fixtures to assist in analysis. Each spectrum consisted of the mean of 16 scans taken with a resolution of  $1\text{ cm}^{-1}$ .

Care was taken to avoid FTIR-ATR scans directly on a leaf blemish or rib. Measurements taken on a leaf rib did not have repeatable spectral response due to inconsistent contact between the IRE and leaf. The IRE was cleaned with an ethanol soaked tissue between leaf samples. Spectra were referenced to background measurements collected in air.

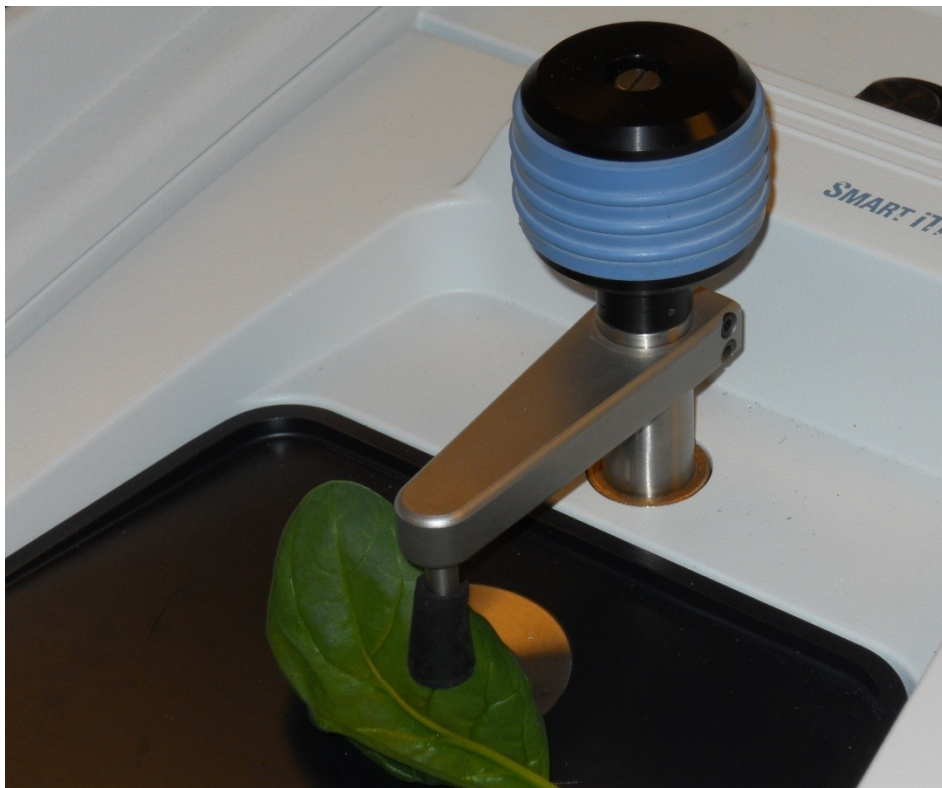


Figure 3. Spinach leaf held against IRE with conformal elastomeric tip during FTIR-ATR spectral scan.

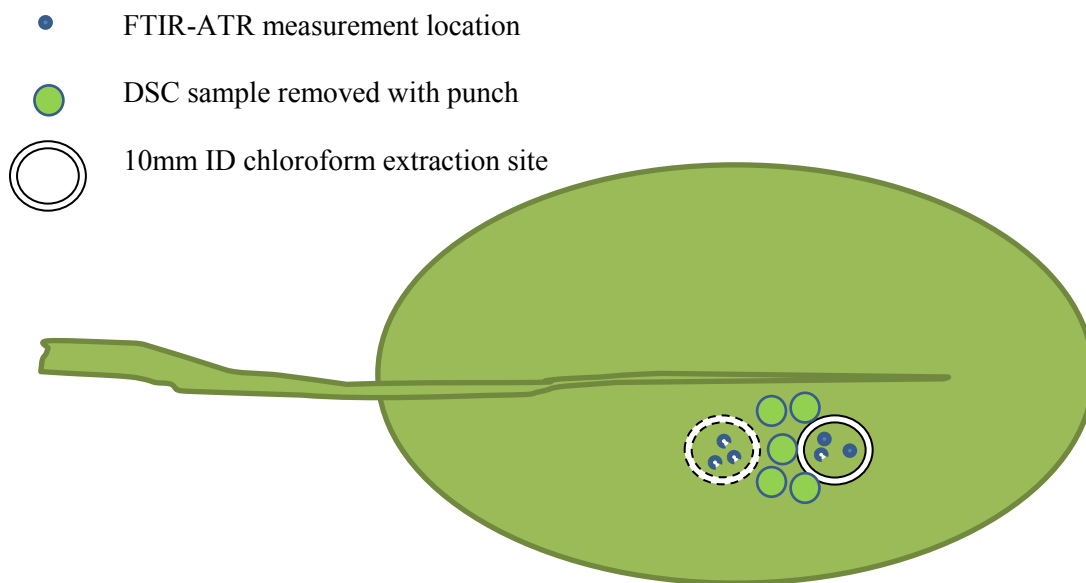


Figure 4. Diagram of spinach leaf sampling protocol for FTIR-ATR, GC and DSC sample set. Dashed lines indicate sampling locations on the back side of the leaf.

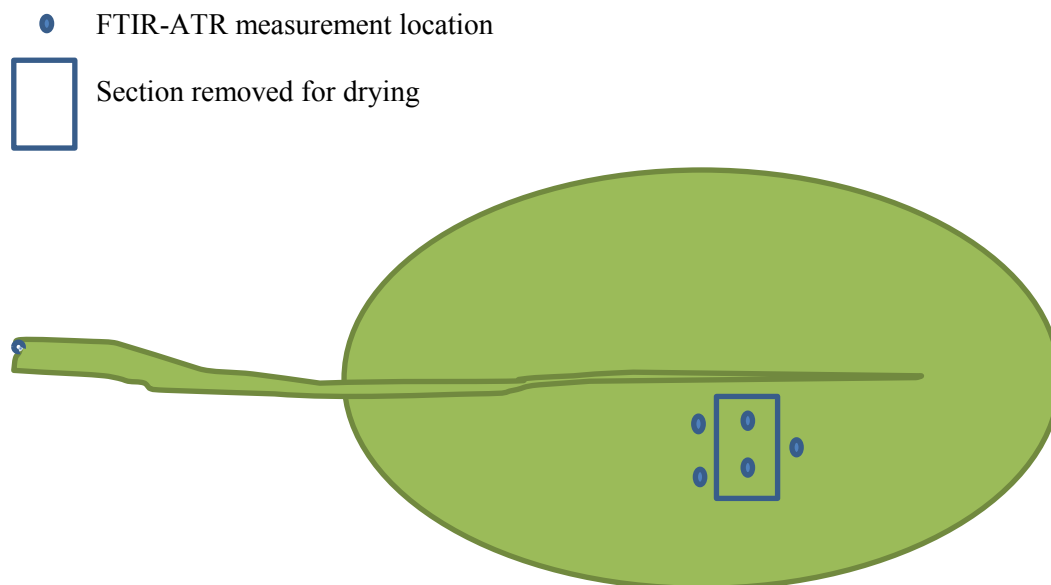


Figure 5. Diagram of spinach leaf sampling protocol for measurement of dried leaf cuticular waxes. Rectangle indicates sampling locations on dried leaf area.

### Chloroform extraction of CM waxes

Cuticular wax for GC analysis was extracted from intact leaves using a protocol adapted from Buschhaus et al. (2007). Leaves were held against an open 7 ml vial containing 2 ml of chloroform with a gloved hand for 30 s at room temperature. The inside diameter of the vial mouth was 10 mm. The vial was gently inverted 10 times during the extraction. The extraction was repeated with another vial in the same location and combined with the first vial. A sample was discarded if significant solvent leaked during extraction. The first extraction vial contained 2  $\mu\text{g}$  each of tetracosane and heptacosanol (Sigma-Aldrich) as internal analytical standards. The second vial was pure chloroform. A similar extraction protocol conducted by Jetter et al. (2000) demonstrated recovery of 95% of waxes in the first extraction thus minor losses of wax or solvent during the second extraction would have a negligible effect on analysis.

Larger samples of cuticular waxes for TLC and DSC and GC protocol development were obtained with a similar process except whole leaves were suspended in chloroform for 30 s two times. Solvent was removed by heating at 40 °C under a stream of nitrogen.

### High performance thin layer chromatography

High performance thin layer chromatography (HPTLC) was used to determine the molecular classes of extracted spinach waxes. Known standards and extracted waxes were spotted onto silica gel HPTLC plates (Analtech Uniplate, model 57527) and developed in a hexane-ether (9:1 and 8:2, with 1% citric acid) mobile phase for component class identification. Wax fractions were visualized by dipping in a 3% cupric acetate and 15% phosphoric acid solution followed by charring on a hot plate. Wax fractions for analysis by GC were isolated on preparatory plates (Analtech Uniplate, model 42511). Individual wax fractions were recovered by eluting bands of silica gel scraped from the plate with hexane-ether (1:1).

## Gas chromatography

Extracted waxes were analyzed by GC to determine wax amount and composition using a protocol adapted from Buschhaus et al. (2007), Jetter and Schaffer (2001) and others to quantify SCL's. After extraction chloroform was evaporated from vials under a stream of nitrogen. Trimethylsilyl (TMS) derivatives of hydroxyl containing compounds were prepared by adding 50ul each of bis-N,O-trimethylsilyltrifluoroacetamide (BTSFA) (Supelco, Bellefonte, PA) and pyridine to the 7 ml vial, vortexing for 10 s and incubating at 70°C for 30 min. Wax components were quantified on a capillary GC (Hewlett Packard 5890 II, Santa Clara, CA) equipped with a FID detector. A 1 ul sample was injected in a splitless configuration (Agilent DB-1, 30 m x 0.25 mm i.d., film thickness 0.25 µm, Santa Clara, CA) with helium as the carrier gas at 1 ml min<sup>-1</sup>. The GC program consists of inlet temperature of 250 °C, oven temperature: 50 °C for 1.75 min, 40 °C min<sup>-1</sup> to 180 °C, 3 °C min<sup>-1</sup> to 320 °C, 10 min at 320 °C. FID was maintained at 350 °C. Injector purge gas was turned on at 1.85 min and off at 59.5 min. A 3 m long retention gap (Agilent model 160-2255-10, Santa Clara, CA) was incorporated and replaced as needed due to fouling by contamination of unpurified samples and non-volatile components (Nass et al. 1998). Semi-quantification of wax components was done by comparing their FID response to tetracosane and heptacosanol internal standards for unchanged and TMS derivatives of wax components respectively. Retention times of authentic standards and GC-MS were used to identify FID peaks.

## Scanning electron microscopy (SEM)

SEM was used to image whole leaves to examine leaf surface topography. Leaf tissue samples were fixed for 2 hours in 2.0% buffered glutaraldehyde solution followed by rinsing in 0.1M phosphate buffer (pH 7.0) for 20 min three times. After one hour in 1% osmium tetroxide specimens were rinsed three times in 0.1M phosphate buffer for 20 min. Dehydration consisted

of an ethanol series of 30%, 50%, 70%, 80%, 90%, 95% and three times in 100% ETOH for 20 minutes each. Finally samples were critical point dried (Bal Tec CPD 030) and mounted on 12 mm aluminum stubs with double-sided adhesive carbon tape and Au-Pd sputter coated (Balzers MED010, Liechtenstein) for 2 min. Images were obtained using a FEI Quanta 600 SEM (Hillsboro, OR) at the Oklahoma State University Microscopy Laboratory.

### Transmission electron microscopy (TEM)

TEM of leaf sections was used to image cuticle thickness directly. The fixation protocol is adapted from one used by Franke et al. (2005). Leaf tissue samples approximately 1.5 mm by 4 mm were cut with a punch and immediately immersed in a vial containing a 2% buffered glutaraldehyde solution. After 2 hours specimens were suspended in buffered wash (pH 7.0) three times for 20 min each followed by a second fixation in 1% osmium tetroxide for 18 hours. Dehydration consisted of an ethanol series of 25%, 50%, 75%, 95% and three times in 100% ETOH for 20 minutes each. Three 20 min washes in transitional solvent propylene oxide followed dehydration. The tissue specimens were then imbedded in a propylene oxide/Spurr's (1:1) resin for 24 h, followed by 24 h in complete Spurr's. Finally tissue specimens were placed in fresh resin in silicon molds and cured at 60°C for 24 hours. Sections 70 nm thick were stained with uranyl acetate for 30 min and Reynold's lead citrate for 20 min. Images were obtained using a JEM 2100 TEM (Jeol, Tokyo, Japan) at the Oklahoma State University Microscopy Laboratory.

### Cuticular membrane isolation

CM were enzymatically isolated intact using an adaptation of a technique described by Orgell (1955). The underlying cell structure was disrupted by immersion of 10 mm diameter leaf discs in a solution of 0.5 g/l Pectinex Ultra SP-L (Novozymes, Denmark) in 0.1M acetate buffer at pH 4.0 for 48-72 h at 50°C followed by gentle agitation and thorough rinsing with distilled water to

remove leaf residues. Wax from isolated cuticles was extracted with chloroform, using a similar procedure for leaf sections, leaving cutin discs. CM and cutin discs were stored in water at 4°C until use.

### Dried leaf cuticle measurement protocol

Sections removed from the fresh leaf after initial FTIR-ATR scans were dried at 50°C for 24 h. Leaf sections were rehydrated in distilled water at 22°C for 2 h. After rehydration, leaf sections were flattened and excess water was removed by gently pressing between two pieces of filter paper for 3 to 4 min. Leaf section area was measured before drying and after rehydration to assess shrinkage. Rehydrated leaves were positioned on the FTIR-ATR IRE such that the area where the conformal clamp contacted the leaf on previous measurements did not overlap the current measurement area.

### Statistical analysis

Principal component analysis (PCA) was used to identify important wavenumbers in the collected spectra. The average reflectance of three (two for dried leaf sections) spectra collected was used as the wax thickness indicator for each leaf region. Prior to averaging, spectral resolution was reduced to 4 cm<sup>-1</sup> to decrease processing time. To further reduce processing time, the spectra were truncated to exclude wavebands that exhibited little inter-sample variance or were primarily a response to water. Wavenumbers between 3300 and 4000 cm<sup>-1</sup>, 1800 and 2800 cm<sup>-1</sup> and 650 to 900 cm<sup>-1</sup> were eliminated. Specific wavenumbers contributing most significantly to variance were isolated by subjecting the training set of 28 reflectance spectra to PCA using the SAS PRINCOMP procedure (SAS Institute Inc., Cary, NC). Using these results, 24 wavenumbers at local maxima and minima values from the first four principal components were selected by inspection for subsequent regression analysis.

Models predicting wax load were then calculated using a subset of these frequencies by multiple linear regression analysis using coefficient of multiple determination ( $R^2$ ) and adjusted coefficient of multiple determination ( $R^2_A$ ) as the variable selection criteria with the SAS REG procedure (SAS Institute Inc. 2004). The SAS CORR procedure was used to evaluate multicollinearity between predictor variables. Response variable measurements were obtained by GC analysis of extracted wax samples. Model performance was verified by comparing root mean squared error (RMSE) of the training set to a validation set containing 13 samples.

### DSC measurements

Five, 6.35 mm diameter leaf discs were cut with a punch from the middle of each leaf (Figure 4) and dried at 40 °C for 24-28 h. Dried disks were then sealed in a hermetically sealed crucible (TA Instruments, TZERO p/n 901683/4) for DSC analysis. Prior investigation has shown that hermetically sealed crucibles are required to mitigate the effects of water vaporization in the wax phase transition range. DSC thermographs of leaf and wax samples were taken with a TA Instruments Q2000 DSC (TA Instruments, New Castle Delaware). Sensitivity of the instrument is 0.2uW with a sampling rate of 50 s<sup>-1</sup>. Measurements were performed using a constant rate temperature ramp of 10 °C/min from 10 to 100 °C. Heat of fusion of pure cuticle wax was determined using the same procedure used for leaf samples. The mass of cuticular wax in each sample was calculated by dividing the sample peak area, in joules, by the heat of fusion of pure wax. Sample peak area of leaf samples was measured over the same temperature range used to determine the heat of fusion of wax. Accuracy of the method was evaluated by comparing the DSC measurement to GC results of extracted wax.

## Results and discussion

### Leaf cuticular wax composition

HPTLC of extract of spinach leaves immersed in chloroform 2 times for 30 s revealed the presence of alkanes, aldehydes, alcohols, fatty acids, and wax esters along with unidentified non-mobile impurities and suspected intracellular compounds from cells disrupted during extraction and handling (Figure 6).

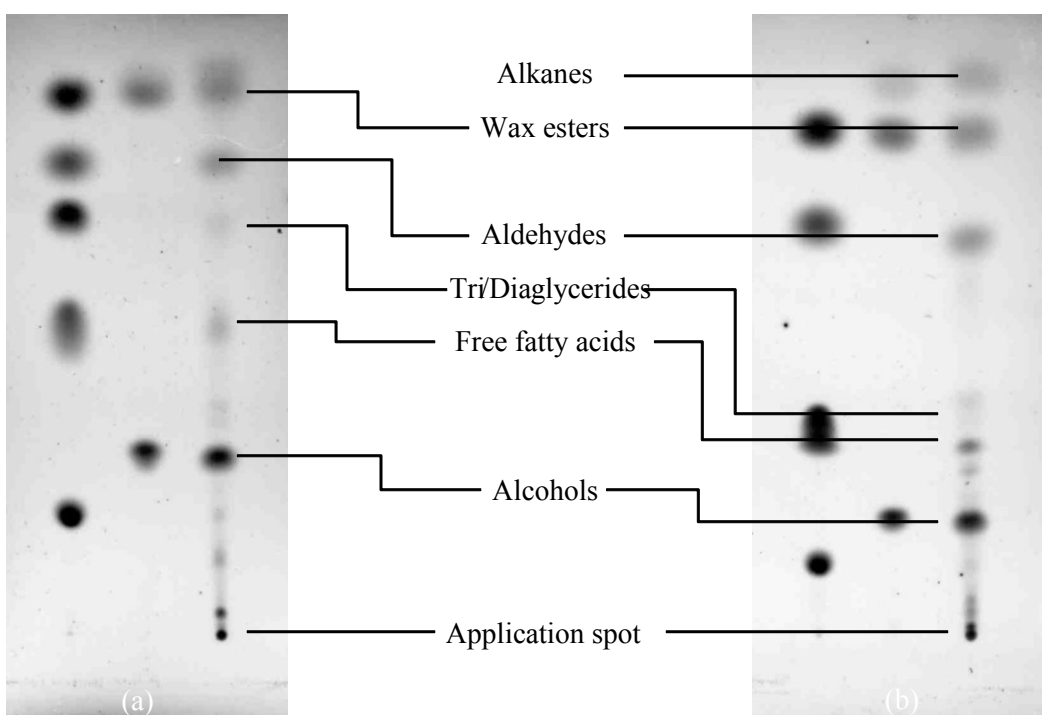


Figure 6. HPTLC plates of chloroform extracted spinach cuticular wax developed with 8:2 (a) and 9:1 (b) hexane - ether mobile phase. Columns 1 and 2 are authentic standards and column 3 is chloroform extracted spinach cuticular wax.

GC was used to identify and quantify the main compounds in the extract. Cuticular waxes consisted mainly of primary alcohols (C<sub>24</sub>, C<sub>26</sub>) and saturated alkanes (nC<sub>29</sub>-nC<sub>33</sub>, with nC<sub>31</sub> dominant) (Figure 7). Aldehydes, wax esters and acids visualized with TLC were low relative to alkanes and alcohols and were not quantified for the purposes of this study. FG and SG leaves had significant differences in the amount of alkanes (P=0.0009) and primary alcohols (P=0.0002)

but not in total wax ( $P=0.7464$ ). SG leaf waxes consisted mainly of primary alcohols while FG waxes were principally alkanes (Table 2). Total cuticular wax and alkane load were not significantly different on abaxial and adaxial sides of the leaves. Adaxial leaf surfaces had more primary alcohols than the abaxial surface ( $1.17$  vs.  $0.89 \mu\text{g cm}^{-2}$ ;  $P=0.0268$ ). Total wax amount increased with chronological plant age although the correlation was poor ( $P=0.0004$ ,  $R^2=0.28$ ). As spinach grows, new leaves emerge in pairs and expand in size. Thus, relationships of wax composition and/or amount to leaf size are also correlated to leaf age. Linear regression analysis showed no consistent pattern of wax load to leaf size so this research provides no insight into a relationship between maturity of individual leaves and wax composition.

Table 2. Composition of cuticular waxes from fast growth (FG) and slow growth (SG) spinach leaves. Amounts shown are the mean and (SD) of waxes extracted mid-leaf from abaxial and adaxial surfaces determined by gas chromatography.

Spinach type	No. of samples	Wax component ( $\mu\text{g cm}^{-2}$ )		
		Alkanes	Primary alcohols	Total waxes
FG	23	1.29 (0.50) a*	0.82 (0.21) a	2.12 (0.50) a
SG	18	0.77 (0.41) b	1.28 (0.48) b	2.06 (0.82) a

\*Means in columns followed by similar letters are not significantly different. (LSD test at  $\alpha=0.05$ )

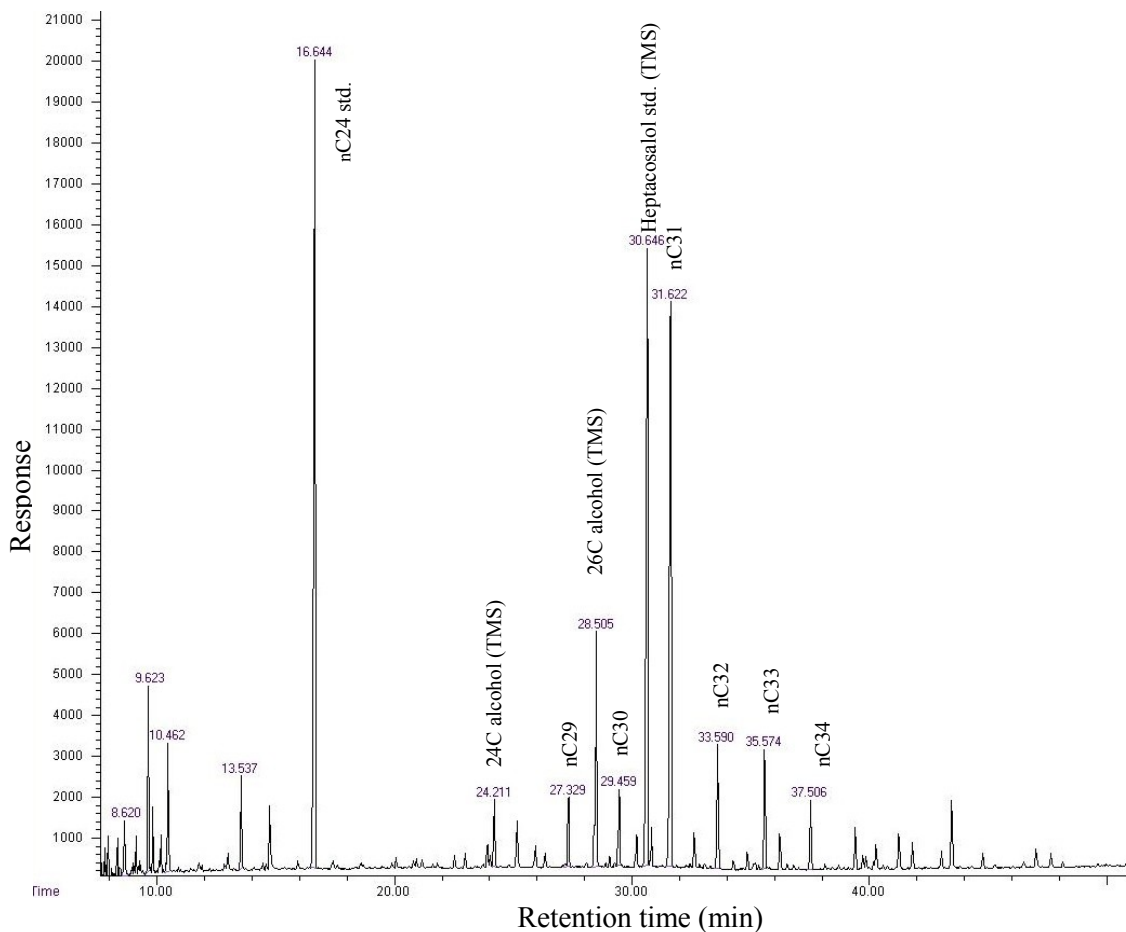


Figure 7. Typical GC response of spinach leaf chloroform extract following TMS derivatization.

### Transmission electron Microscopy

Measurement of cuticle thickness by transmission electron microscopy (TEM) was inconclusive. Differentiation of the cuticle from cell walls was not consistent and epicuticular waxes were not conserved. Some images did have good differentiation (Figure 8, left) while others (Figure 8, right) did not. Furthermore, work effort and expense would have been prohibitive to use this technique for quantifying the cuticle thickness. TEM Images did support published reports of a cuticular structure consisting of a faintly lamellar cutin structure merging with an inner reticulate region next to the cell wall (Jeffrey 2006).

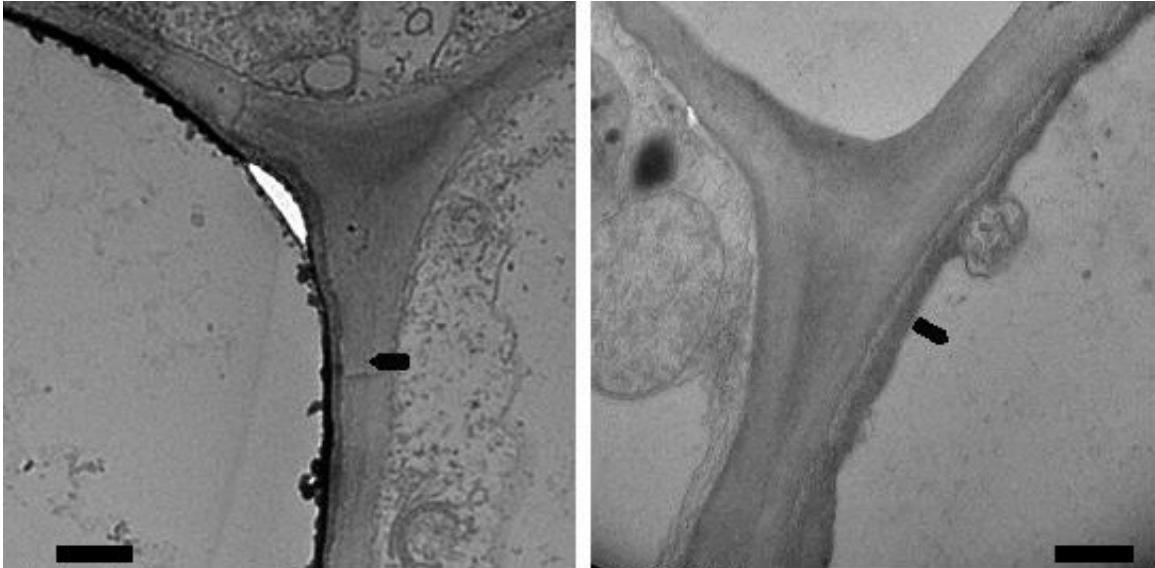


Figure 8. Representative transmission electron microscope images of spinach leaf epidermis. Pointer is indicating base of cuticle. Scale bar is 500 nm.

Scanning electron microscope images of the surface of spinach leaves revealed a generally smooth leaf surface (Figure 9, top row) at moderate magnification. Small scale surface roughness (Figure 9, bottom row) is obscured by the relatively large 1.5 mm diameter sensing area of the FTIR optics.

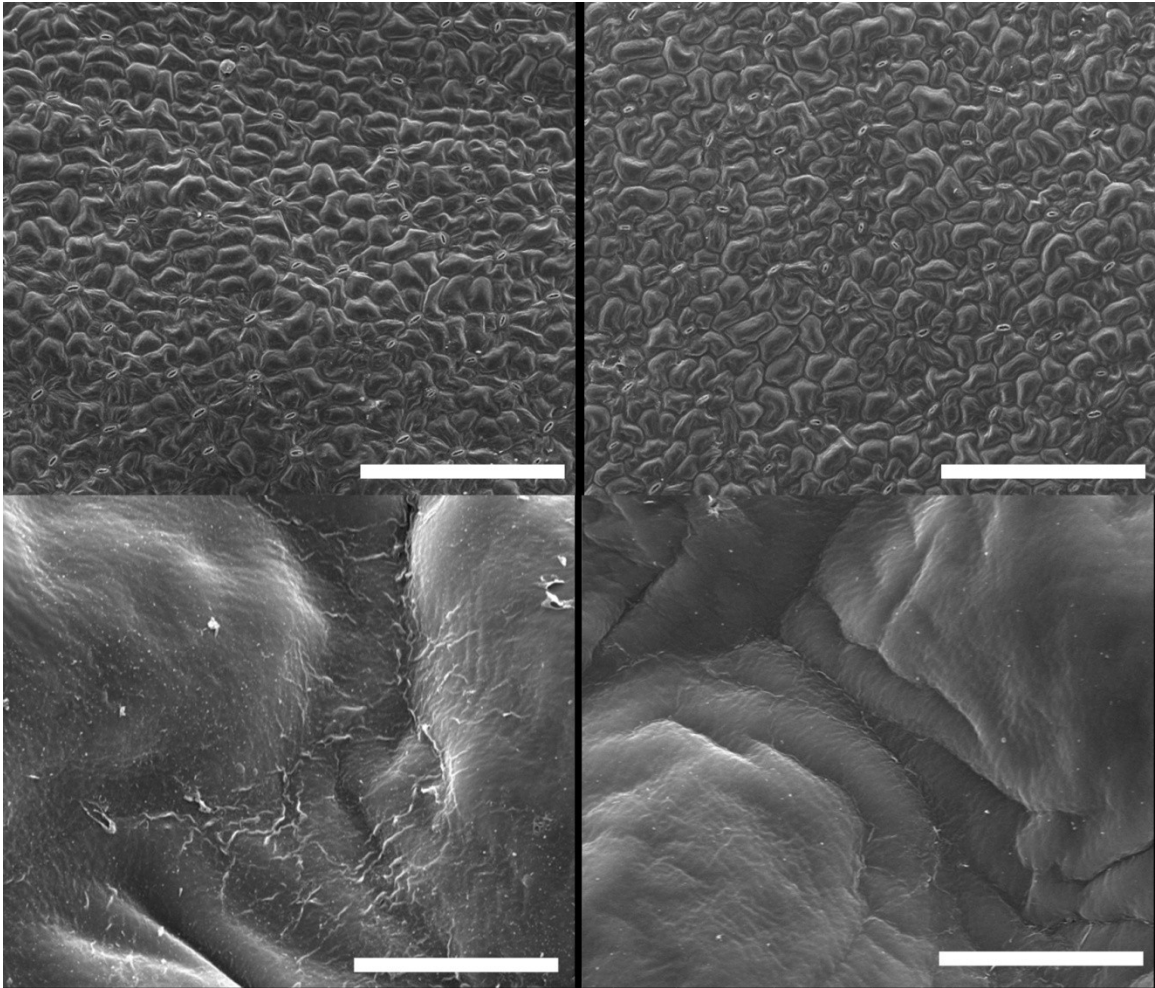


Figure 9. SEM images of FG (left images) and SG (right images) spinach leaf surface. Scale bar is 300  $\mu\text{m}$  in top images and 10  $\mu\text{m}$  in bottom images.

### FTIR-ATR spectra

For FTIR-ATR spectral measurements to be a viable indicator of cuticle wax thickness, attenuation at distinct wavelengths by the various leaf components in the leaf epidermal layer must be correlated to thickness. FTIR-ATR spectrum of a whole leaf (Figure 10, A) is a composite of the spectra of isolated epidermal components (Figure 10, B-E). Thickness of each of the isolated components is much greater than the penetration depth of the evanescent wave and thus these spectra represent attenuation by pure substances. An optical leaf model made up of layers of these pure components would not represent a real leaf because the boundaries between layers are not well differentiated. The cuticle membrane consists primarily of wax and cutin but

also has residual polysaccharides embedded within it. Furthermore, thicknesses of the various layers within the cuticle are not constant within the measurement window of an FTIR-ATR instrument.

Wax displayed strong attenuation at 2915 and 2850  $\text{cm}^{-1}$  (typical of C-C stretching) while other epidermal components had essentially no attenuation at those wavelengths. Water and cellulose both have broad absorbance bands centered at 3300  $\text{cm}^{-1}$  (O-H stretching), and 1632  $\text{cm}^{-1}$  (O-H absorption) due to high incidence of hydroxyl groups. Close examination shows that these bands are present, but much less pronounced, in wax and cutin which also contain a relatively small amount of hydroxyl groups. Cutin and cellulose showed interfering absorptive bands at 1000  $\text{cm}^{-1}$  (C-O stretching in cellulose) however at 900 to 950  $\text{cm}^{-1}$  cutin showed considerably more attenuation which concurs with the findings of Nuopponen et al. (2005). The whole leaf spectrum has the primary shape of water overlain by wax, polysaccharides and cutin.

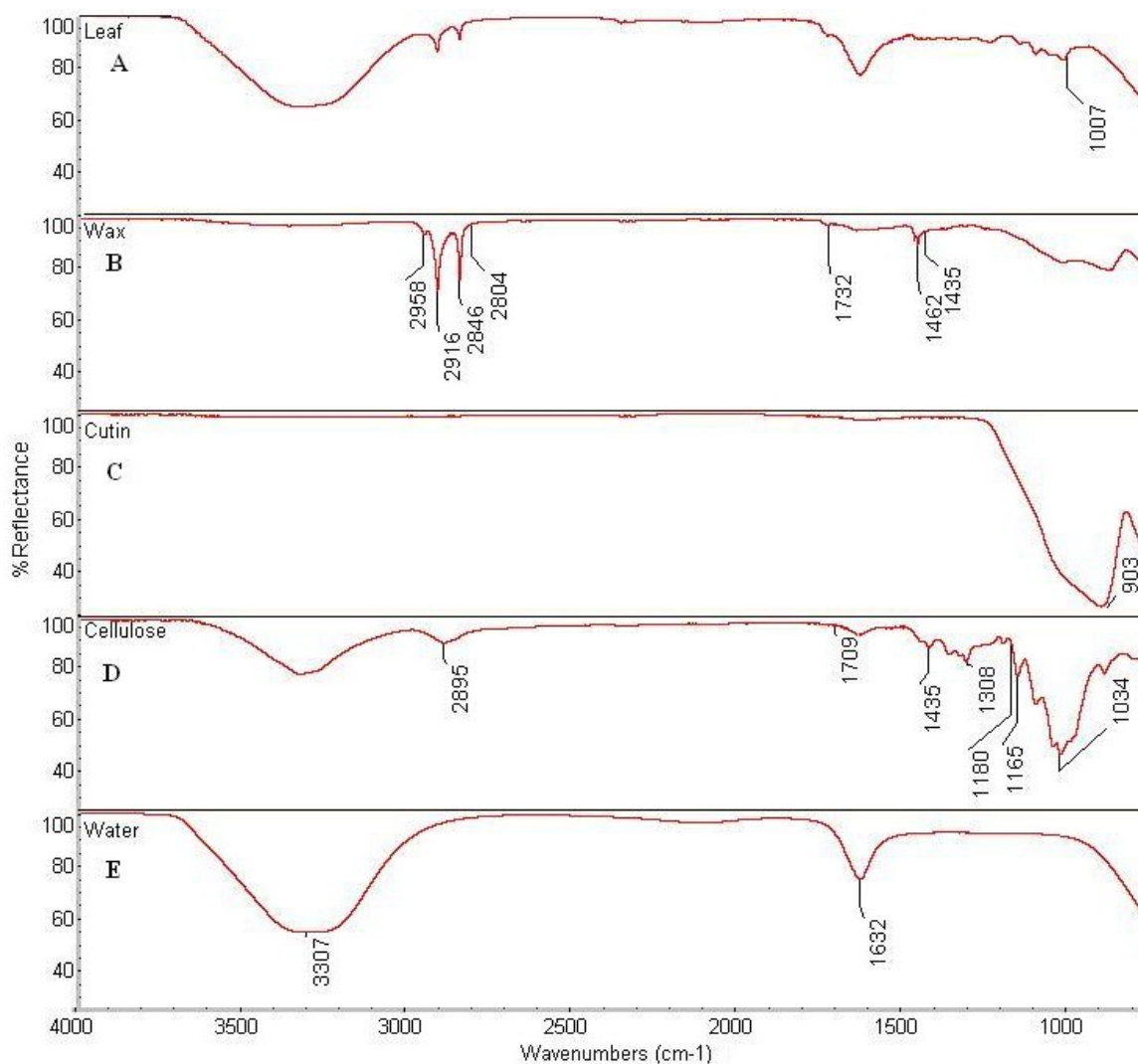


Figure 10. FTIR-ATR reflectance spectra of spinach: (A) leaf, (B) extracted cuticular wax, (C) dewaxed isolated cutin, (D) cellulose, and (E) water.

### Wax quantification on fresh leaves using FTIR-ATR

The first four eigenvectors (Figure 11) from PCA analysis accounted for 97.7% of the variation in the reflectance spectra while the first eigenvector accounted for 69% (Table 3). Twenty-four local maxima/minima values from the first four principal components were selected for regression analysis (Figure 11). As the number of predictor variables in the best linear model increased, the coefficient of multiple determination ( $R^2$ ) also increased (Figure 12). Models with four or more

predictor variables had values of  $R^2$  approaching 0.9. Based on this preliminary analysis, final models were limited to a maximum of five predictor frequencies.

Table 3. Principal component analysis results of training spectra of spinach. (N=28)

<u>Principal component</u>	<u>Eigenvalue</u>	<u>Proportion of variance</u>	<u>Cumulative</u>
1	252.78	69.3%	69.3%
2	77.27	21.2%	90.4%
3	18.71	5.1%	95.6%
4	7.70	2.1%	97.7%

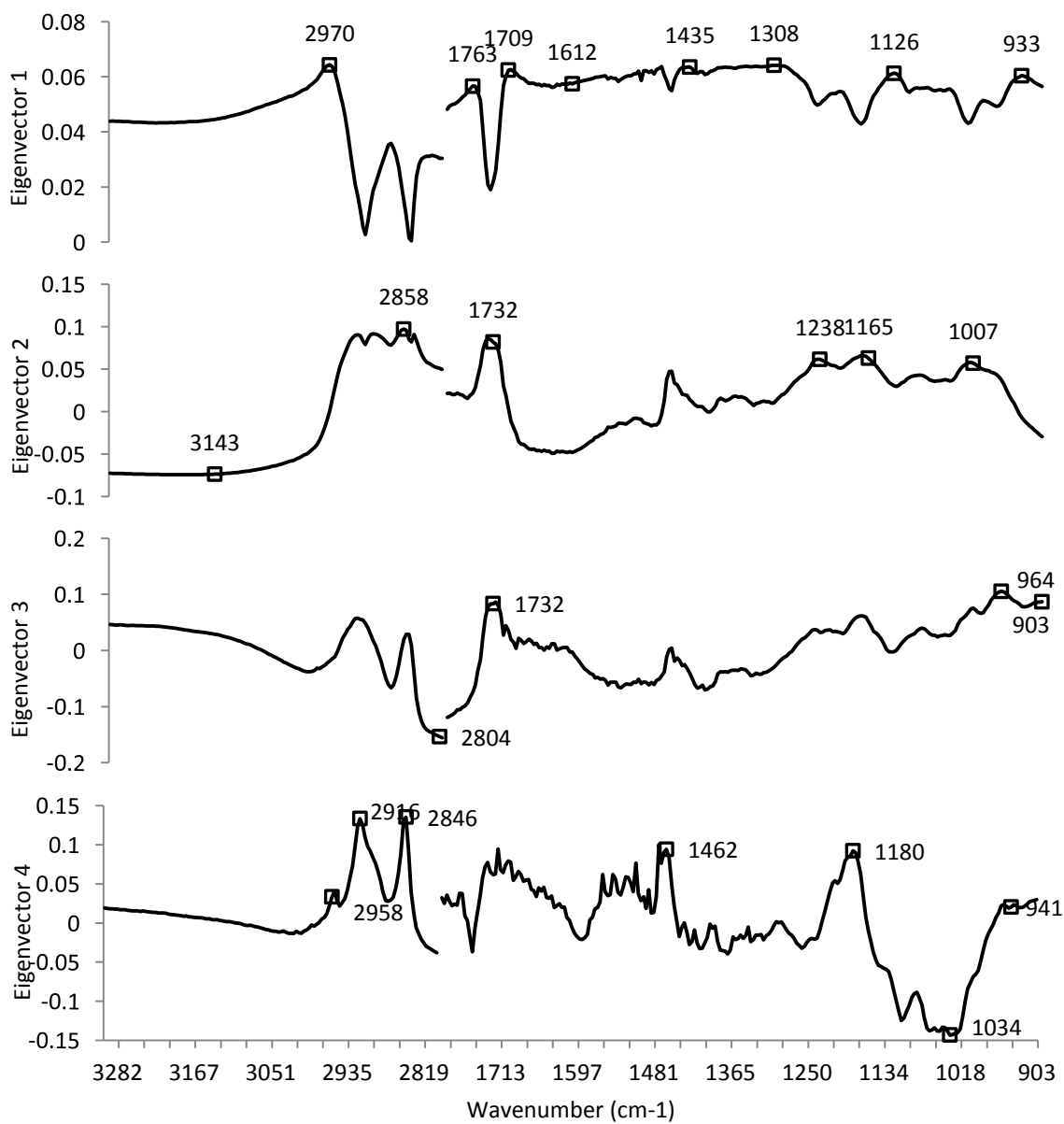


Figure 11. First four eigenvectors for 28 training spectra. Wavenumbers of frequencies selected for regression modeling are represented by  $\square$  on graph.

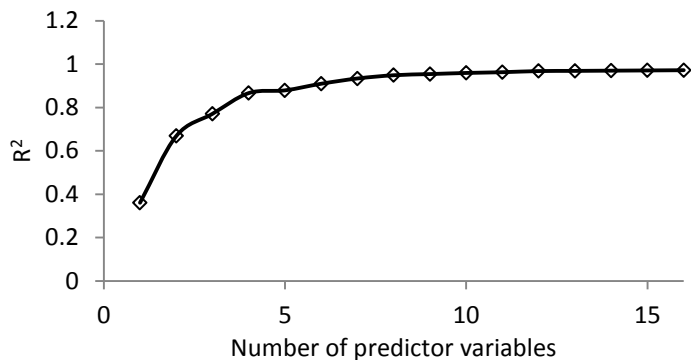


Figure 12. Effect of predictor variable quantity on coefficient of variation for the best fitting linear models.

Adjusted coefficient of multiple determination ( $R^2_A$ ) was used as the selection criteria for the final multiple linear regression models to mitigate the effects of over fitting. Examination of the top models reveals that specific wavenumbers were shared between various models. Most influential in most of the models was the  $2958\text{ cm}^{-1}$  waveband in combination with wavenumbers  $2916$  or  $2846\text{ cm}^{-1}$  (C-C stretching) attributable to waxes. Wavenumbers  $1709\text{ cm}^{-1}$  (C-O stretching) and  $1435\text{ cm}^{-1}$  are influenced by cell wall polysaccharides and cellulose. The best model with five predictor wavenumbers had an  $R^2$  of 0.879 (Table 4, model 1). In that model, wavenumber  $1007\text{ cm}^{-1}$  was not significant at  $\alpha=0.05$  ( $P=0.145$ ). The best model with four predictor variables (Table 4, model 11) contained the same wavenumbers as model one, except wavenumber  $1007\text{ cm}^{-1}$  was removed. This had minimal effect on model fit or on reducing RMSE of the training and validation sets (Table 4). Models 11 and 14, each with four variables, had RMSE of 0.51 and  $0.45\text{ }\mu\text{g cm}^{-2}$  respectively, the lowest of any of the models for the validation set although the differences between residuals of any two of the remaining models was not significant ( $P=0.0899$  to  $0.5474$ ). For model 11 the 95% confidence prediction interval varied across the range of wax loads in the training set from  $\pm 0.63$  to  $\pm 0.76\text{ }\mu\text{g cm}^{-2}$ . All but one of the 13 validation samples fell within the prediction interval of model 11 (Figure 14).

Table 4. Comparison of best linear regression models based on  $R^2_A$  for training, validation and field grown samples.

Model number	Number of predictor variables	$R^2$	$R^2_A$	Wax prediction RMSE ( $\mu\text{g cm}^{-2}$ )		
				Training set (n=28)	Validation set (n=13)	Field samples (n=8)
1	5	0.879	0.851	0.32	0.62	0.96
2	5	0.879	0.851	0.33	0.87	1.89
3	5	0.877	0.850	0.33	1.33	0.90
4	5	0.874	0.845	0.33	0.77	1.63
5	5	0.873	0.845	0.33	1.33	1.05
6	5	0.873	0.845	0.33	0.72	1.12
7	5	0.873	0.844	0.33	1.29	1.30
8	5	0.873	0.844	0.34	0.71	1.44
9	5	0.873	0.844	0.33	0.61	1.08
10	5	0.872	0.843	0.33	0.54	1.00
11	4	0.866	0.843	0.34	0.51	1.04
12	4	0.856	0.830	0.36	1.17	1.01
13	4	0.844	0.817	0.37	0.84	0.96
14	4	0.837	0.809	0.38	0.45	0.88

Model	Regression equation*
1	WAX=16.0273+2.1896(W2958)-0.4325(W2846)-0.8151(W1709)-1.2346(W1435)+0.1211(W1007)
2	WAX=12.7782+1.9594(W2958)-0.3914(W2846)+0.6569(W1732)-1.1145(W1435)-1.2599(W1180)
3	WAX=25.5174-0.4073(W3143)+3.1976(W2970)-1.5925(W2804)-1.0914(W1462)-0.3882(W1238)
4	WAX=20.7718+1.7959(W2958)-0.4031(W2846)+0.6574(W1732)-1.0456(W1308)-1.2479(W1180)
5	WAX=13.5418-0.3391(W3143)+3.2592(W2970)-1.3172(W2804)-1.1681(W1462)-0.5915(W1308)
6	WAX=-2.1426+2.6332(W2958)-0.3113(W2916)-1.2564(W1709)-1.5172(W1435)+0.4628(W941)
7	WAX=17.5658-0.3761(W3143)+3.0871(W2970)-1.4802(W2804)-1.2961(W1462)-0.1379(W1034)
8	WAX=23.5327-1.7722(W2970)+2.9333(W2958)-0.5659(W2846)+0.5685(W1732)-1.4430(W1165)
9	WAX=18.5074+2.0257(W2958)-0.4310(W2846)+0.0689(W1732)-0.7294(W1709)-1.1438(W1435)
10	WAX=17.5632+2.1804(W2958)-0.3999(W2846)-1.0064(W1709)-1.1388(W1435)+0.1743(W941)
11	WAX=15.1526+2.1661(W2958)-0.4065(W2846)-0.7407(W1709)-1.1933(W1435)
12	WAX=22.2144-0.3469(W3143)+2.7528(W2970)-1.3553(W2804)-1.2856(W1462)
13	WAX=8.08438-0.1001(W3143)+1.8798(W2958)-0.4992(W2846)-1.3970(W1435)
14	WAX=24.2537+1.900(W2958)-0.4059(W2846)-0.6940(W1709)-1.0798(W1308)

\*WAX in  $\mu\text{g cm}^{-2}$ , Wnnnn is the FTIR-ATR reflectance (0 to 1) at wavenumber nnnn  $\text{cm}^{-1}$ .

Several of the best performing models (Table 4, models 3, 5, 7, 12 and 13) included the  $3143 \text{ cm}^{-1}$  wavenumber. Response at this frequency is affected largely by water in the leaf (Figure 11E).

Models containing wavenumber  $3143 \text{ cm}^{-1}$  were rejected as predictors of wax load because the

amount of water within a leaf can change rapidly. Furthermore, those models resulted in poor predictions for the validation set. FTIR-ATR spectra of a wilted leaf compared to a fully hydrated leaf, showed much less absorption from water in the broad peak centered at  $3300\text{ cm}^{-1}$  (Figure 13). However, at  $1615$ ,  $1308$  and  $1020\text{ cm}^{-1}$ , absorption increased in the partially desiccated leaves, likely due to polysaccharide concentration increasing in the evanescent wave field. The effects of leaf desiccation and reduction of the water absorbance did not substantially change wax absorbance at  $2958$ ,  $2916$ ,  $2846$ ,  $1709$  and  $1435\text{ cm}^{-1}$ , wavenumbers contained in the best fitting models (Figure 13, Table 4).

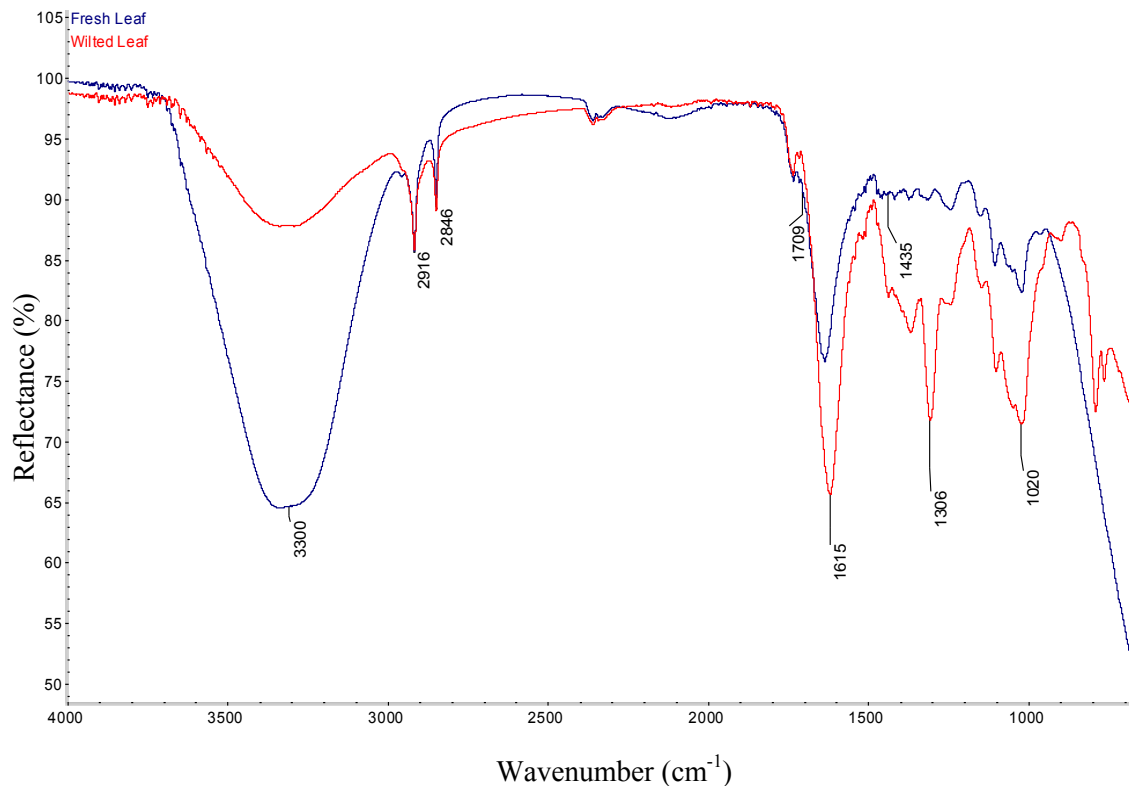


Figure 13. Typical FTIR-ATR spectra of fresh and wilted spinach leaves.

Multicollinearity is expected between wavenumbers in a spectral dataset even after pruning and regression steps to reduce the number of predictor variables. Pearson correlation coefficients (PCC) confirm significant multicollinearity between some of the variables in the best linear regression models (Table 5). An example of the effects of having variables with a high degree of

multicollinearity is illustrated in models 11 and 14. They have the same variables except that model 14 contains wavenumber 1308 which replaces 1435 in model 11 (Table 4). These two wavenumbers are highly correlated with a PCC of 0.99 (Table 5) and both models yield similar estimates of wax load. Wavenumbers 2916 and 2846 are both associated with C-C stretching in wax and are highly correlated ( PCC=0.98,  $p<0.001$ ). Models 6 and 10 are the same except for these wavenumbers and result in similar performance (Table 4). Wavenumber 2970 or 2958 appear in all models in Table 4 and are also highly correlated ( PCC=0.90,  $p<0.001$ ). Conversely, wavenumbers 2970 and 2958 are not significantly correlated ( $p>0.271$ ) to the wax wavenumbers of 2916 and 2846. One wavenumber from each of these two pairs appear in all models except for those that contain water wavenumber 3143 and are important to account for variation among the spectra (Table 4).

When the models for FG and SG spinach were applied to spectra of a different spinach cultivar grown under field conditions, wax prediction was poor and RMSE increased in all models except for several models that contained wavenumber 3143 (Table 4, Figure 14). This suggests that recalibration of the model will be necessary when evaluating different cultivars of plants. The FTIR-ATR spectral profiles of other plant species have a pattern similar to spinach leaves (Appendix B) indicating that the empirical methods used to construct models for measuring spinach wax could be applied to them. Some plants, such as certain varieties of apples and tomatoes have cuticles that may be too thick for accurate FTIR-ATR measurements of wax (Jeffrey 2006). These methods may also have application on dried and processed plant materials. In any case, recalibration or reformulation of the models would likely be required when applied to new applications.

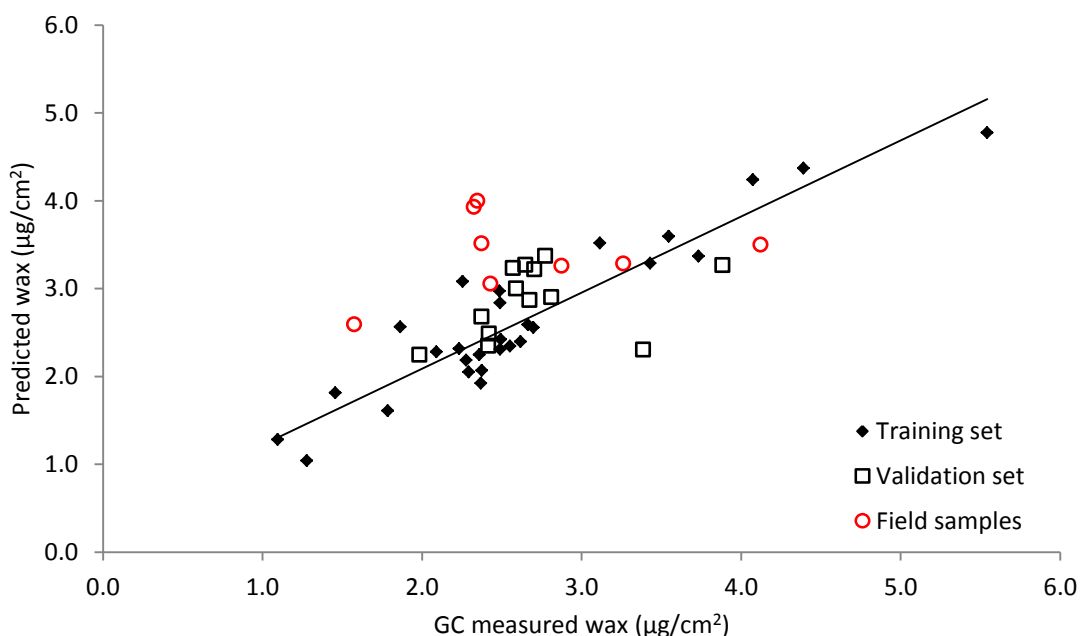


Figure 14. Comparison of cuticular wax measured by GC to predicted amount from FTIR-ATR using the model:  $WAX = 15.1526 + 2.1661(W2958) - 0.4065(W2846) - 0.7407(W1709) - 1.1933(W1435)$ .

Table 5. Pearson correlation coefficients for selected predictor variables in important wax prediction models. P values in parenthesis.

	WN2970	WN2916	WN2958	WN2846	WN1435	WN1308
WN2970	1	-0.19 -0.327	0.9 ( $<.001$ )	-0.21 -0.282	0.98 ( $<.001$ )	0.98 ( $<.001$ )
WN2916	-0.19 -0.327	1	0.22 -0.271	0.98 ( $<.001$ )	-0.06 -0.758	-0.1 -0.629
WN2958	0.9 ( $<.001$ )	0.22 -0.271	1	0.18 -0.356	0.93 ( $<.001$ )	0.91 ( $<.001$ )
WN2846	-0.21 -0.282	0.98 ( $<.001$ )	0.18 -0.356	1	-0.07 -0.72	-0.12 -0.556
WN1435	0.98 ( $<.001$ )	-0.06 -0.758	0.93 ( $<.001$ )	-0.07 -0.72	1	0.99 ( $<.001$ )
WN1308	0.98 ( $<.001$ )	-0.1 -0.629	0.91 ( $<.001$ )	-0.12 -0.556	0.99 ( $<.001$ )	1

### Wax quantification on dried spinach leaves using FTIR-ATR

The surface texture of dried leaves was rougher than fresh leaves. Surface texture after rehydration was in between the fresh and dried states (Figure 15). Initial leaf sample MC was 86.8 % wet basis (SD = 2.8%). After rehydration leaf MC was 54.4% (SD=7.8%). Rehydrated leaf sections covered 75.4% of their original area. The amount of shrinkage was similar in the longitudinal and transverse directions.



Figure 15. Typical leaf surface texture from left to right of fresh, dried at 50 °C for 24 h, and rehydrated spinach in water at 22 °C for 2 h. Images represent a 1.5 by 1.5 mm area.

The FTIR-ATR instrument used in these experiments has an active sampling area 1.5 mm in diameter. Roughness on the scale found on dried leaves (Figure 15, center) would cause non-uniform contact with the FTIR-ATR IRE. FTIR-ATR measurements on dried samples produced erratic results although it is unknown whether this was caused by non-uniform contact with the IRE due to surface roughness or by cracks in the leaves that resulted from stresses imparted by the sample holder, or both. Rehydration by immersing the dried leaves in water at 22 °C for 2 h produced consistent spectral scans although samples were subject to damage from clamping forces and measurements could not be repeated in the same area.

Cuticular wax amounts were calculated from FTIR-ATR spectra obtained from the same leaf in the fresh and rehydrated state using each of the models derived from regression analysis of

FTIR\_ATR spectra to GC results (Table 4). These models over predicted the amount of wax on the rehydrated leaves and there was considerable variation within the sample population (Table 6). This prediction trend was expected because after drying and rehydration the leaves shrunk to 75.4% (SD=4.4%) of their fresh size increasing the cuticle thickness. Performance improved when model predictions for rehydrated leaves were corrected to account for leaf area shrinkage (Table 6). Models 4 and 14 contained wavenumber  $1308\text{ cm}^{-1}$  and had poor correlations between fresh and rehydrated leaves with RMSE of 154.8% and 193.2% respectively. These models over predicted wax on rehydrated leaves by 64.6% (SD=41.0%) and 61.2% (SD=46.8%) respectively. It is unknown how this predictor frequency contributed to poor model performance on dried samples. Wavenumber 1308 is significant in the cellulose spectra (Figure 10) and attention at this frequency was much more apparent in wilted leaves than fully hydrated leaves (Figure 13). For the other models, error in wax predictions on rehydrated leaves after correcting for shrinkage ranged from 18.2% to 59.3% of fresh wax load. Model 11, previously identified as the best performing model with four predictor frequencies, resulted in RMSE of 41.9% for wax predictions of rehydrated leaves. Wax was over predicted by a mean of 24.3% (SD=26.9%). After correcting for shrinkage due to drying/rehydration RMSE was reduced to 23.8% and wax on rehydrated leaves was under predicted by 6.3% (SD=23.1%).

The differences in wax quantities predicted by the current models on fresh and rehydrated leaves are too large to recommend using FTIR-ATR as a method for in situ measurement of wax on dried spinach. The method may ultimately work if the models are recalibrated. This would require repeating the protocol used to produce the original models for fresh leaves, with modifications to the extraction procedures as needed to accommodate rehydrated leaves.

Table 6. Root mean square error and mean difference between fresh and rehydrated spinach leaf (n=48) cuticular wax load predicted by each of the 14 best performing models with 4 or 5 predictor frequencies. Rehydrated leaf cuticular wax predictions for corrected model output were multiplied by 75.4% to account for shrinkage due to drying/rehydration process.

Model	Uncorrected model			Corrected model		
	RMSE ( $\mu\text{g cm}^{-1}$ )	RMSE %	Mean difference %	RMSE ( $\mu\text{g cm}^{-1}$ )	RMSE %	Mean difference %
1	1.23	35.8%	21.9% (23.7%)	0.82	20.9%	-8.1% (20.1%)
2	2.37	60.4%	46.6% (27.6%)	1.12	28.4%	10.5% (23.6%)
3	1.12	35.7%	20.0% (22.5%)	0.82	21.4%	-9.6% (20.1%)
4	4.85	154.8%	118.4% (49.6%)	2.88	96.4%	64.6% (41.0%)
5	2.53	66.9%	51.8% (28.7%)	1.20	32.5%	14.4% (24.3%)
6	0.99	29.9%	1.9% (29.0%)	1.15	31.1%	23.2% (24.3%)
7	1.16	31.1%	15.0% (22.5%)	1.03	22.0%	-13.3% (12.0%)
8	1.83	95.4%	44.1% (36.7%)	1.09	59.3%	8.6% (33.2%)
9	1.42	43.2%	25.4% (26.7%)	0.91	24.1%	-5.5% (23.0%)
10	1.05	32.7%	15.8% (24.5%)	0.88	23.1%	-12.7% (20.9%)
11	1.33	41.9%	24.3% (26.9%)	0.87	23.8%	-6.3% (23.1%)
12	1.16	30.4%	19.3% (19.2%)	0.84	18.2%	-10.1% (17.0%)
13	2.06	60.6%	37.1% (33.5%)	1.18	33.0%	3.3% (28.7%)
14	3.80	193.2%	114.0% (56.6%)	2.30	128.6%	61.2% (46.8%)

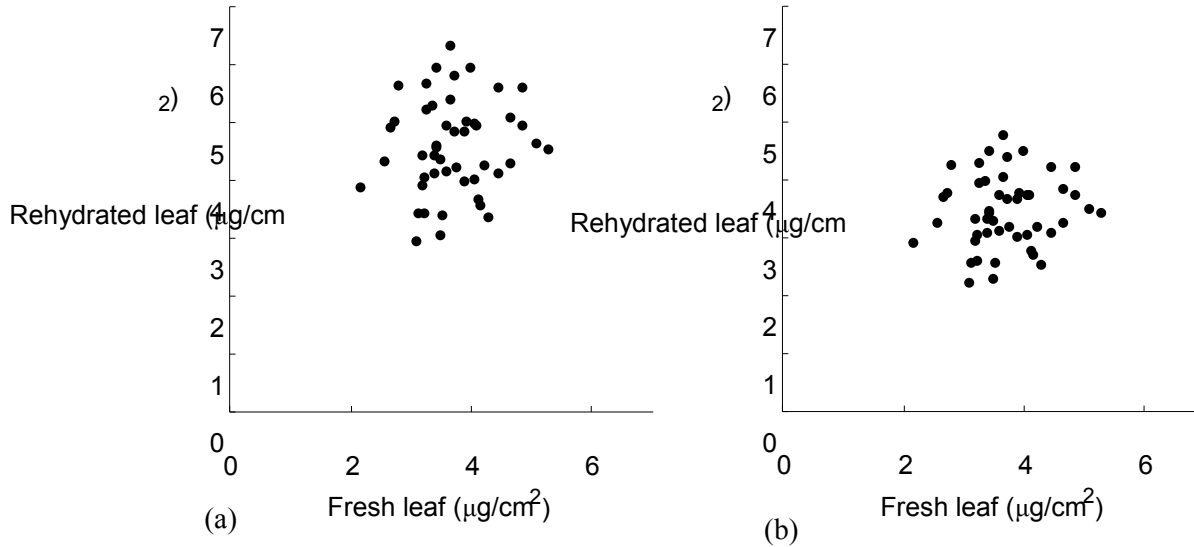


Figure 16. Comparison of wax predictions from model 11 on leaves (n=48) in the fresh and rehydrated state. Graphs represent uncorrected model output (a) and rehydrated leaf wax corrected for shrinkage (b).

## Wax quantification using DSC

The heat of fusion of extracted spinach cuticular wax was found to be  $88.8 \text{ uJ } \mu\text{g}^{-1}$  ( $n=3$ ,  $SE=2.0$ ) over a broad temperature range of 40 to 73 °C (Figure 17). DSC of leaf material remaining after chloroform extraction of SCLs showed no phase transitions over this same temperature range indicating other components within the leaf did not overlap with the cuticular wax transition. Wax quantity was calculated from the integrated heat flow between 40 and 73 °C on dried leaf samples (Figure 18).

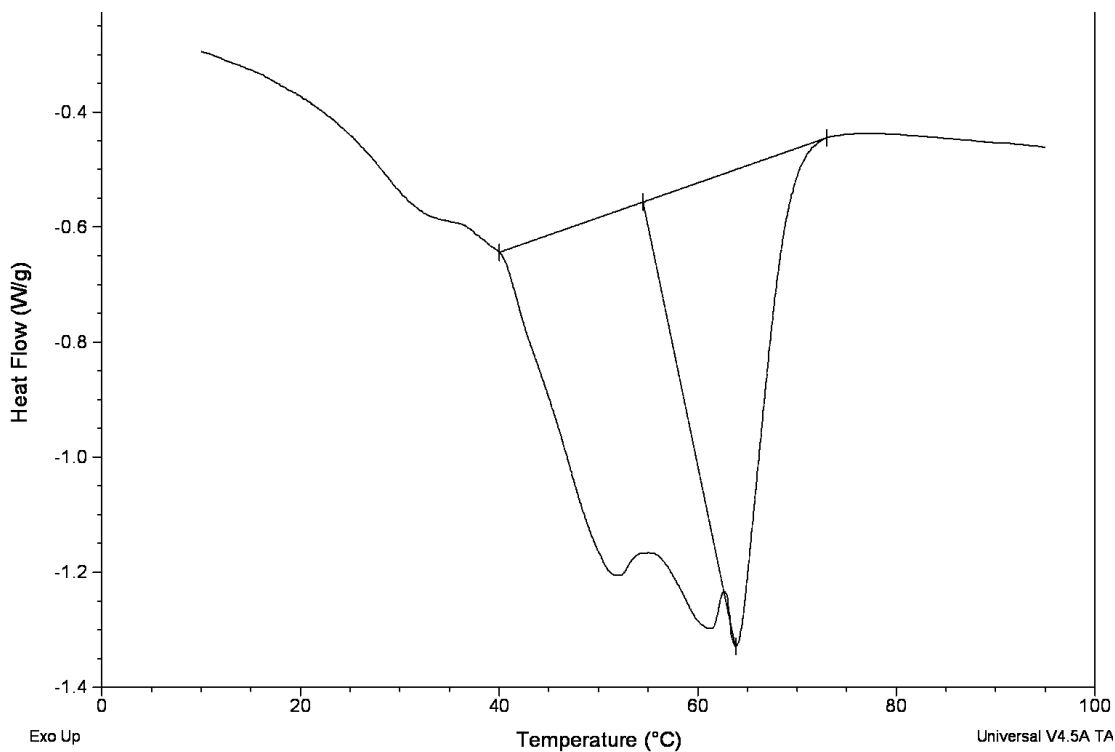


Figure 17. Representative differential scanning calorimetry thermalgram of spinach cuticular wax.

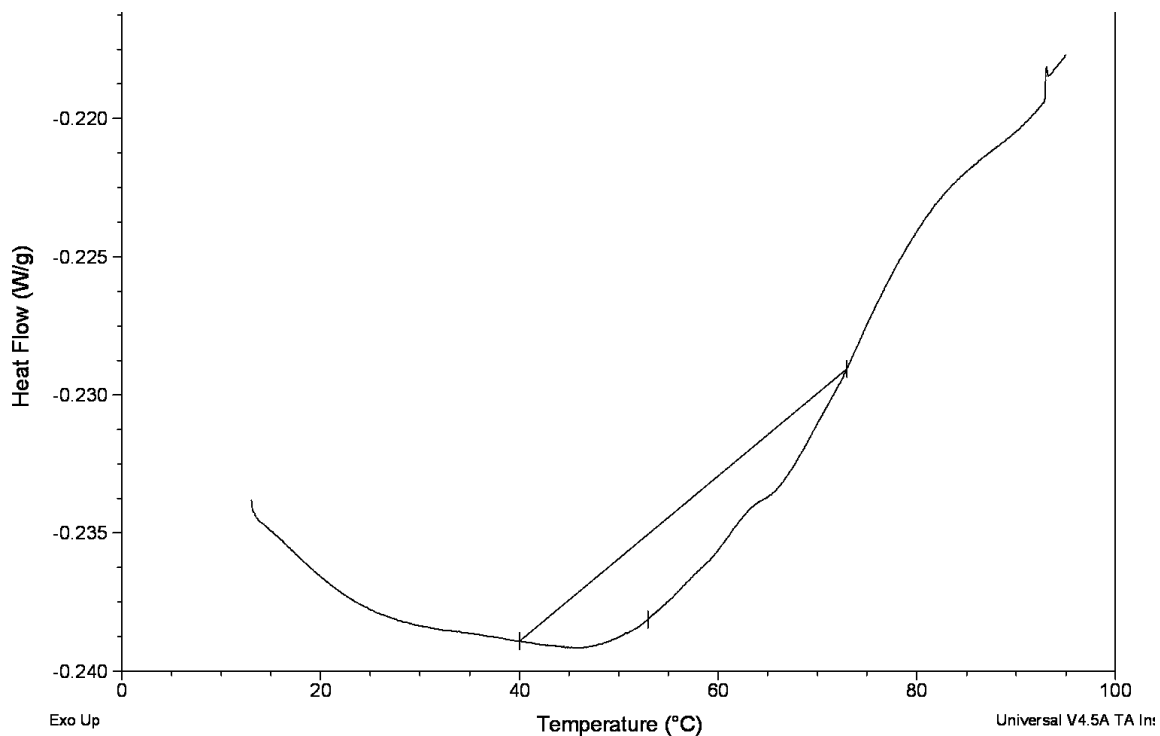


Figure 18. Typical DSC thermalgram of leaf sample showing peak area measured between 40 and 73 °C.

The correlation of DSC to GC measured wax quantity was poor (Figure 19). Two groupings of data are evident on Figure 19. The bottom group of eight points correlates to the GC measurements to some extent. Linear regression of only those eight points results in an  $R^2$  of 0.31 and overestimated wax content by 34% compared to the GC measurement. No justification for eliminating specific outliers from the results could be identified.

The calculation used to determine wax transition energy assumed a flat baseline in the thermalgram (Figure 18). It was assumed that an empirically determined baseline correction would be needed to compensate for leaf dry matter effects and to calibrate the model to match GC results. Given the scattered nature of the DSC data compared to GC measurements that process is not justified. The DSC results of several leaf samples were discarded because integrating the peak area of the thermalgram using a linear or sigmoidal baseline was not possible due to the shape of the heat flux trace. Another suspected problem with the protocol was maintaining

consistent thermal conductance from the leaf material to the crucible for all samples. Lower heat flux rates on process verification samples did not mitigate the problem.

Quantifying cuticular wax in situ using DSC was initially proposed with a low confidence of success because the amount of wax on a leaf is only about 0.1% of mass on a dry basis. This is approaching the sensitivity limit of laboratory instruments. Furthermore this measurement procedure requires drying discs removed from leaves and is not as fast of FTIR-ATR or GC methods.

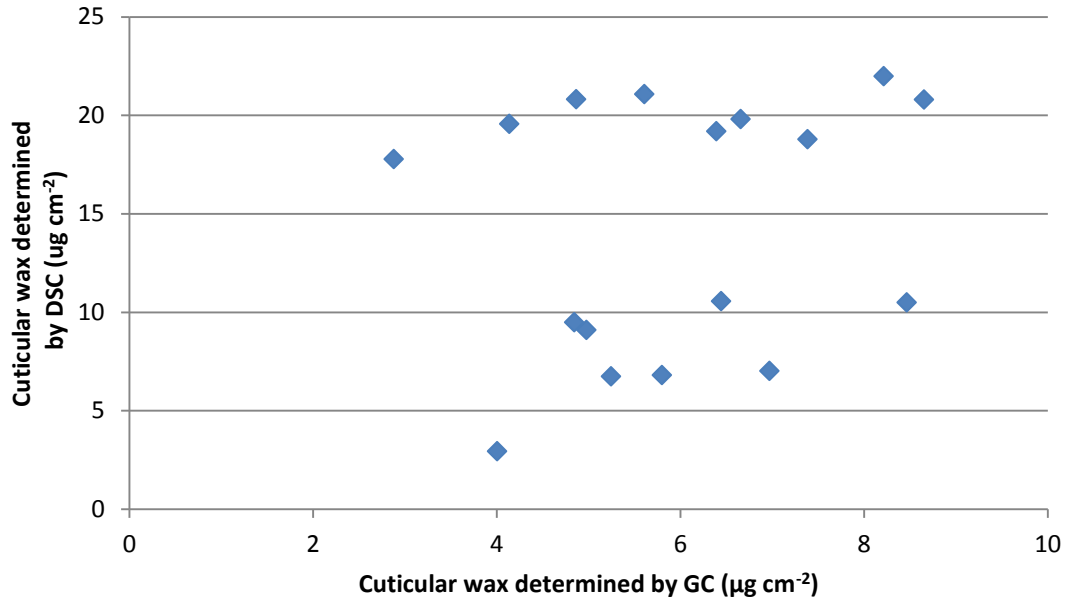


Figure 19. Comparison of spinach cuticular wax determined by GC and DSC. (N=17)

### Conclusion

FTIR-ATR shows promise as a method for rapid in situ measurement of cuticular waxes on leaves. Empirically derived linear regression models for spinach leaves using FTIR-ATR spectral responses correlated well with GC measurements of extracted cuticular waxes ( $R^2 > 0.86$ ). The model development technique presented can be used to extend this measurement method to other plant cultivars, organs and species. Portable and ruggedized FTIR-ATR instruments are

currently available and would allow for infield measurements. A purpose-built ATR sensor that analyzes several infrared frequencies specific to cuticular measurements would be a significant, but achievable, engineering design challenge.

Two methods were investigated for quantifying cuticular wax on dried leaf samples. The first used the regression models developed for fresh leaves on rehydrated dried leaves. After correcting for leaf shrinkage, FTIR-ATR on rehydrated leaves produced results with RMSE of wax load from 18.2% to 59.3% compared to fresh leaf measurements. Model 11, previously identified as the best performing model with four predictor frequencies, resulted in RMSE of 23.8% for wax predictions of rehydrated leaves. This model under predicted wax on rehydrated leaves by an average of 6.3% (SD=23.1%). Recalibration of the regression models specifically for rehydrated leaves may yield acceptable wax predictions. DSC experiments produced erratic results. The cuticular wax content of spinach leaves is approximately 0.1% of dry leaf mass. This is too low to overcome the confounding thermal transitions of other leaf materials. A new approach to DSC measurements of cuticular waxes is required.

## References

- Bargel, H., K. Koch, Z. Cerman, and C. Neinhuis. 2006. Structure-function relationships of the plant cuticle and cuticular waxes - a smart material? *Functional Plant Biology* 33 (10): 893-910.
- Bauer, S., E. Schulte, and H.-P. Thier. 2004. Composition of the surface wax from tomatoes: II. Quantification of the components at the ripe red stage and during ripening. *European Food Research and Technology A* 219: 487-491.
- Buschhaus, C., H. Herz, and R. Jetter. 2007. Chemical Composition of the Epicuticular and Intracuticular Wax Layers on Adaxial Sides of *Rosa canina* Leaves. *Ann Bot* 100 (7): 1557-1564.
- Calvert, J. G., R. G. Derwent, J. J. Orlando, G. S. Tyndall, and T. J. Wallington. 2008. *Mechanisms of Atmospheric Oxidation of the Alkanes* Oxford University Press.
- Casado, C. G., and A. Heredia. 2001. Specific heat determination of plant barrier lipophilic components: biological implications. *Biochimica et Biophysica Acta (BBA) - Biomembranes* 1511 (2): 291-296.
- Coret, J., and A. Chamel. 1994. Effect of some ethoxylated alkylphenols and ethoxylated alcohols on the transfer of [<sup>14</sup>C] chlorotoluron across isolated plant cuticles. *Weed Research* 34 (6): 445-451.
- Dubis, E. N., A. T. Dubis, and J. W. Morzycki. 1999. Comparative analysis of plant cuticular waxes using HATR FT-IR reflection technique. *Journal of Molecular Structure* 511-512: 173-179.

- Edelmann, H., C. Neinhuis, and H. Bargel. 2005. Influence of Hydration and Temperature on the Rheological Properties of Plant Cuticles and Their Impact on Plant Organ Integrity. *Journal of Plant Growth Regulation* 24 (2): 116-126.
- Els, A. V., L. Jeroen, M. N. Bart, and I. Joseph. 2003. Spectroscopic Evaluation of the Surface Quality of Apple.
- Franke, R., I. Briesen, T. Wojciechowski, A. Faust, A. Yephremov, C. Nawrath, and L. Schreiber. 2005. Apoplastic polyesters in Arabidopsis surface tissues - A typical suberin and a particular cutin. *Phytochemistry* 66 (22): 2643-2658.
- Gibbs, A., and J. G. Pomonis. 1995. Physical properties of insect cuticular hydrocarbons: The effects of chain length, methyl-branching and unsaturation. *Comparative Biochemistry and Physiology Part B: Biochemistry and Molecular Biology* 112 (2): 243-249.
- Greene, P. R., and C. D. Bain. 2005. Total internal reflection Raman spectroscopy of barley leaf epicuticular waxes in vivo. *Colloids and Surfaces B: Biointerfaces* 45 (3-4): 174-180.
- Hohne, G. W. H., W. F. Hemminger, and H. J. Flammersheim. 2003. *Differential Scanning Calorimetry*. 2nd ed. Berlin: Springer-Verlag.
- Holloway, P. J. 1974. Intracuticular lipids of spinach leaves. *Phytochemistry* 13 (10): 2201-2207.
- Holloway, P. J., G. A. Brown, and J. Wattendorff. 1981. Ultrahistochemical Detection of Epoxides in Plant Cuticular Membranes. *J. Exp. Bot.* 32 (5): 1051-1066.
- Islam, M., H. Du, J. Ning, H. Ye, and L. Xiong. 2009. Characterization of Glossyl-homologous genes in rice involved in leaf wax accumulation and drought resistance. *Plant Molecular Biology* 70 (4): 443-456.

- Ivanova, D. G., and B. R. Singh. 2003. Nondestructive FTIR monitoring of leaf senescence and elicitin-induced changes in plant leaves. *Biopolymers* 72 (2): 79-85.
- Jeffree, C. E. 1984. The cuticle, epicuticular waxes and trichomes of plants, with reference to their structure, functions and evolution. In *Insects and plant surfaces*, edited by B. E. Juniper and T. R. E. Southwood. London: Edward Arnold.
- Jeffree, C. E. 2006. The fine structure of the plant cuticle. In *Biology of the plant cuticle*, edited by M. Riederer and C. Muller. Oxford: Blackwell Publishing.
- Jenks, M. A., H. A. Tuttle, S. D. Eigenbrode, and K. A. Feldmann. 1995. Leaf Epicuticular Waxes of the Eceriferum Mutants in Arabidopsis. *Plant Physiol.* 108 (1): 369-377.
- Jetter, R., M. Riederer, and K. J. Lenzian. 1996. The effects of dry O<sub>3</sub>, SO<sub>2</sub> and NO<sub>2</sub> on reconstituted epicuticular wax tubules. *New Phytologist* 133 (2): 207-216.
- Jetter, R., and S. Schaffer. 2001. Chemical Composition of the Prunus laurocerasus Leaf Surface. Dynamic Changes of the Epicuticular Wax Film during Leaf Development. *Plant Physiol.* 126 (4): 1725-1737.
- Jetter, R., S. Schäffer, and M. Riederer. 2000. Leaf cuticular waxes are arranged in chemically and mechanically distinct layers: evidence from *Prunus laurocerasus* L. *Plant, Cell & Environment* 23 (6): 619-628.
- Jetter, R., and R. Sodhi. 2010. Chemical composition and microstructure of waxy plant surfaces: triterpenoids and fatty acid derivatives on leaves of *Kalanchoe daigremontiana*. *Surface and Interface Analysis* 9999 (9999): n/a.

- Kacuráková, M., P. Capek, V. Sasinková, N. Wellner, and A. Ebringerová. 2000. FT-IR study of plant cell wall model compounds: pectic polysaccharides and hemicelluloses. *Carbohydrate Polymers* 43 (2): 195-203.
- Kane, S. R., P. D. Ashby, and L. A. Pruitt. 2009. ATR-FTIR as a thickness measurement technique for hydrated polymer-on-polymer coatings. *Journal of Biomedical Materials Research Part B: Applied Biomaterials* 91B (2): 613-620.
- Kosma, D. K., B. Bourdenx, A. Bernard, E. P. Parsons, S. Lu, J. Joubes, and M. A. Jenks. 2009. The Impact of Water Deficiency on Leaf Cuticle Lipids of Arabidopsis. *Plant Physiol.* 151 (4): 1918-1929.
- Kunst, L., A. L. Samuels, and R. Jetter. 2005. The plant cuticle: formation and structure of epidermal surfaces. In *Plant lipids*, edited by D. J. Murphy. Oxford: Blackwell Publishing.
- Lopez-Casado, G., A. J. Matas, E. Dominguez, J. Cuartero, and A. Heredia. 2007. Biomechanics of isolated tomato (*Solanum lycopersicum* L.) fruit cuticles: the role of the cutin matrix and polysaccharides. *J. Exp. Bot.* 58 (14): 3875-3883.
- Lu, H.-F., J.-B. Shen, X.-Y. Lin, and J.-L. Fu. 2008. Relevance of Fourier transform infrared spectroscopy and leaf anatomy for species classification in *Camellia* (Theaceae). *Taxon* 57: 1274-1278E.
- Matas, A. J., J. Cuartero, and A. Heredia. 2004. Phase transitions in the biopolyester cutin isolated from tomato fruit cuticles. *Thermochimica Acta* 409 (2): 165-168.
- Merk, S., A. Blume, and M. Riederer. 1997. Phase behaviour and crystallinity of plant cuticular waxes studied by Fourier transform infrared spectroscopy. *Planta* 204 (1): 44-53.

- Muller, G., and K. Abraham-Fuchs. 1993. Matrix Dependence in single and multilayer IRS spectra. In *Internal Reflection Spectroscopy: Theory and Applications*, edited by F. M. Mirabella. New York: Marcel Dekker.
- Nass, R., C. Markstädter, V. Hauke, and M. Riederer. 1998. Quantitative gas chromatographic analysis of plant cuticular waxes containing long-chain aldehydes. *Phytochemical Analysis* 9 (3): 112-118.
- Nuopponen, M. H., G. M. Birch, R. J. Sykes, S. J. Lee, and D. Stewart. 2005. Estimation of Wood Density and Chemical Composition by Means of Diffuse Reflectance Mid-Infrared Fourier Transform (DRIFT-MIR) Spectroscopy. *Journal of Agricultural and Food Chemistry* 54 (1): 34-40.
- Orgell, W. H. 1955. The Isolation of Plant Cuticle with Pectic Enzymes. *Plant Physiology* 30 (1): 78-80.
- Percy, K. E., S. Manninen, K.-H. Häberle, C. Heerdt, H. Werner, G. W. Henderson, and R. Matyssek. 2009. Effect of 3 years' free-air exposure to elevated ozone on mature Norway spruce (*Picea abies* (L.) Karst.) needle epicuticular wax physicochemical characteristics. *Environmental Pollution* 157 (5): 1657-1665.
- Perkins, M. C., C. J. Roberts, D. Briggs, M. C. Davies, A. Friedmann, C. Hart, and G. Bell. 2005. Macro and microthermal analysis of plant wax/surfactant interactions: plasticizing effects of two alcohol ethoxylated surfactants on an isolated cuticular wax and leaf model. *Applied Surface Science* 243 (1-4): 158-165.
- Peschel, S., R. Franke, L. Schreiber, and M. Knoche. 2007. Composition of the cuticle of developing sweet cherry fruit. *Phytochemistry* 68 (7): 1017-1025.

- Petracek, P. D., and M. J. Bukovac. 1995. Rheological Properties of Enzymatically Isolated Tomato Fruit Cuticle. *Plant Physiol.* 109 (2): 675-679.
- Rashotte, A., M. Jenks, A. Ross, and K. Feldmann. 2004. Novel eceriferum mutants in *Arabidopsis thaliana*. *Planta* 219 (1): 5-13.
- Reynhardt, E. C., and M. Riederer. 1991. Structure and molecular dynamics of the cuticular wax from leaves of *Citrus aurantium* L. *Journal of Physics D: Applied Physics* 24 (3): 478.
- Rezvani, M. P., and D. Wilman. 1998. Cell wall thickness and cell dimensions in plant parts of eight forage species. *The Journal of Agricultural Science* 131 (01): 59-67.
- Ribeiro da Luz, B. 2006. Attenuated total reflectance spectroscopy of plant leaves: a tool for ecological and botanical studies. *New Phytologist* 172 (2): 305-318.
- Riedel, M., A. Eichner, and R. Jetter. 2003. Slippery surfaces of carnivorous plants: composition of epicuticular wax crystals in *Nepenthes alata* Blanco pitchers. *Planta* 218 (1): 87-97.
- Riederer, M., and L. Schreiber. 2001. Protecting against water loss: analysis of the barrier properties of plant cuticles. *Journal of Experimental Botany* 52 (363): 2023-2032.
- Ristic, Z., and M. A. Jenks. 2002. Leaf cuticle and water loss in maize lines differing in dehydration avoidance. *Journal of Plant Physiology* 159 (6): 645-651.
- Samuels, L., L. Kunst, and R. Jetter. 2008. Sealing plant surfaces: Cuticular wax formation by epidermal cells. *Annual Review of Plant Biology* 59: 683-707.
- SAS Institute Inc. 2004. *SAS/STAT 9.1 User's Guide*. Cary, NC, USA: SAS Institute Inc.
- Schreiber, L., and J. Schönherr. 2009. *Water and Solute Permeability of Plant Cuticles* Berlin: Springer-Verlag

- Stork, N. E. 1980. Role of waxblooms in preventing attachment to brassicas by the mustard beetle, &lt;i>Phaedon cochleariae&lt;/i>. *Entomologia Experimentalis Et Applicata* 28 (1): 100-107.
- Stuchebyukov, S. D., and V. M. Rudoy. 1992. Quantitative approach to the sample contact problem in attenuated total reflection spectroscopy: Theoretical considerations. *Vibrational Spectroscopy* 4 (1): 95-104.
- Turakhozhaev, M., M. Khodzhaeva, N. Burkhanova, S. Yugai, and M. Yunusov. 1997. Structure and properties of apple pectin. *Chemistry of Natural Compounds* 33 (6): 620-623.
- Uppalapati, S. R., Y. Ishiga, V. Doraiswamy, M. Bedai, S. Mittal, J. Chen, J. Nakashima, Y. Tang, M. Tadege, P. Ratet, R. Chen, H. Schultheiss, and K. S. Mysore. 2012. Loss of Abaxial Leaf Epicuticular Wax in *Medicago truncatula* irg1/palm1 Mutants Results in Reduced Spore Differentiation of Anthracnose and Nonhost Rust Pathogens. *Plant Cell* 24 (1): 353-370.
- Wilson, R. H., A. C. Smith, M. Kacurakova, P. K. Saunders, N. Wellner, and K. W. Waldron. 2000. The Mechanical Properties and Molecular Dynamics of Plant Cell Wall Polysaccharides Studied by Fourier-Transform Infrared Spectroscopy. *Plant Physiol.* 124 (1): 397-406.
- Yang, P., X. Meng, Z. Zhang, B. Jing, J. Yuan, and W. Yang. 2005. Thickness Measurement of Nanoscale Polymer Layer on Polymer Substrates by Attenuated Total Reflection Infrared Spectroscopy. *Analytical Chemistry* 77 (4): 1068-1074.
- Ye, X., K. Sakai, S.-i. Asada, and A. Sasao. 2008. Application of narrow-band TBVI in estimating fruit yield in citrus. *Biosystems Engineering* 99 (2): 179-189.

Zhang, J.-Y., C. Broeckling, L. Sumner, and Z.-Y. Wang. 2007. Heterologous expression of two *Medicago truncatula* putative ERF transcription factor genes, WXP1 and WXP2, in *Arabidopsis* led to increased leaf wax accumulation and improved drought tolerance, but differential response in freezing tolerance. *Plant Molecular Biology* 64 (3): 265-278.

## CHAPTER III

### ESTIMATION OF PECAN YIELD USING TERRESTRIAL MICROWAVE SENSING

Abstract: Accurate estimates of pecans [*Carya illinoensis* (Wang.) K. Koch] in an orchard prior to harvest are critically important for marketing and production management decisions such as nut thinning, irrigating and nutrition supplementing. Current methods of estimating pecan yield in situ are not sufficiently accurate and are time consuming. Research using satellite based microwave imaging has enabled scientists to identify trends in orchard crop condition but precision is inadequate for yield sensing. Ground based radar schemes using antenna within the orchard resolve many of the power, resolution and sensitivity limitations of satellite radar imagery. The objective of this research is to determine if pecan nuts can be quantified in situ using backscattered microwaves from antenna located in the orchard. Pecan tree canopy samples (leaves and secondary branches) and nuts were collected at five growth stages (water stage through shuck split) and placed in a polystyrene foam test fixture located between horn antennae spaced 1 m apart. Reflection and transmission measurements were recorded with a vector network analyzer at frequencies from 1 to 18 GHz while the amount of nuts were varied from 0 to approximately 30% of the canopy mass. Regression analysis revealed no specific frequencies to quantify nut mass however response to total canopy water and dry mass over a wide range of frequencies had  $R^2 > 0.63$  and 0.78 respectively. This relationship combined with range finding and appropriate crop model algorithms may ultimately be the basis used to developing pecan yield monitoring technology. Furthermore, if successful in pecans, the technology has potential for extension to other orchard fruit and nut crops.

## Introduction

Pecans [*Carya illinoensis* (Wang.) K. Koch] are an economically important nut crop grown commercially across 13 states in the USA. Annual production in 2011 was 122.8M kg with a commercial value of \$683M. Exports of inshell and shelled pecans totaled \$192.8M. Production and exports of pecan have both seen significant increases in recent years. Over 80% of the world's pecans are produced in the United States (Geisler 2012).

Accurate estimates of pecans in an orchard prior to harvest are critically important for both production management decisions and marketing. Under normal conditions pecan trees exhibit alternate bearing where they produce nuts heavily one year followed by a smaller crop the next (Conner and Worley 2000). The mechanisms causing alternate bearing are complex and are an area of active research. Recommended practices to reduce alternate bearing include fruit thinning, timed fertilizer applications, pruning and other cultural practices (McCraw et al. 2007). Accurate, in situ measurement of crop load is important for these and other management decisions such as irrigation and pest control measures. Pecan producers, processors and marketers have identified control of alternate bearing and improved accuracy of crop estimates as primary research priorities for the industry (Weckler and Smith 2011).

Current methods of estimating pecan yield in situ include empirically derived formulas and sampling techniques where a subset of nuts are visually counted in the orchard (Wright et al. 1990). These methods are not sufficiently accurate nor do they provide cost effective yield information on a per tree basis that is needed for precision agriculture applications. Technological innovations to improve the accuracy and/or speed of infield pecan estimates will have direct benefit to producers, processors and marketers. Precision agricultural practices, including in situ yield estimates, have been applied successfully to a variety of field crops and pecans represent a

similar opportunity (Lee et al. 2010). Furthermore, if successful in pecans, the technology has potential for extension to other orchard fruit and nut crops.

### Existing remote sensing technologies for estimating pecan yield in situ

Remote sensing from satellites and airplanes to estimate yield of agricultural crops has been applied to many different commodities using a wide range of the visible, IR and microwave spectrum. Applications of remote sensing in both the visible and microwave regions of the electromagnetic spectrum have been successfully demonstrated for field crops such as corn, rice, soybeans and wheat (Bouvet et al. 2009; McNairn et al. 2009; Shao et al. 2001). Plots of these crops appear homogeneous at resolutions detectable by current sensors. Crop type, condition and yield data can be inferred by correlating the reflected electromagnetic energy to ground truth data. Forests and orchards are more heterogeneous and estimating tree crop condition and yields using satellite remote sensing has had limited success to date.

Recent research using satellite based optical imaging has enabled scientists to identify trends in orchard crop yield but precision is inadequate. Ye et al. (2008) used 1.2 m resolution hyperspectral vis-NIR data to estimate citrus yield and found that the best model performance accounted for less than 75% of actual variation in the citrus crop. In a study on Pistachio, Moazenpour et al. (2006) showed that satellite data was inadequate for yield prediction. Even when satellite data was combined with other orchard data (soil, cultivar and management practices) only marginally accurate estimates of yield resulted. Both of these studies used statistical analysis to develop models that predict yield using optical spectral response of the overall tree in combination with other non-sensed variables. Vis-NIR electromagnetic energy does not penetrate effectively through leafy tree canopies, thus the image data is not directly influenced by fruits that are often fully or partially hidden from the field of view.

Microwaves have longer wavelengths (1 cm to 1 m) than vis-NIR radiation so they can penetrate vegetation more effectively and thus may be more appropriate for yield monitoring of pecan. Microwaves have an advantage over vis-NIR imaging in that they are able to penetrate clouds that would obscure optical wavelengths. By definition, remote sensing is concerned with reflected or backscattered energy. For biological materials, backscattered microwaves are largely dependent on the frequency and polarization of the incident signal and on the geometry and dielectric properties of the target. Geometric properties such as surface roughness and orientation effect whether reflections are specular or diffuse. Vegetation usually returns diffuse reflections to remote sensors due to the generally random orientation of leaves. However, plants are often arranged with underlying patterns, such as vertical stalks in grains or upward facing leaves that reflect certain orientations of electromagnetic waves more strongly (Bouvet et al. 2009). If incident energy is polarized, the intensity of resulting reflections can be either enhanced or reduced providing useful information about the target. Similarly, plant structural orientation can result in polarized energy reflecting from a non-polarized source.

Satellite based radar images of vegetation consist of a composite of backscattered electromagnetic energy. Some energy is directly reflected back to the receiver by leaves, stalks/stems or soil while a portion undergoes multiple reflections before returning. Early investigations of crops by backscattered microwaves used models that assumed the vegetative layer was a cloud of absorbing material over the soil surface (Ulaby et al. 1984). Performance of vegetation canopy models of field crops have been improved by differentiating between leaf and stem layers (Paris 1986).

Researchers have been able to identify and provide estimates of corn crop acreage and their condition at a field scale by analyzing backscattered satellite radar imagery (McNairn et al. 2009; Soria-Ruiz et al. 2007). In these approaches, more comprehensive crop information such as yield

estimation is inferred from measured parameters. For example, taller stands of corn generally correlate to better plant condition and thus higher yields. The actual kernel content does not significantly affect the sensed signal. Further refinements have been incorporated into microwave backscatter models for forest canopies that include reflections from leaf, branch, trunk, and soil layers (de Jong and Herben 2004; Ulaby et al. 1990). In these models, the trunk is represented as a single vertical cylinder while branches commonly take the form of semi-randomly oriented cylinders of various sizes. Individual thin disks or a cloud of material can represent leaves. In general, leaves and small branches result in isotropic reflections and the trunk and primary branches have directional reflections. Imagery from satellite synthetic aperture radar (SAR) investigations has shown the ability to provide canopy level information correlating with density of stems and leaves, leaf area and understory canopy type (Imhoff 1995; Kovacs et al. 2008). Detecting differences in the nut content at the tree or orchard level with satellite based radar remains well beyond the sensitivity of current technology.

The dielectric properties, or permittivity, of a material determine how the electric field of an electromagnetic wave interacts with it. Permittivity is represented as a complex number; the real component is a measure of how much of the electric field is stored in the material while the imaginary component represents how much is absorbed by the sample, and generally dissipated as heat. The stored energy component can be either reflected back, or transmitted through the sample to intercept another surface.

The dielectric constant (K) of a material is the ratio of the material's permittivity over the permittivity of free space. Water has a very high K, usually given as 80 at 1 GHz. Free space, by definition, has a dielectric constant of one. The dielectric constant of a material is not a constant; it varies with frequency and temperature. Materials containing water generally have a high K. The K of a leaf increases as it takes on water and decreases as it dries out (Shrestha et al. 2007).

Many plants exhibit a diurnal water cycle where water stored in tissues is released during the day through transpiration. Similar responses have been detected due to irrigation and soil water levels (Dobson 1988). Solutions containing sugars, salts and lipids have unique K values. As the concentration of these changes over time in a plant the electromagnetic response of the plant changes. The state of water in a plant also influences K. Water can exist in a free state or it can be chemically bound in tissues. Each tissue in a plant has its own electromagnetic signature that is dependent on its chemical makeup, structure, quantity and state of water.

Mature pecan nuts, like many seeds, are high in lipids and have a lower K value than leaves and stems (Nelson 1991; Nelson et al. 1992). The developing pecan nut expands to its full size early in its development. When it reaches its ultimate size it is dominated by a large central vacuole filled with cytoplasm, which is commonly called the “water stage” of development. The cytoplasm is an aqueous solution containing elemental ions and sugars that maintain turgor pressure in the developing nut. The edible embryo and cotyledons of the pecan develop and expand to fill the liquid filled void (Wells and Wood 2008). Fruit thinning decisions are made at the water stage before significant plant resources are diverted to development of the kernel. The effectiveness of microwaves to estimate yield will likely be maximum at this stage when the nuts have high water content and a correspondingly high K. As nutrients are diverted from other tree tissues to the developing kernel, there may be sensible changes in the K profile necessitating different models to predict pecan load throughout the season.

Short-range terrestrial backscattered microwaves can resolve many of the resolution and sensitivity limitations of satellite radar imagery. The radar equation (Eq. 1) can be used to illustrate fundamental relations between the characteristics of the radar, the target, and power of the transmitted and received signals.

$$P_r = P_t G^2 \sigma \frac{\lambda^2}{(4\pi)^3 R^4} \quad (1)$$

In this equation  $P_t$  and  $P_r$  represent the power of the transmitter and receiver respectively,  $\lambda$  is signal wavelength,  $\sigma$  is the radar backscattering coefficient of the target,  $R$  is the distance to the target, and  $G$  is the gain of the antenna (ESA 2011). Equation 1 is written in a form that assumes that microwaves are transmitted and received from the same antenna.

The radar backscatter coefficient, or radar cross section, lumps together a number of parameters associated with the target. It is influenced by the dielectric constant, physical properties and area of the target, factors that are frequency, polarization and directionally variable.

Equation 1 shows that returned signal power is inversely proportional to the distance from the receiver to the target raised to the fourth power. By placing the transmitter/receiver closer to the target, higher received signal strengths, and thus, increased sensitivity, are attainable.

Background noise will be lower which potentially improves signal to noise ratio. Another related advantage that close proximity to the pecan tree provides is that reflections from the far side of the tree are much further from the antenna relative to reflections from the front side. Reflected signals from the backside will be weaker by the ratio of distances to the fourth power.

Lower frequencies tend to be preferred on satellite-based radars because the reflected power of short wavelengths is lower (Eq.1) unless the target is tuned to specific wavelengths. For example, tripling the wavelength increases returned signal power by a factor of nine. In most cases, satellites have limited power available; a problem that ground based systems can generally overcome. Another advantage of dedicated ground based radar is that imagery can be taken when needed from orientations not dictated by set satellite orbits. Imaging of the pecan canopy could use upward looking radar, which removes reflections from the soil and trunks in the returned signal. All models that use satellite imagery must account for the confounding effects of reflections from the ground. Ground reflections are influenced by soil moisture from rainfall and irrigation, vegetation cover and soil conditions. McDonald et al. (1991) investigated microwave

backscatter response of a walnut orchard to ground based X band (9.6 GHz) radar. The configuration used in the experiments of McDonald et al. employed a boom-mounted antenna pointed towards the ground at an angle of 35-50°. Diurnal water response of the tree was detectable with their configuration. Their antenna also received reflections from the soil but the effects were less influential than in satellite systems because of the proximity of the antenna to the tree and ground resulted in less interference with canopy backscatter. This study illustrated the ability to detect relatively minor physiological differences in a tree with short-range ground based radar.

The ability of microwave energy to penetrate through vegetation has enabled satellite-based radars to identify trends in orchard crop condition but precision is inadequate for yield sensing. Short-range ground based radars resolve many of the power, resolution and sensitivity limitations of satellite radar imagery and are a potential technology for estimation of pecan nut yield. The objective of this research was to determine the feasibility of pecan nut quantification in situ using backscattered microwaves from antenna located in the orchard. The specific experimental objectives were to obtain baseline empirical microwave backscatter response of a pecan tree canopy in a laboratory setting and identify spectral features that may allow quantification of nuts in situ. This information will assist in specifying radar systems and experiments for future research efforts.

## Materials and Methods

### Plant materials

Pecan nuts and canopy samples were collected from the Oklahoma State University Cimarron Valley Research Station near Perkins, OK. The orchard contained 26-year-old 'Maramec' trees on 'Apache' seedling rootstocks in a Teller sandy loam soil (fine-loamy, mixed, active, thermic

Udic Argiustoll). Trees were diagonally spaced 24.4 by 24.4 m with Bermudagrass [*Cynodon dactylon* (L.) Pers.] ground cover. A 3 m wide vegetation-free area was maintained the entire row length with herbicides. Natural rainfall of 51.9 cm from Jan. through Oct. 2011 was supplemented by traveling gun irrigation. Mean daily temperatures were 4.0 °C above average during June through Aug. 2011. Commercial management for pests and fertilization were used. Diammonium phosphate and urea were each applied in a band application at rate of 482 kg·ha<sup>-1</sup> in March of 2011. Specimens were collected periodically from water stage through harvest to determine the effects of ontogeny on electromagnetic properties. On each collection date, canopy samples from three trees randomly selected at the start of the study were cut where the branch diameter reached approximately 2 cm. Samples were taken from trees approximately 2 to 4 m above the ground. Additional nuts were collected from the same trees to supplement nuts in the canopy samples. Plant materials were immediately placed over ice in coolers until tested.

#### Vector network analyzer measurements

Microwave response to the pecan canopy samples was observed at the Biosystems and Agricultural Engineering Sensor lab at Oklahoma State University in Stillwater, Oklahoma. Microwave reflection and transmission measurements of test samples in various configurations were taken using a vector network analyzer (VNA) (model N5230A PNA-L, Agilent, Santa Clara, CA) attached to double-ridged waveguide horn antennae (model 3117, ETS-Lindgren, Cedar Park, TX). The antenna supported a frequency range of 1 to 18 GHz. The antennae were mounted vertically facing each other 1 m apart in a PVC frame with a midlevel specimen support shelf (Figure 20). Port 1 of the VNA was connected to the bottom antenna. To minimize reflections from the tile covered concrete floor a microwave absorbent panel 61 by 61 cm was positioned under the antenna set (model C-RAM LF-79, Cuming Microwave, Avon, MA). The VNA was calibrated with a SOLT (short-open-load-through) procedure prior to taking

measurements on pecan canopy samples. This procedure consisted of sequentially connecting a short circuit, open circuit and matched load to each of the VNA ports to calibrate reflection response. After this, the antennae were connected to the VNA ports to calibrate the through response in empty space. Temperatures were between 21 and 23 °C for all tests.

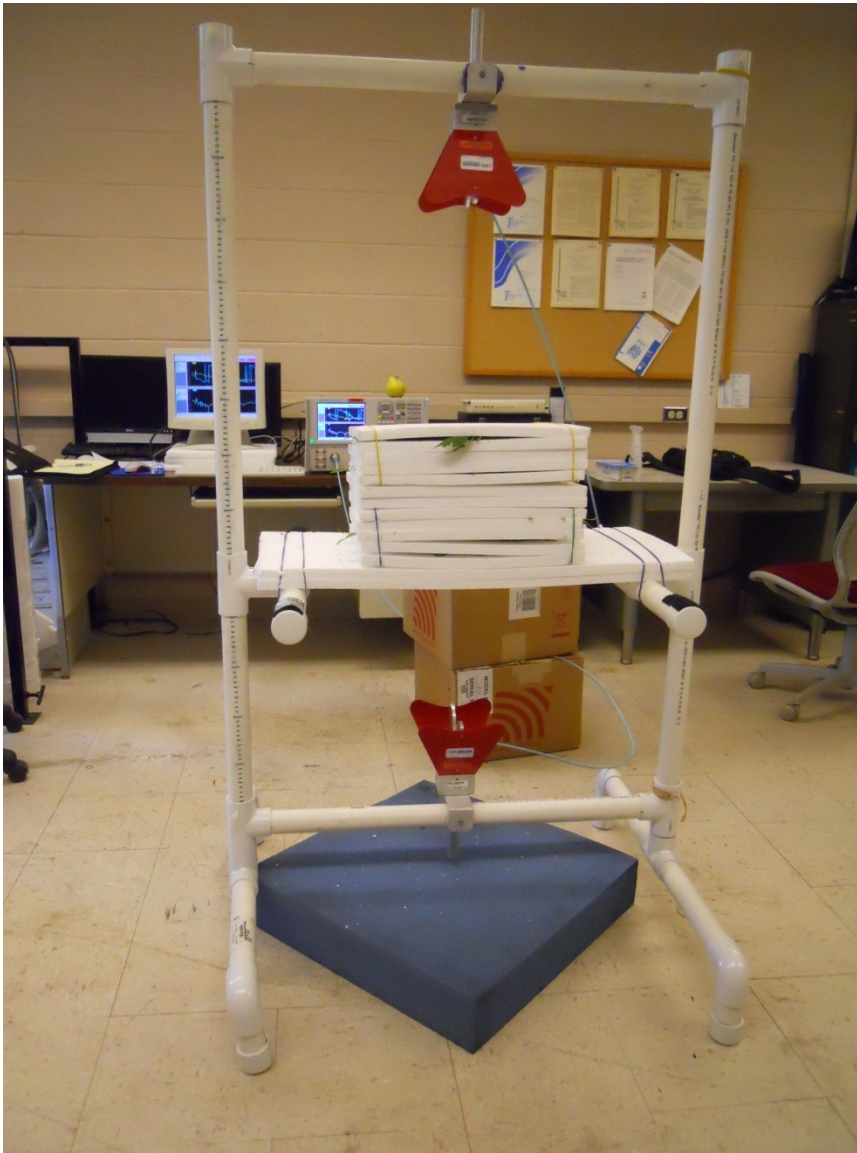


Figure 20. Pecan canopy test stand showing antenna, specimen holder on support shelf, absorbent material on floor and VNA in background.

For each configuration tested, the magnitude of scattering matrix parameters  $S_{11}$ ,  $S_{22}$ ,  $S_{21}$  and phase of  $S_{21}$  were collected. Each measurement consisted of the average of 20 spectral scans

from 1 to 18 GHz divided into 401 measurements resulting in a spectral resolution of 42.4 MHz. VNA transmit power was set at -5 dBm and each scan took 11 ms.

### Sample holder and measurement procedure

A specimen holder with dimensions of 35 by 40 cm and consisting of 12 layers of 1.8 cm thick closed cell expanded polystyrene (EPS) was used to position plant materials for measurement in the test stand (Figure 21). EPS has a dielectric constant of 1.03, which is very near that of air, thus the specimen holder has little effect on the antenna field (Trabelsi and Nelson 2004). Layers 2, 4, 9 and 11 had an open space 25 x 30 cm to hold leaves and branch material in a secure position. This allowed multiple measurements to be taken with the leaves and branches in the same position as nuts were sequentially added to 9 holes arranged in a 3 by 3 grid with 10 cm spacing in layers 6 and 7 (Figure 21). The layers of the specimen holder allowed air to circulate through it so that plant materials could be partially dried in their original position by placing the loaded specimen holder in an oven so that the effect of leaf moisture content (MC) on dielectric properties could be measured.

Each canopy specimen was subjected to two sets of 11 VNA measurements. First, the empty specimen holder was measured with the VNA to establish a baseline. Then the specimen holder was loaded with approximately 200 g of leaves and current year growth plus 200 g of prior year growth and branch material divided approximately equally between the 4 void spaces. Plant materials were randomly layered which allowed a few leaves and stems to protrude from the specimen block. Elastic bands held layers 1-5 and 8-12 together during subsequent measurements. After loading the specimen block with leaves and branches, a series of 10 VNA measurements were taken with zero through nine nuts sequentially added to randomly selected holes (Figure 21).

Following the 10 VNA measurements with fresh leaves, the specimen holder was placed in an oven for 30 minutes at 50 °C to reduce leaf MC. The specimen block was weighed after the drying cycle to determine leaf moisture loss. The VNA measurements were repeated on configurations with zero through nine nuts. After the final VNA measurement, plant materials were dried at 70 °C for 72 hours to determine MC at the two levels of hydration. Nuts were dissected to determine maturity stage at time of measurement. Six repetitions at five maturity stages were tested. Attenuation of nuts without leaves and branches were also measured to identify significant attenuation frequencies.



Figure 21. Typical sample of leaves and branches (left) and nuts (right) being loaded into specimen holder for VNA measurements.

### Data analysis

Key predictive frequencies were identified by partial least squares (PLS) and linear regression analysis in MATLAB (Natick, MA). Analysis was conducted on two sample formations: on fresh leaves and on fresh and partially dried leaves pooled together. Statistical analysis of the spectral data investigated significant main effects by frequency for pecan and canopy mass, and water content. Plant material property data were analyzed using SAS GLM (SAS Institute Inc., Cary, NC) for mean separations.

## Results and discussion

### Plant materials

Pecan canopy samples were collected on five occasions where the maturity stage of the nuts ranged from water stage through shuck split initiation (Table 7, Figure 22). Due to abnormally low seasonal rainfall in 2011, which was partially supplemented with irrigation, MC and mass of nuts at water stage were low on the first sampling date in August. The orchard received significant rainfall before the second sampling date on Aug. 17 and mean nut mass increased from 8.1 g to 13.9 g. Nuts continued to increase in size through the growing season. Leaf MC ranged from 55.9% at the first sampling and generally decreased through the season to 52.4% while MC of branches exhibited an irregular trend over the sampling period. Leaf MC was reduced by 10.8% to 16.5% after partial drying for 30 min at 50 °C (Table 7). Drying for 30 min at 50 °C had little influence on branch moisture levels therefore those effects were not analyzed in these experiments.

Table 7. Pecan canopy materials used in microwave experiments with associated moisture content (MC).

Sample date	Nut development stage	Mean nut mass (g)	Nut MC (% w.b.)	Leaf MC initial (% w.b.)	Leaf MC after desiccation (% w.b.)	Branch MC (% w.b.)
3-Aug	Water stage	8.1	78.2% a <sup>z</sup>	55.9% a	43.1% a	39.7% a
17-Aug	Gell stage	13.9	79.9% b	53.2% b c	42.4% a	40.7% a c
6-Sep	Developing kernel	20.2	73.1% c	54.8% a b c	41.8% a	43.0% b
27-Sep	Mature kernel	23.7	68.9% d	54.9% a b	40.6% a	42.3% b c
25-Oct	Shuck split	25.5	67.1% e	52.4% c	35.9% b	42.5% b c

<sup>z</sup>Means followed by the same letter are not significantly different as determined by LSD test (P≤0.05).

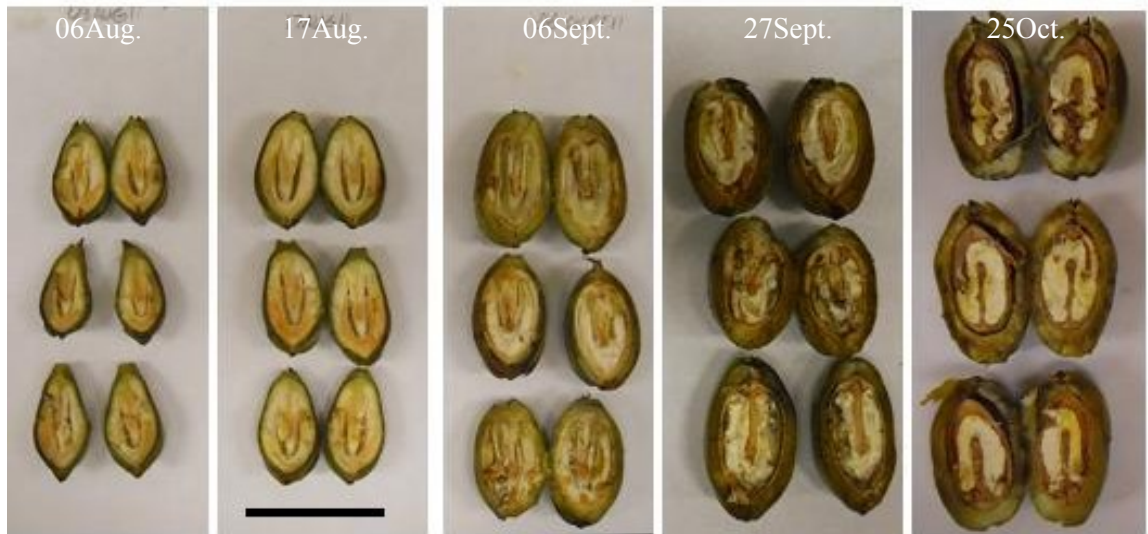


Figure 22. Sectioned 'Maramec' pecan nuts at each sampling date in 2010. Bar = 5 cm.

### VNA measurements

Trends in the VNA spectral response of the canopy samples as nuts were sequentially added (Figure 23) were not evident from inspection. Small changes in the orientation of the samples in the antenna field could not be precisely controlled and this resulted in variation in the VNA measurements that often obscured differences as nuts were added. This was especially evident in the phase behavior of through measurements where large changes were observed as nuts were sequentially added (Figure 23, top right).

A consistent resonance, centered at 1.9 GHz, occurred throughout the testing. This resulted in positive insertion losses and attenuation in the range of 1-3 GHz. The source of the resonance is unknown, however, reflections from the ceiling and absorber (S11 and S22 measurements respectively) and diffuse reflections from the canopy samples impinging on the receiving antenna (S21 measurements) are suspected contributing factors. During calibration in open space, no energy is diffusely reflected by the canopy samples and this energy would have bypassed the antenna and been excluded from the received signal. Backscattered measurements in the test configuration included energy reflected from the opposing antenna that would not exist in a field

measurement. Testing in an anechoic chamber or open field site would reduce interfering reflections from the surroundings and should be considered for future measurements.

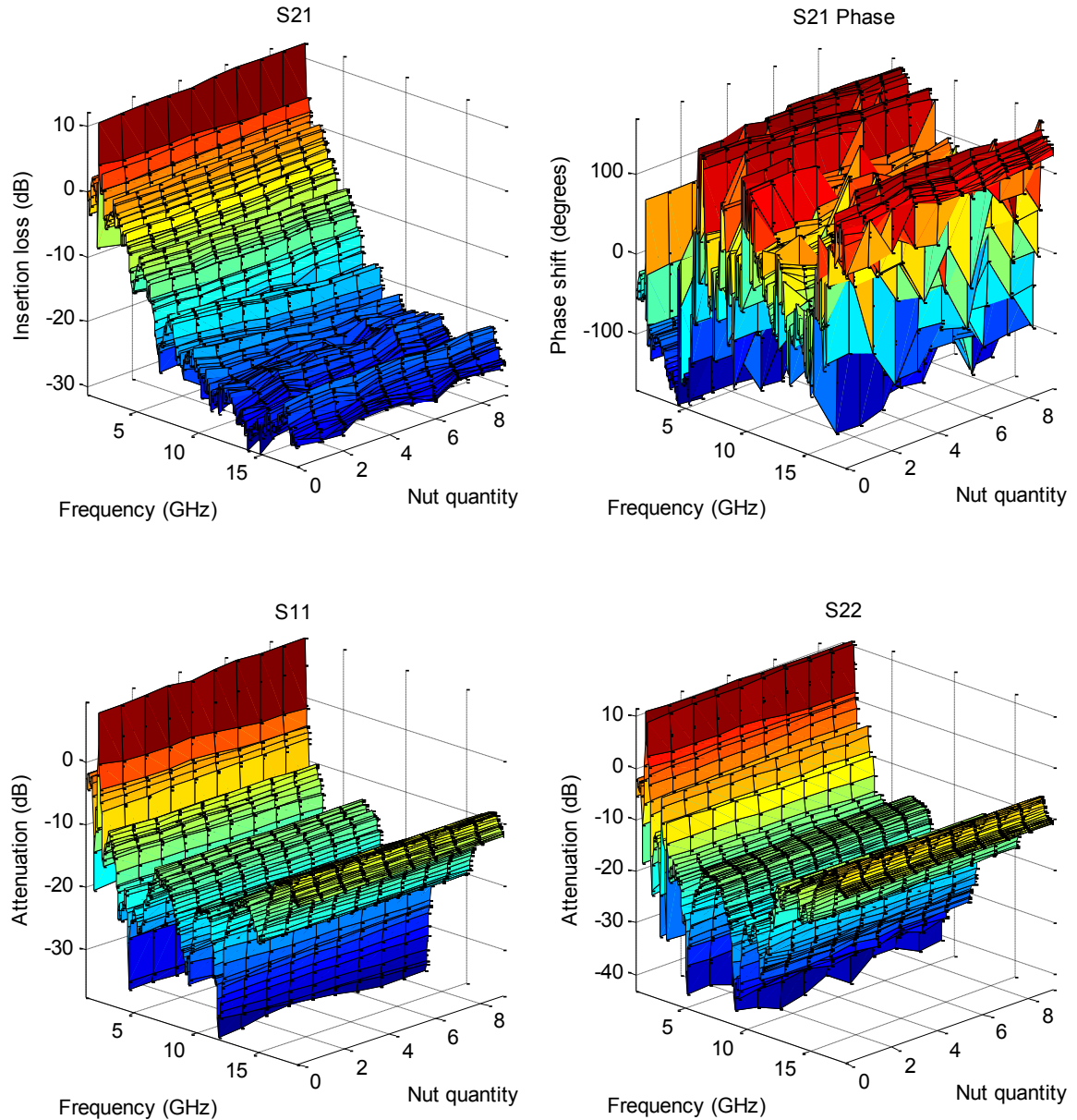


Figure 23. VNA spectral response of representative canopy sample with 0 to 9 pecan nuts. Top row is insertion loss and phase of through measurement. Bottom row is reflection of ports 1 and 2 respectively. (Mean of Oct 27 fresh leaf sample (n=6)).

Baseline reflection response was generally greater than -40 dB except at the low range of the spectrum (Figure 24, bottom). For signals transmitted through the canopy samples, insertion losses were generally low starting at 1 GHz and increased to approximately -30 dB at 18 GHz

(Figure 24, top left). Attenuation of the reflected signals (S11 and S22) decreased with increasing frequency in a pattern complementary to the through measurements (Figure 24, bottom). A strong attenuation band occurred at 11.8 GHz in nuts, and in leaves and branches in the reflected signal from antenna 1. The signal from antenna 2 exhibited attenuation at this same frequency although the magnitude was lower (Figure 24, bottom row). The difference between reflected signals from nuts and from leaves and branches was greater than 5 dB across the spectrum of antenna 1 except around 4 GHz. Antenna 2 had a similar response although there were several additional bands between 9.1 and 14.4 GHz that showed low attenuation difference.

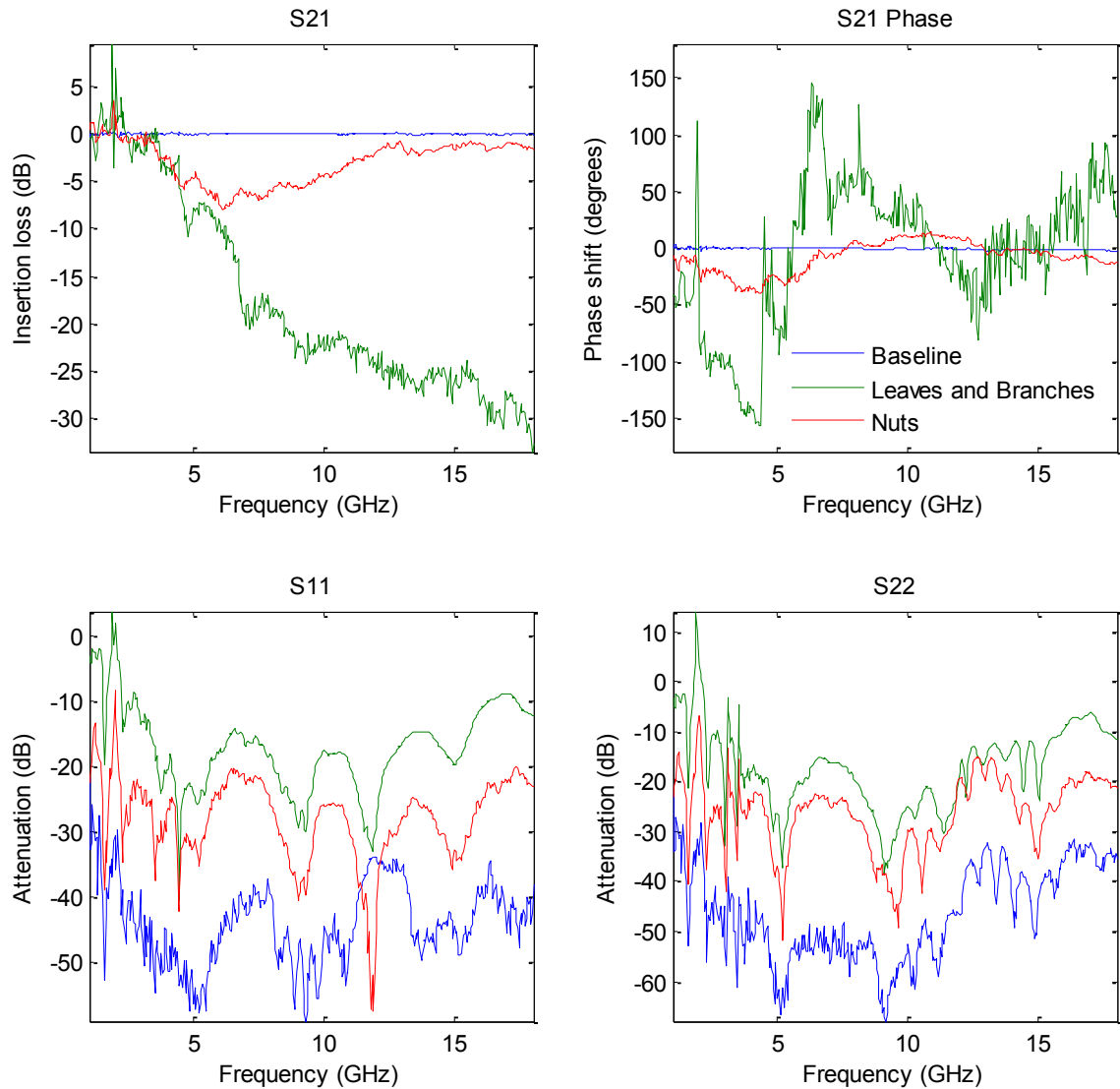


Figure 24. Mean VNA spectral response for pecan leaves and branches ( $n=60$ ), and nuts (9 nuts, 24 samples). The top row is insertion loss and phase of through measurement. The bottom row is reflection of ports 1 and 2 respectively.

Microwave signal attenuation of leaves and branches generally increased with frequency (Figure 24, top left). Longer wavelengths are able to penetrate deeper into the tree canopy (Karam et al. 1992). Pecan nut samples caused maximum attenuation of the through signal in a broad frequency band centered around 5 GHz (Figure 24, top left). In this same band, the magnitude of attenuation increased through the season as nut mass increased (Figure 25, top left and Table 7). In the reflected signals (Figure 25, bottom row), increasing nut mass resulted in a stronger reflected signal up to about 12 GHz. At higher frequencies, the pattern is not well defined.

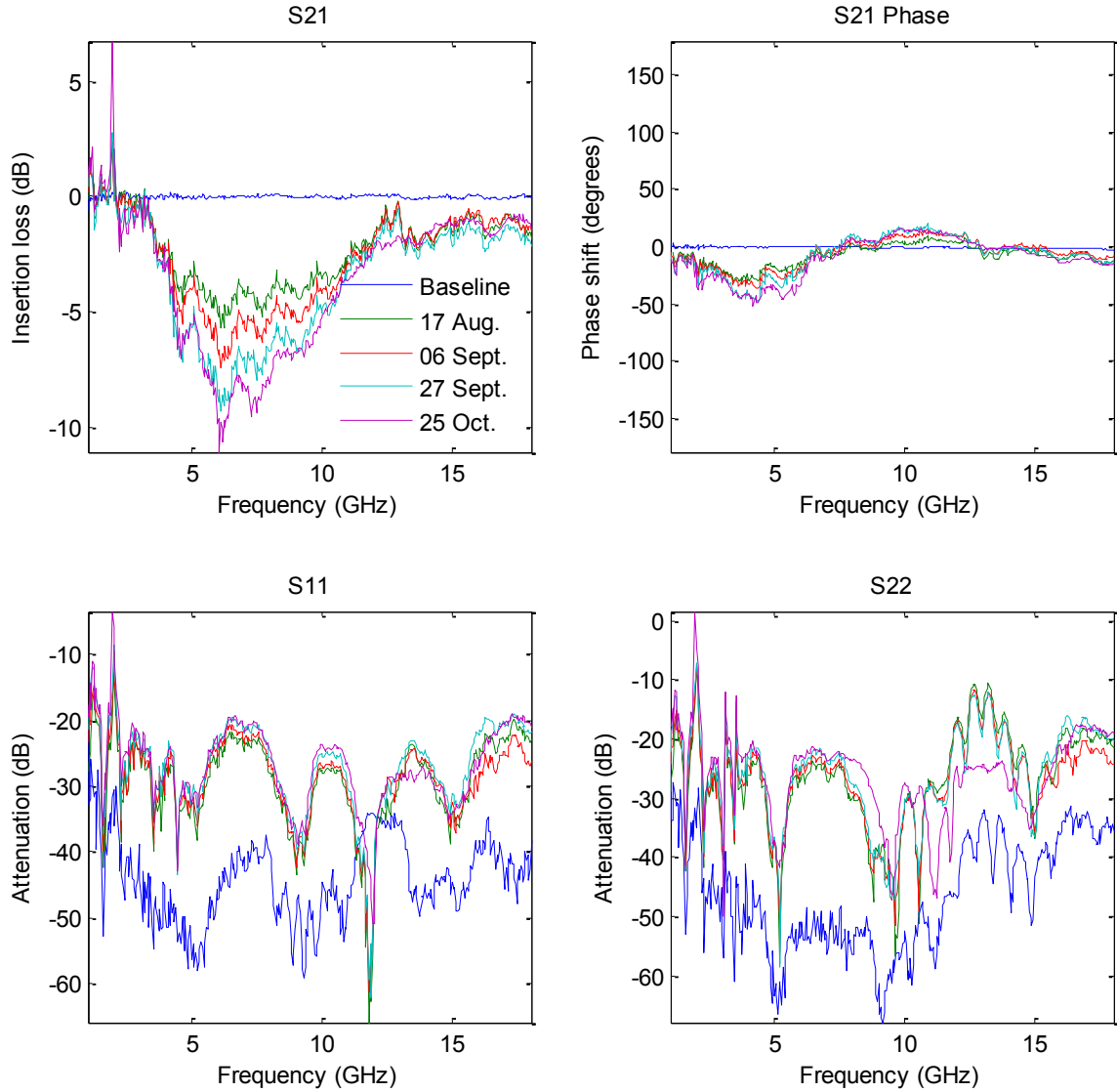


Figure 25. Effect of harvest date on mean VNA spectral response for nuts (9 nuts, 6 samples per date) . The top row is insertion loss and phase of through measurement. The bottom row is reflection of ports 1 and 2 respectively.

PLS regression analysis was conducted on spectral data of fresh leaves and on fresh and partially dried leaves pooled together with nut, canopy water, and canopy mass as independent variables.

Weights of the five most influential eigenvectors indicate several frequency bands that were responsible for a large part of the variance among the samples (Figure 26). An analysis of the ten peaks with the strongest correlation to nut mass in each of the first five eigenvectors shows that several frequencies between 1 and 5.5 GHz, plus bands around 9, 12 and 15 GHz were the most

influential in accounting for variance among the samples. This pattern was consistent for all maturity stages with the 9 GHz band being the most prominent for all dates (Figure 27).

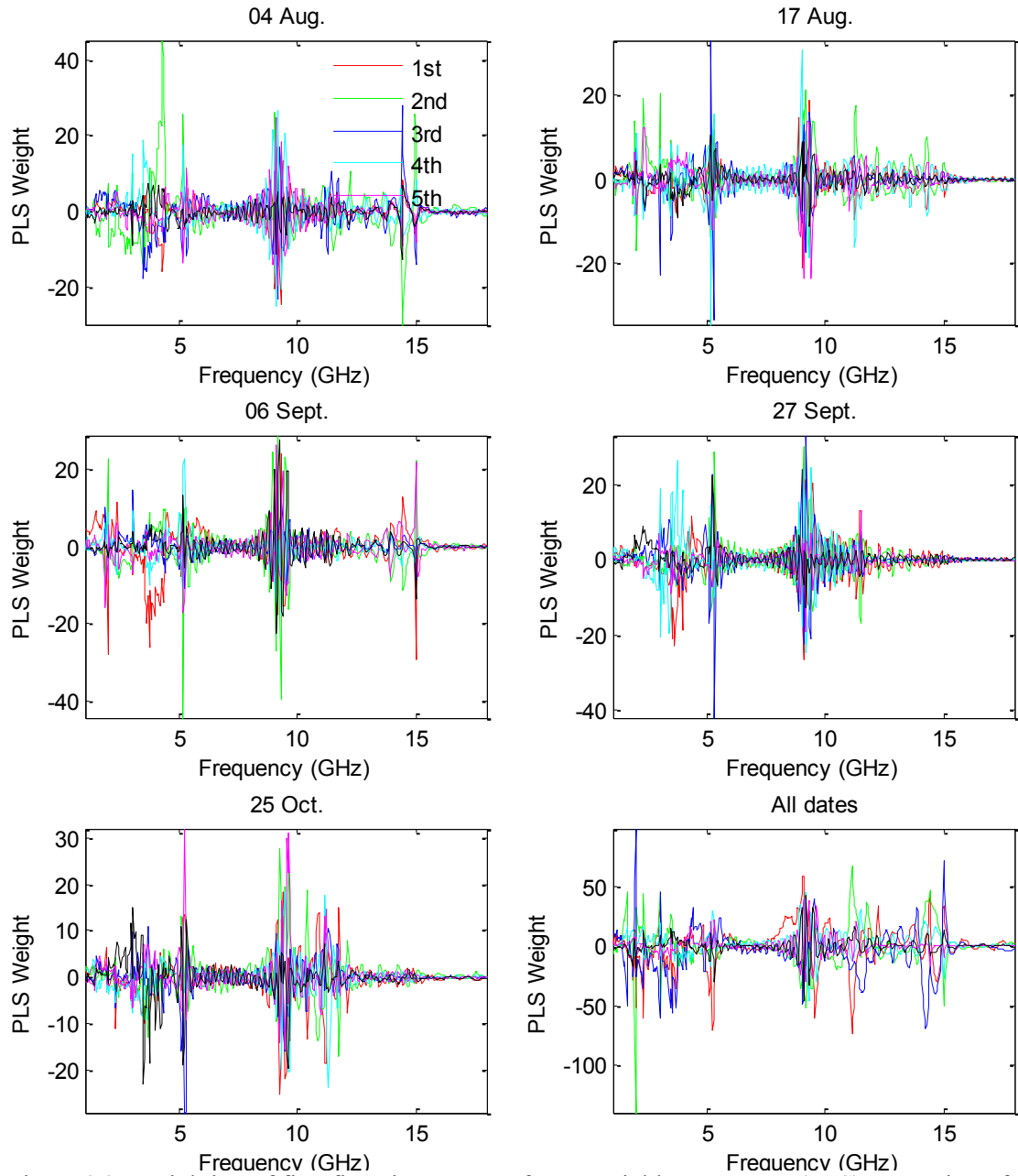


Figure 26. Weighting of first five eigenvectors from partial least squares (PLS) regression of canopy samples for nut mass at individual harvest dates and all dates pooled together. (S11 shown)

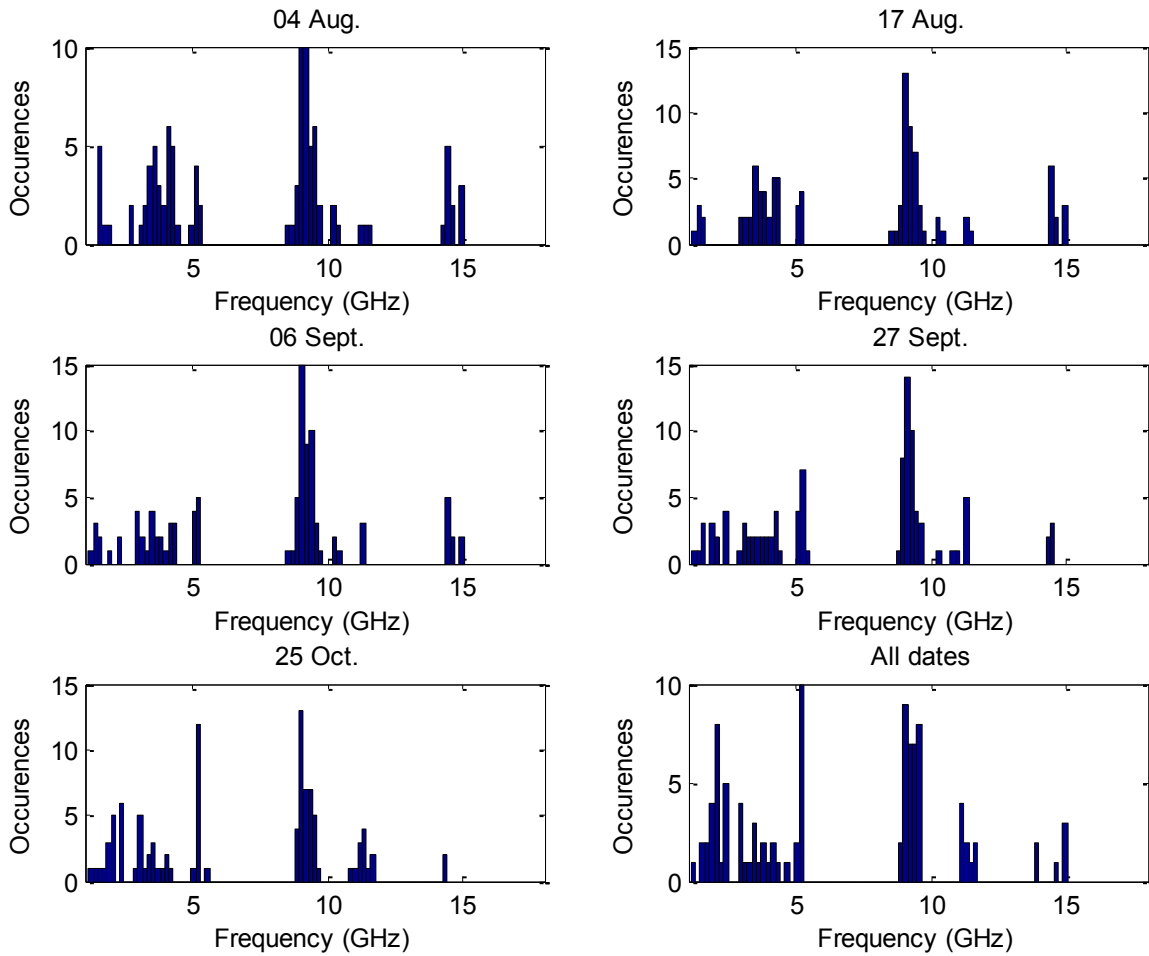


Figure 27. Distribution of the ten most influential frequencies from each of the first five eigenvectors from partial least squares (PLS) regression of canopy samples for nut mass at individual harvest dates and all dates pooled together. (S11 shown)

The amount of variance explained by PLS regression analysis increased as more PLS components were added. With one PLS component, between 19 and 66% of the variance in nut mass was recovered in the reflection measurements (Figure 28). The through measurements exhibited the best performance although backscattered microwaves were of primary interest in this study. PLS analysis of individual dates was better than when all dates were pooled together suggesting that physiological changes during canopy ontogeny have an effect on microwave response. A similar pattern was observed when the fresh leaves were analyzed with the partially dried leaves except the magnitude of variance recovered was lower (Figure 29). The primary difference between the two sample sets was the water content of the leaves.

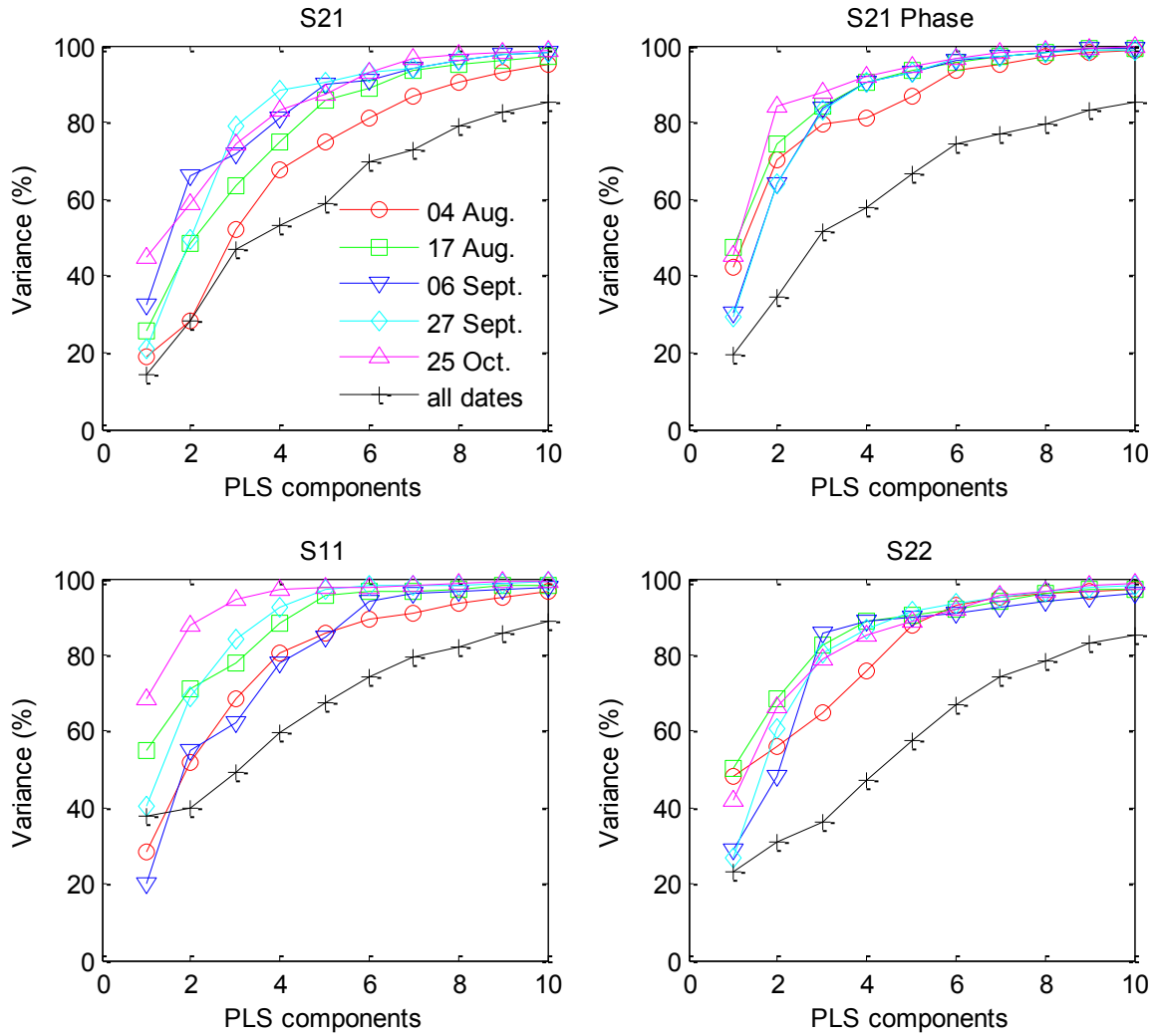


Figure 28. Variance accounted for by the first 10 eigenvectors from partial least squares (PLS) regression of fresh leaf canopy samples for nut mass at individual harvest dates and all dates pooled together. The top row is the attenuation and phase shift of through measurements; the bottom row is reflection measurements from antenna one and two respectively.

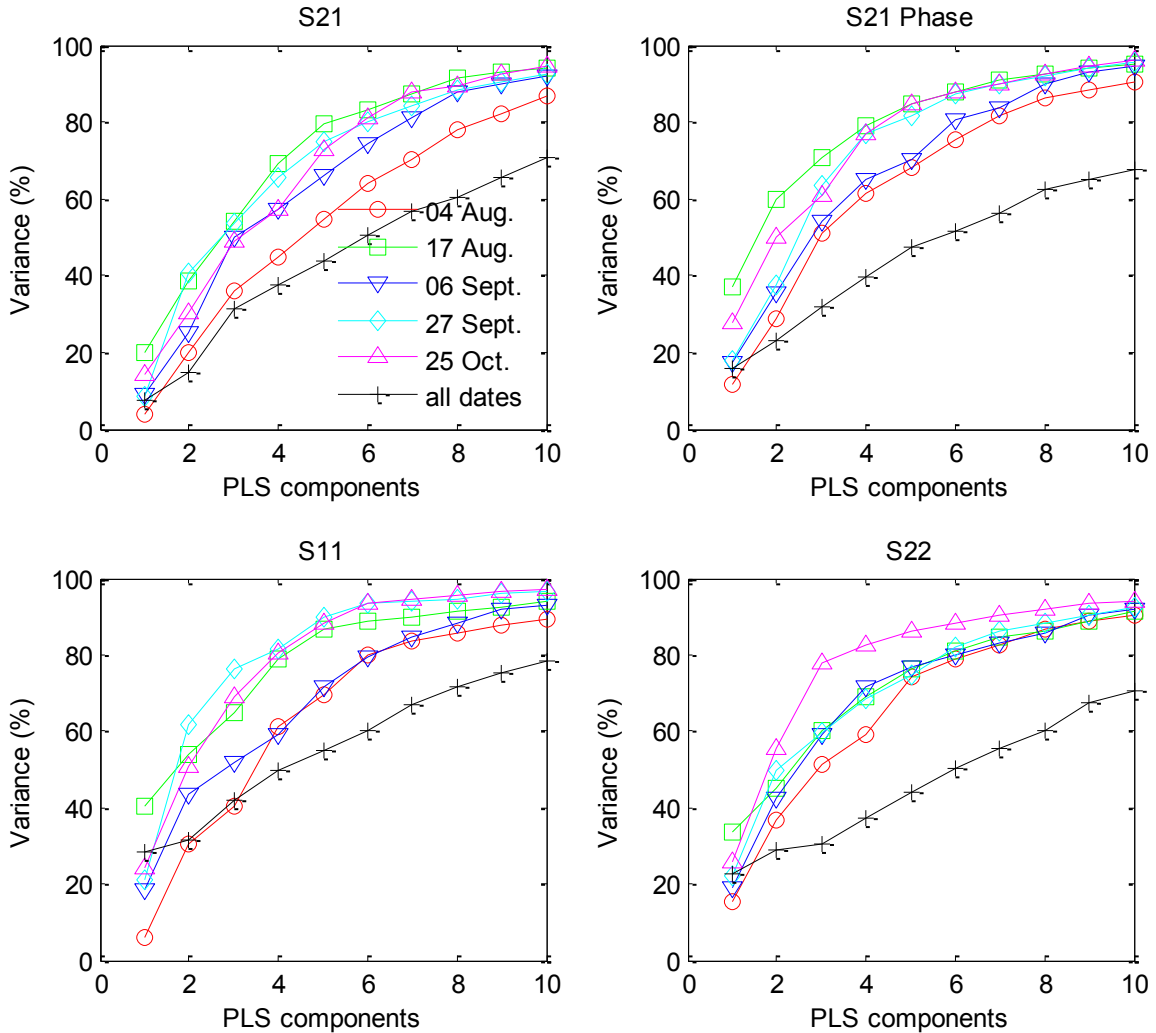


Figure 29. Variance accounted for by the first 10 eigenvectors from partial least squares (PLS) regression of fresh and partially dried canopy samples for nut mass at individual harvest dates and all dates pooled together. The top row is the attenuation and phase shift of through measurements; the bottom row is reflection measurements from antenna one and two respectively.

The variance recovered in PLS regression is a function of the entire spectra although weighting of individual frequencies is governed by the eigenvectors. The correlation of nut mass to a single frequency is of practical interest to radar applications. Simple linear regression of nut mass to each frequency in all samples resulted in significant correlations at several frequency bands however model error was relatively high and there was significant variability among the dates. The maximum coefficient of determination ( $R^2$ ) occurred from 1 to 4.5 GHz for all dates. The maximum  $R^2$  observed was 0.32 ( $P < 0.0001$ ) at 4.145 GHz in the 25 Oct. samples. In general,

correlations at all frequencies were poor with  $R^2 < 0.3$  (Figure 30). The poor correlations suggest that direct sensing of nut mass within a canopy sample using backscattered microwaves is not feasible because no strong nut specific microwave interactions were found.

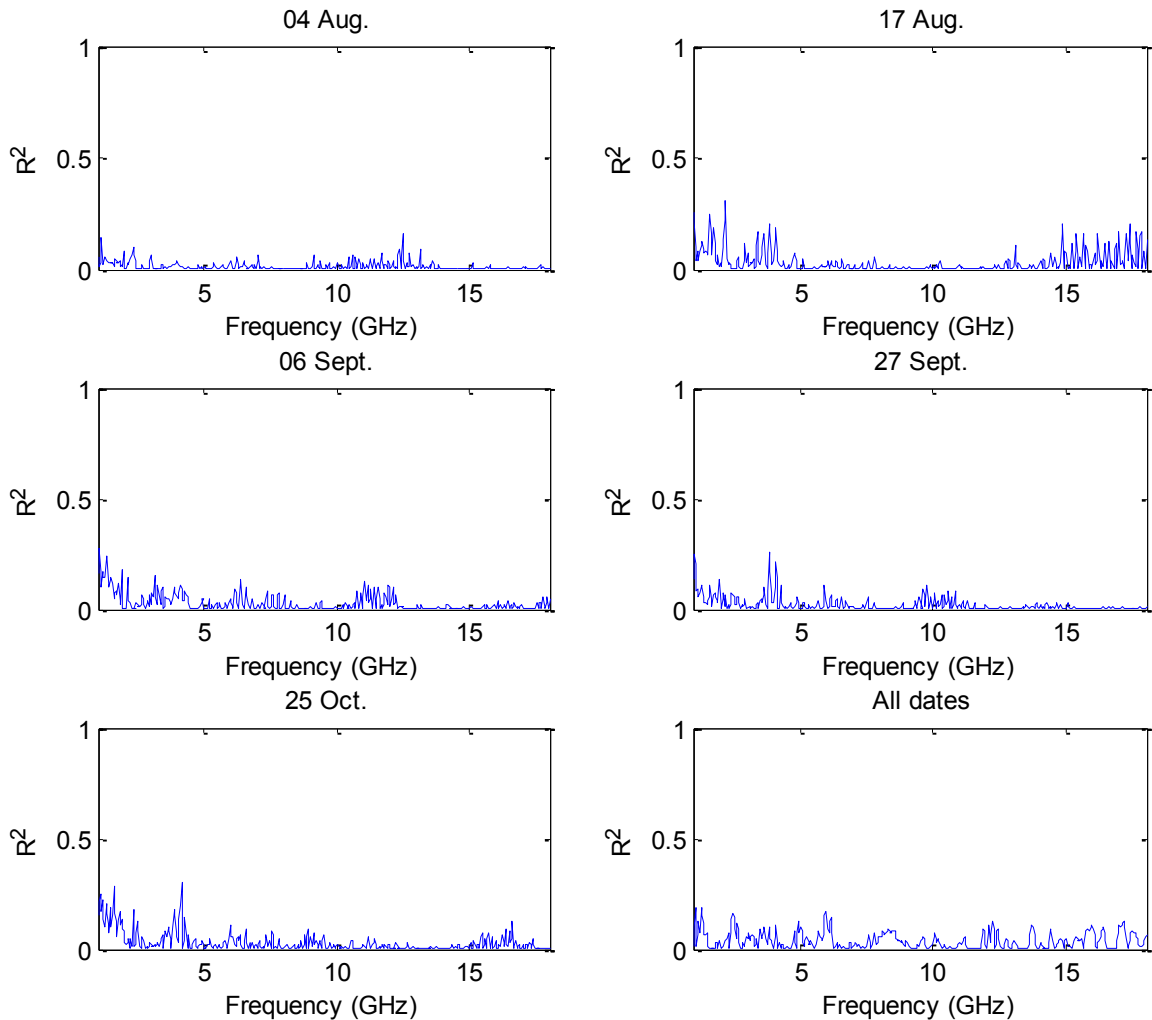


Figure 30. Coefficients of determination ( $R^2$ ) from linear regression of nut mass at each frequency from canopy samples for individual harvest dates and all dates pooled together. (S11 shown)

The dry mass and water mass in the samples with 0 to 9 nuts ranged from 166 to 301 and 138 to 359 g respectively. Significantly improved correlations result when PLS and linear regressions were conducted on the sample set which includes the baseline empty sample holder observations plus the observations that contain 0 to 9 nuts. The dry and water mass in these data ranged from

0 to 301 g and 0 to 359 g respectively. The magnitude of the first eigenvector from PLS regression is much greater than the others across most of the measured spectrum when the baseline samples were included (Figure 31 and Figure 32). Eigenvectors 2 through 5 indicate that frequency bands at 5.5, 9, 12 and 15 GHz were also influential in accounting for variance among the samples. The pattern in eigenvectors 2 through 5 is similar to the previous analysis when the baseline observations were not included. In the present analysis, the first eigenvector accounts for more than 67% of variance in all maturity stages of the reflected measurements for total water (Figure 33). For dry matter mass, the first eigenvector accounts for more than 83% of variance among the samples (Figure 34).

Simple linear regression of total water at each frequency resulted in significant correlations across large portions of the spectrum. A consistent broad peak from approximately 5.5 to 8 GHz had  $R^2 > 0.63$  ( $P < 0.0001$ ) for total water and  $R^2 > 0.78$  ( $P < 0.0001$ ) for total dry matter for all dates analyzed individually and pooled together. Non-significant results were found in various dates at narrow frequency bands around 2, 5.2, 9, 12 and 15 GHz for total water and dry mass (Figure 35 and Figure 36).

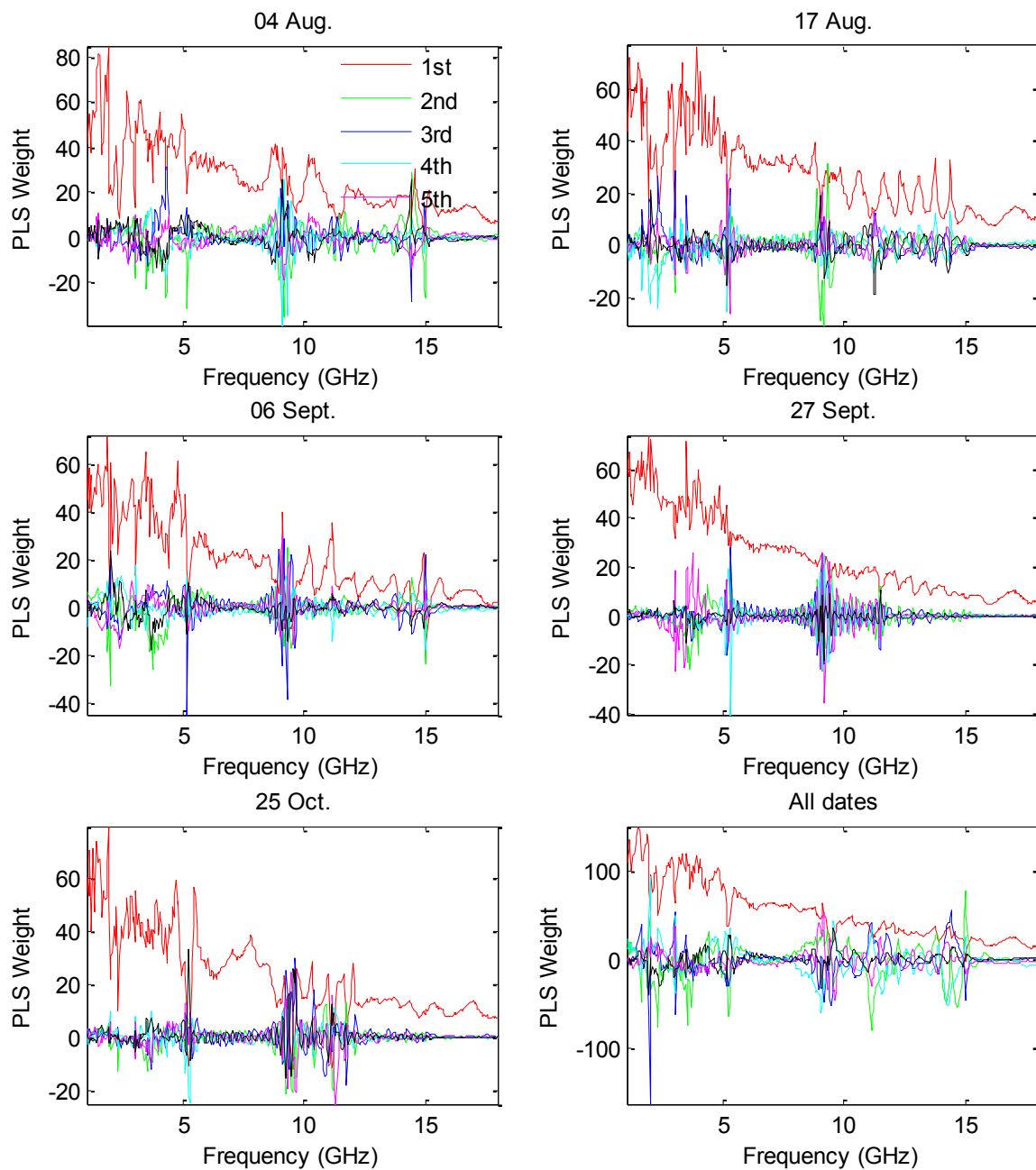


Figure 31. Weighting of first five eigenvectors from partial least squares (PLS) regression of baseline and canopy samples for total water mass at individual harvest dates and all dates pooled together.

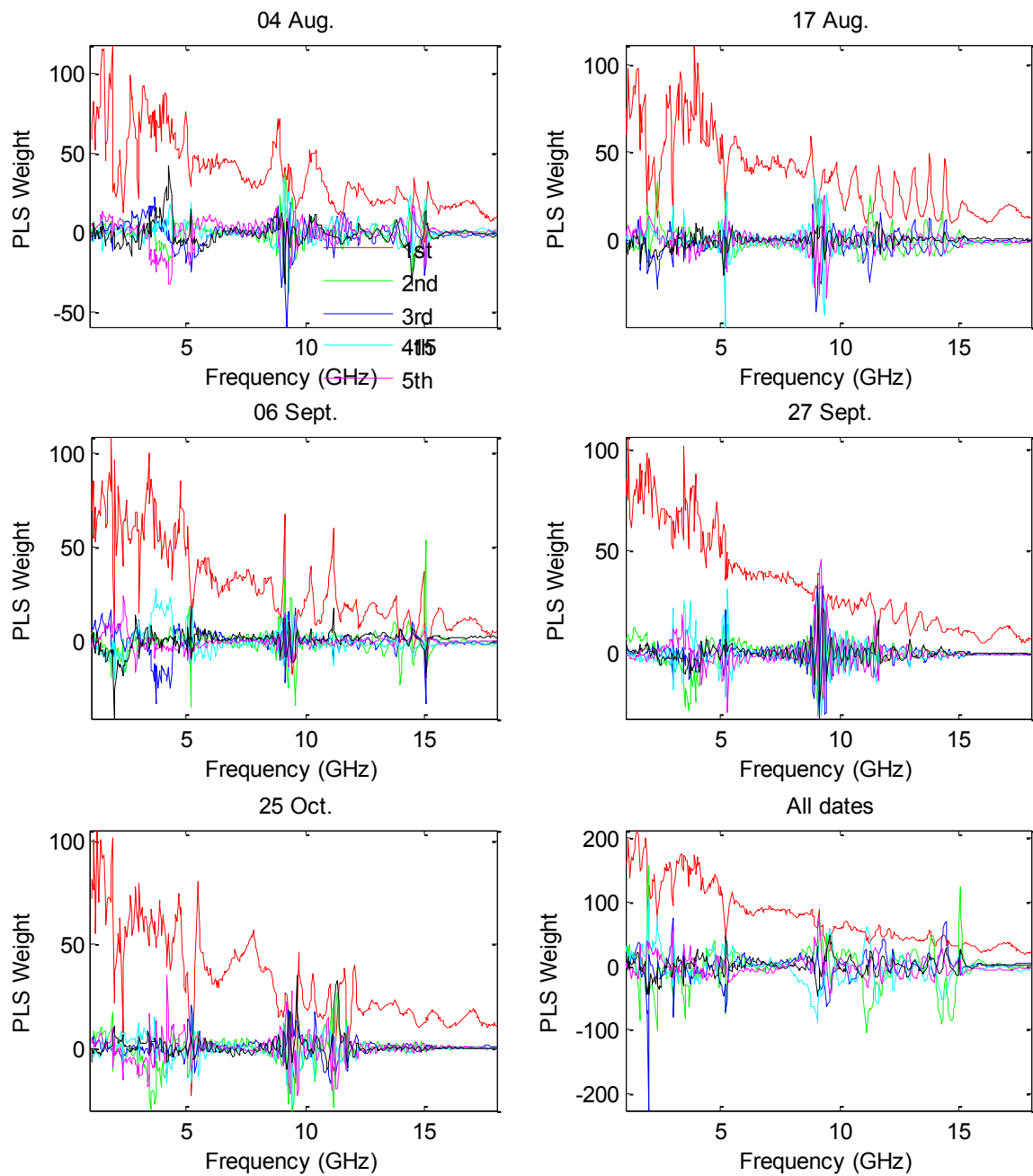


Figure 32. Weighting of first five eigenvectors from partial least squares (PLS) regression of baseline and canopy samples for total dry mass at individual harvest dates and all dates pooled together.

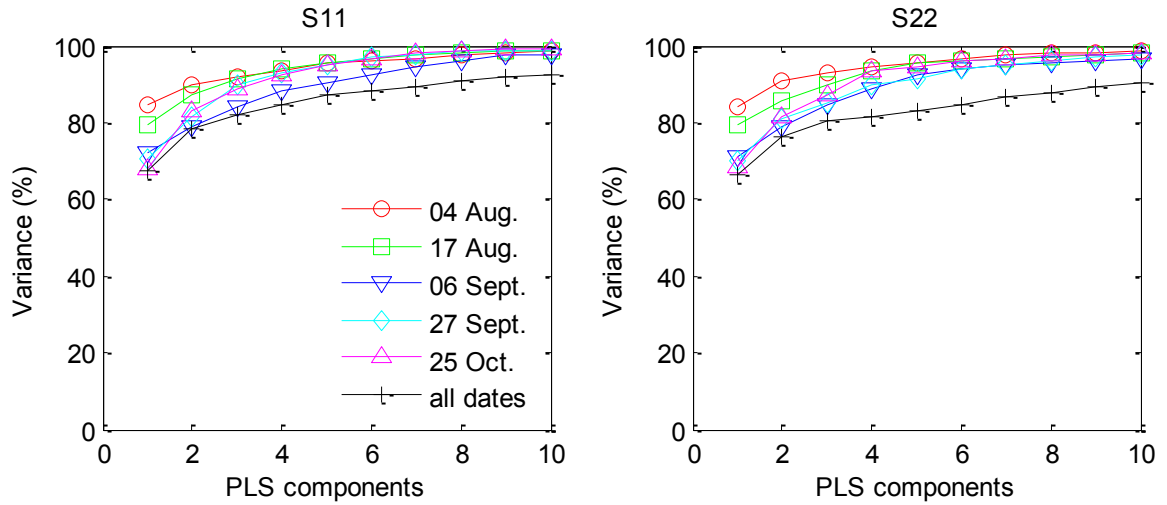


Figure 33. Variance accounted for by the first 10 eigenvectors from partial least squares (PLS) regression of baseline an canopy samples for total water mass at individual harvest dates and all dates pooled together. S11 and S22 represent reflection measurements from antenna one and two respectively.

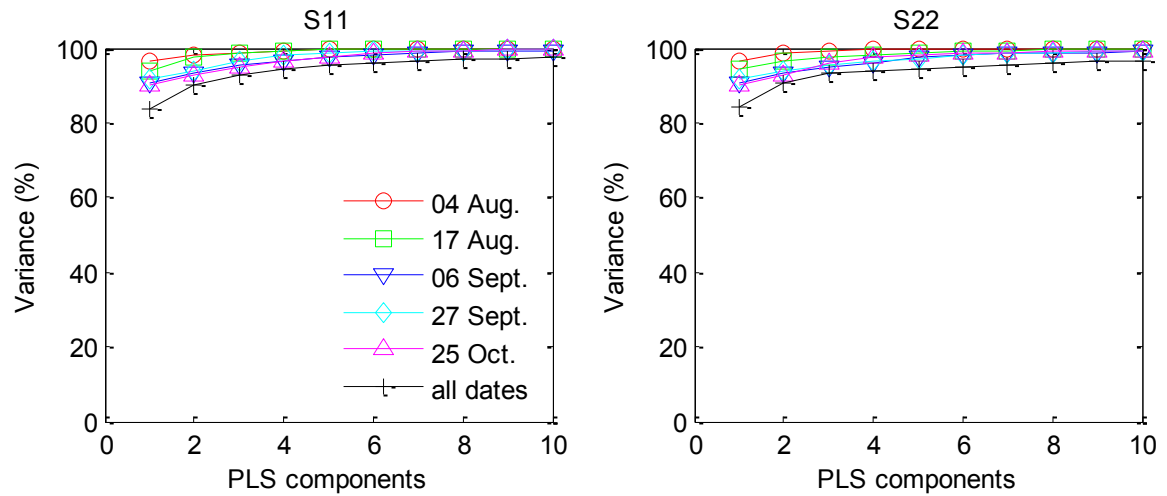


Figure 34. Variance accounted for by the first 10 eigenvectors from partial least squares (PLS) regression of baseline an canopy samples for total dry mass at individual harvest dates and all dates pooled together. S11 and S22 represent reflection measurements from antenna one and two respectively.

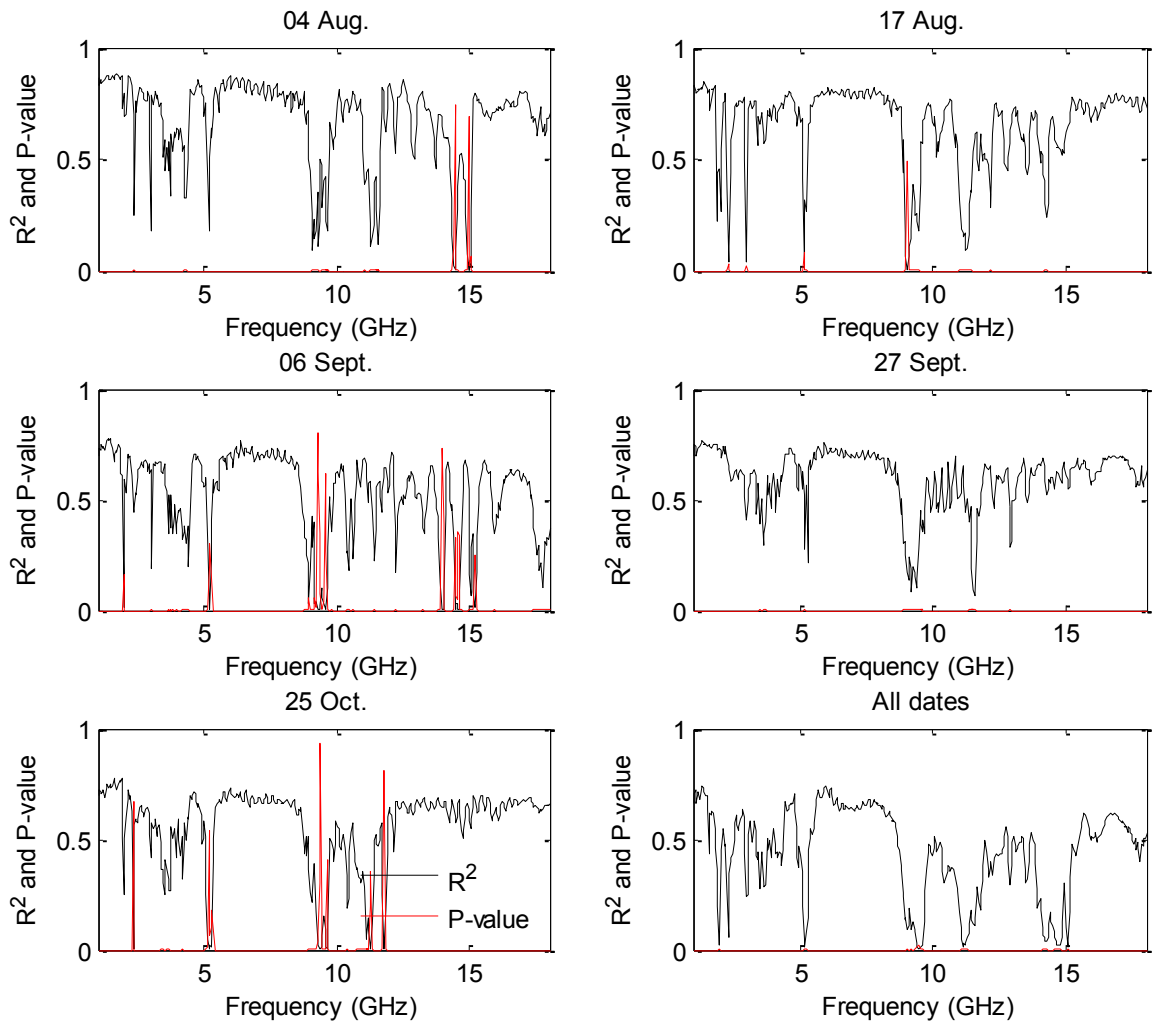


Figure 35. Coefficients of determination ( $R^2$ ) and P-values from linear regression of total water mass at each frequency from baseline and canopy samples for individual harvest dates and all dates pooled together.

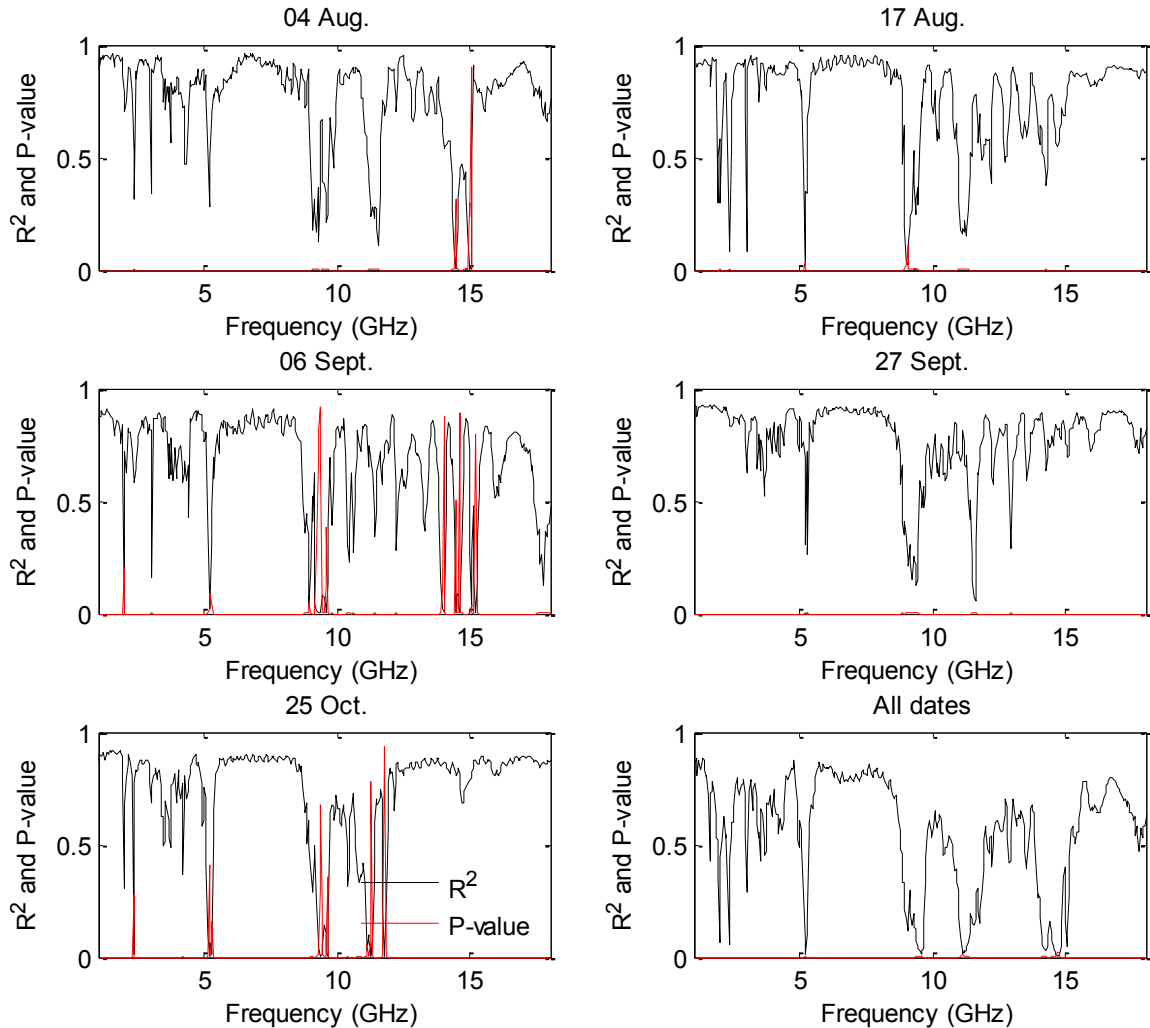


Figure 36. Coefficients of determination ( $R^2$ ) and P-values from linear regression of total dry mass at each frequency from baseline and canopy samples for individual harvest dates and all dates pooled together.

### Implications for future investigations

The microwave backscatter behavior of a pecan tree canopy is dependent on both the geometry and composition of the components illuminated by the antenna. The permittivity and loss factor of leaves and branches have been shown to increase with increasing water content (El-Rayes and Ulaby 1987; Shrestha et al. 2007). In this investigation, regression relationships for total dry mass were more closely correlated to microwave backscatter response than was total water. This

indicates that the backscattered microwaves were more highly influenced by the geometry of the leaves, branches and nuts than by their composition or water content.

These experiments were designed to minimize the variability of leaf and branch mass among the samples in order to test the effects of changing nut quantity on backscattered microwaves. In an orchard, there will be variability in distance from the antenna and in the spatial arrangement of the canopy components. No frequencies were identified that directly correlated to nut mass however yield estimates may be indirectly derived from mass changes sensed in the canopy. To do this, spatial distributions of biomass within an orchard could be compared at different dates. The sensing system would require distance measuring and positioning capabilities in order to construct a three dimensional distribution of canopy biomass. Additional studies to optimize sensor parameters including directionality, power, gain, frequency, bandwidth and polarity also need to be performed.

Technology developed to sense pecan yield in situ can potentially be extended to other pecan tree sensing applications and to other orchard fruit and nut crops. Orchard crops such as citrus, peaches and apples have higher fruit mass in the canopy compared to pecans and may be better suited to microwave yield sensing.

## Conclusions

Sensing of backscattered microwaves originating from antenna located within an orchard is a potential solution for in situ estimation of pecan nut yield. Short-range microwaves resolve many of the power, resolution and sensitivity problems that limit utility of satellite radar systems. VNA measurements of microwave energy reflected from, and transmitted through pecan tree canopy samples with varying nut content were taken to characterize the microwave response of pecan trees. PLS regression of the spectral data did not reveal frequencies that were specifically

sensitive to varying nut content. Linear regression analysis identified significant correlations of pecan canopy water and dry mass to backscattered microwave response over a large portion of the 1 to 18 GHz spectrum tested. Most notably a broad peak from 5.5 to 8 GHz had  $R^2 > 0.63$  for total water and  $R^2 > 0.78$  for total dry matter. Non-significant correlations were found in various dates at narrow frequency bands around 2, 5.2, 9, 12 and 15 GHz for total water and dry mass.

These results indicate that short-range backscattered microwaves are a promising technology for in situ estimation of pecan yield. Furthermore, the same methods may be extensible to other sensing applications in pecans and other orchard crops.

## References:

- Bouvet, A., T. Le Toan, and L.-D. Nguyen. 2009. Monitoring of the Rice Cropping System in the Mekong Delta Using ENVISAT/ASAR Dual Polarization Data. *Geoscience and Remote Sensing, IEEE Transactions on* 47 (2): 517-526.
- Conner, P. J., and R. E. Worley. 2000. Alternate bearing intensity of pecan cultivars. *Hortscience* 35 (6): 1067-1069.
- de Jong, Y. L. C., and M. H. A. J. Herben. 2004. A tree-scattering model for improved propagation prediction in urban microcells. *Vehicular Technology, IEEE Transactions on* 53 (2): 503-513.
- Dobson, M. C. 1988. Diurnal and seasonal variation in the microwave dielectric constant of selected trees In *IGARSS*. IEEE.
- El-Rayes, M. A., and F. T. Ulaby. 1987. Microwave Dielectric Spectrum of Vegetation-Part I: Experimental Observations. *Geoscience and Remote Sensing, IEEE Transactions on* GE-25 (5): 541-549.
- ESA. 2011. *The radar equation*. European Space Ag.2011 [cited July 16 2011]. Available from [http://earth.esa.int/applications/data\\_util/SARDOCS/spaceborne/Radar\\_Courses/Radar\\_Course\\_III/radar\\_equation.htm](http://earth.esa.int/applications/data_util/SARDOCS/spaceborne/Radar_Courses/Radar_Course_III/radar_equation.htm).
- Geisler, M. 2012. *Pecans*. USDA 2012 [cited May 29 2012]. Available from [http://www.agmrc.org/commodities\\_\\_products/nuts/pecans.cfm](http://www.agmrc.org/commodities__products/nuts/pecans.cfm).

- Imhoff, M. L. 1995. A theoretical analysis of the effect of forest structure on synthetic aperture radar backscatter and the remote sensing of biomass. *Geoscience and Remote Sensing, IEEE Transactions on* 33 (2): 341-352.
- Karam, M. A., A. K. Fung, R. H. Lang, and N. S. Chauhan. 1992. A microwave scattering model for layered vegetation. *Geoscience and Remote Sensing, IEEE Transactions on* 30 (4): 767-784.
- Kovacs, J. M., C. V. Vandenberg, J. Wang, and F. Flores-Verdugo. 2008. The Use of Multipolarized Spaceborne SAR Backscatter for Monitoring the Health of a Degraded Mangrove Forest. *Journal of Coastal Research*: 248-254.
- Lee, W. S., V. Alchanatis, C. Yang, M. Hirafuji, D. Moshou, and C. Li. 2010. Sensing technologies for precision specialty crop production. *Computers and Electronics in Agriculture* 74 (1): 2-33.
- McCraw, D., M. W. Smith, and W. Reid. 2007. Pecan Crop Load Management Fact sheet HLA-6251.
- McDonald, K. C., M. C. Dobson, and F. T. Ulaby. 1991. Modeling multi-frequency diurnal backscatter from a walnut orchard. *Geoscience and Remote Sensing, IEEE Transactions on* 29 (6): 852-863.
- McNairn, H., J. Shang, C. Champagne, and X. Jiao. 2009. TerraSAR-X and RADARSAT-2 for crop classification and acreage estimation. In *Geoscience and Remote Sensing Symposium, 2009 IEEE International, IGARSS 2009*, II-898-II-901.
- Moazenpour, M., A. Farshad, and A. A. Abkar. 2006. Use of remote sensing (RS) in pistachio yield estimation. *Acta Hort.* 726: 464-470.

- Nelson, S. 1991. Dielectric Properties of Agricultural Products. *IEEE Transactions on Electrical Insulation* 26 (5): 845-869.
- Nelson, S. O., K. C. Lawrence, and A. W. Kraszewski. 1992. Sensing moisture content of pecans by RF impedance and microwave resonator measurements. *Transactions of the ASAE* 35 (2): 617-623.
- Paris, J. F. 1986. The effect of leaf size on the microwave backscattering by corn. *Remote Sensing of Environment* 19 (1): 81-95.
- Shao, Y., X. Fan, H. Liu, J. Xiao, S. Ross, B. Brisco, R. Brown, and G. Staples. 2001. Rice monitoring and production estimation using multitemporal RADARSAT. *Remote Sensing of Environment* 76 (3): 310-325.
- Shrestha, B. L., H. C. Wood, and S. Sokhansanj. 2007. Modeling of Vegetation Permittivity at Microwave Frequencies. *Geoscience and Remote Sensing, IEEE Transactions on* 45 (2): 342-348.
- Soria-Ruiz, J., H. McNairn, Y. Fernandez-Ordonez, and J. Bugden-Storie. 2007. Corn monitoring and crop yield using optical and RADARSAT-2 images. In *International Geoscience and Remote Sensing Symposium*. Barcelona: IEEE International.
- Trabelsi, S., and S. O. Nelson. 2004. Microwave dielectric properties of shelled and unshelled peanuts. *Transactions of the ASABE* 47 (4): 1215-1222.
- Ulaby, F. T., C. T. Allen, G. E. III, and E. Kanemasu. 1984. Relating the microwave backscattering coefficient to leaf area index. *Remote Sensing of Environment* 14 (1-3): 113-133.

- Ulaby, F. T., K. Sarabandi, K. McDonald, M. Whitt, and M. C. Dobson. 1990. Michigan microwave canopy scattering model. *International Journal of Remote Sensing* 11 (7): 1223-1253.
- Weckler, P. W., and M. W. Smith. 2011. Pecan development workshop. Ardmore, OK: USDA SCRI.
- Wells, M. L., and B. W. Wood. 2008. Foliar Boron and Nickel Applications Reduce Water-stage Fruit-split of Pecan. *Hortscience* 43 (5): 1437-1440.
- Wright, G. C., J. B. Storey, M. K. Harris, and P. T. Sprinz. 1990. Pre-harvest Pecan Yield Estimation. *Hortscience* 25 (6): 698-700.
- Ye, X., K. Sakai, A. Sasao, and S.-i. Asada. 2008. Potential of airborne hyperspectral imagery to estimate fruit yield in citrus. *Chemometrics and Intelligent Laboratory Systems* 90 (2): 132-144.

## CHAPTER IV

### IN SITU MEASUREMENT OF PECAN LEAF NITROGEN CONCENTRATION USING A CHLOROPHYLL METER AND VIS-NIR MULTISPECTRAL CAMERA

Abstract: Knowledge of foliar nitrogen (N) concentration is important in pecan [*Carya illinoensis* (Wang.) K. Koch] management protocols. Lower cost and/or rapid methods to determine foliar N are desirable and may result in improved management strategies as well as enable precision agricultural practices to be deployed in pecan production. This study investigates using a portable chlorophyll meter and Vis-NIR camera to rapidly determine pecan foliar N in situ. Relationships of SPAD values from a chlorophyll meter (Minolta SPAD 502Plus) and vegetative indices calculated from camera image data to foliar N determined by chemical analysis were investigated. SPAD readings were taken monthly from May through October on ‘Pawnee’, ‘Kanza’ and ‘Maramec’ pecan cultivars in Oklahoma in 2010. Images of the same ‘Pawnee’ and ‘Kanza’ trees were collected in September and October of 2010 with a truck mounted multispectral camera using ambient light. Correlation of foliar N to SPAD values was poor in May for all cultivars but distinct significant linear relationships were found for ‘Maramec’ and ‘Pawnee’ for each of the other months tested with  $R^2$  ranging from 0.40 to 0.87. Data from ‘Kanza’ had significant relationships in June and October with  $R^2$  of 0.39 and 0.72, respectively. Normalized difference vegetative index (NDVI) and reflectance data extracted from Vis-NIR camera images were significantly correlated to foliar N in both months of the study on ‘Pawnee’ but only in September for ‘Kanza’. The various relationships had  $R^2$  between 0.21 and 0.51.

## Introduction

Nitrogen management in pecan orchards is important for tree health, optimizing yield and managing alternate bearing (Conner and Worley 2000; Smith et al. 2007; Wood et al. 2004). Over application of N wastes resources and can cause environmental harm. Availability of N depends not only on fertilizer application rate, type and time, but also on a variety of cultural practices and environmental conditions including soil nutrients and properties, weather and climate, irrigation practices, tree condition, orchard floor management and nut production (McDonald et al. 1991; Soria-Ruiz et al. 2007; Ye et al. 2008). Soil tests and leaf analysis are used to measure N; however, leaf analysis is widely used commercially in pecan to assess N concentration during the growing season because it provides a direct measurement of nutrient status in the tree.

The traditional practice for measuring N levels in a pecan orchard consists of hand harvesting specific leaves that are then dried and sent off to a lab for chemical analysis. This process takes considerable time and is typically used to guide the subsequent year's fertility program rather than adjusting N in the current year. Generally only a subset of the trees in an orchard is tested to reduce cost. A sensor that provides an immediate indication of pecan foliar N in the field would be desirable if it provides adequate performance at a reasonable cost. Such a sensor would also be a key component to enable precision agriculture practices in pecan production.

Much of the N in a leaf is partitioned in chlorophyll, thus a sensor that measures chlorophyll can often be used to quantify the amount of N in a leaf (Filella et al. 1995). The basis for most optical sensing of N in leaves is based on chlorophyll's spectral response to light. Chlorophyll absorbs blue and red light ( $\lambda \approx 450$  and  $650$  nm, respectively) and reflects near infrared (NIR) light ( $\lambda > 750$  nm). The intensity of transmitted and/or reflected light at these wavelengths can be used to

form empirical relationships which estimate chlorophyll, and consequently, N concentration in a leaf (Richardson et al. 2002).

A SPAD meter (Konica Minolta, Osaka, Japan) is a handheld device that measures light intensity at wavelengths of 650 and 940 nm transmitted through a 2 by 3 mm area of a leaf clamped in the instrument. The SPAD meter calculates a unit-less value between 1 and 100 that has been shown to be positively correlated to leaf chlorophyll concentration. Regression analysis can then be used to predict foliar N from SPAD readings (Markwell et al. 1995). Originally developed for rice, SPAD meters have found utility on a variety of field and tree crops for predicting N concentrations (Chang and Robison 2003; Gianquinto et al. 2004; Neilsen et al. 1995; Perry and Davenport 2007; Simorte et al. 2001; van den Berg and Perkins 2004; Wood et al. 1992).

Reflectance measurements of Vis-NIR light have also been used to estimate chlorophyll and N status of plants. Normalized difference vegetative index (NDVI) is the most widely used measurement and is computed from the intensity of reflected red and NIR light using the following equation:  $NDVI = (I_{NIR} - I_{red}) / (I_{NIR} + I_{red})$ . Empirical relationships of NDVI to chlorophyll concentration and N status have been developed for many crops (Hansen and Schjoerring 2003; Jones et al. 2007; Ma et al. 1995; Plant et al. 2000; Reyniers and Vrindts 2006). NDVI can be calculated from remotely acquired multispectral digital camera images or from close-proximity sensors. Remote imaging systems generally measure reflected ambient light while some close proximity sensors collect reflected light that originates from the sensor itself (Jones et al. 2007). In both cases the intensity of incident light is required to accurately determine relative intensity of the reflected light to control sensor error.

At high levels of biomass, NDVI tends to become less sensitive to chlorophyll concentration because reflected red light intensity from leaves asymptotically approaches a minimum. In plant systems where chlorophyll density is high, vegetative indices (VI) that include green reflectance

may have better performance predicting foliar N than NDVI. Gitelson et al. (1996) compared NDVI to green-NDVI (GNDVI) obtained from satellite images of Norway maple (*Acer platanoides* L.) and horse chestnut (*Aesculus hippocastanum* L.) trees and found GNDVI resulted in more accurate predictions of chlorophyll content with full canopies. GNDVI is calculated from the intensities of reflected NIR and green light using the formula:  $GNDVI = (I_{NIR} - I_{green}) / (I_{NIR} + I_{green})$ . Numerous other VI using red, green and NIR reflected light have been proposed and evaluated on various plants over the years (Zarco-Tejada et al. 2005).

A SPAD meter and/or a suitable ground based multispectral camera may have utility for assessing the N status of pecan leaves in an orchard. The optical properties of leaves vary among plant species and can change throughout ontogeny and with growth conditions (Qi et al. 2003). Foliar N levels on fruiting and vegetative shoots of pecan decreased over the growing season (Diver et al. 1984). Chang and Robison (2003) found that the regression relationships of SPAD readings to foliar N concentration on four species of hardwood tree leaves were different among species and crown position, and changed throughout the growing season. In a similar study on citrus, Jifon et al. (2005) found that growth conditions resulted in a variation of leaf thickness and changed the regression relationship of SPAD readings to chlorophyll and N concentration. Similarly, corrections for variation in pecan leaf optical properties may need to be included in a measurement protocol using a SPAD meter or multispectral camera to measure foliar N.

The efficacy of multispectral cameras and/or portable chlorophyll meters to quantify N in pecan leaves has not been reported. The objectives of these experiments were to evaluate the performance of: 1) a SPAD meter and 2) a ground based Vis-NIR multispectral camera using ambient light for rapid in situ measurement of foliar N in a pecan orchard during the growing season.

## Materials and methods

### Site descriptions

The study contained trees in two locations in Oklahoma. An orchard near Cleveland, OK, USA contained 17-year-old ‘Pawnee’ and ‘Kanza’ pecan on ‘Giles’ seedling rootstocks with 12.2 by 12.2 m diagonal spacing. Soil was a Dennis silt loam (fine, mixed, active, thermic Aquic Argiudoll). Rainfall in this non-irrigated orchard during the study period (April through October 2010) was about 640 mm. A 1.8 m wide vegetation-free strip centered on the tree was maintained with selected herbicides while the remainder of the orchard floor was mowed as needed. Trees received commercial management for pests. Fertilizer treatments in the Cleveland, OK orchard were varied to induce greater variability of foliar N for this study (Table 8). All ‘Pawnee’ trees, and one subplot of ‘Kanza’, received a base rate of 280 kg·ha<sup>-1</sup> of diammonium phosphate (18N-20P-0K) applied in a continuous band 1.8 m from the trunk during March. Various subplots also received between 0 and 975 kg·ha<sup>-1</sup> of urea (46N-0P-0K) hand broadcast from the trunk to the drip line of the tree (Table 8). One subplot of ‘Kanza’ trees was seeded with ‘Durana’ white clover (*Trifolium repens* L.) and received no other N supplements. This orchard was used for both the SPAD and Vis-NIR camera studies.

A second orchard at the Cimarron Valley Research Station near Perkins, OK contained 25-year-old ‘Maramec’ trees on ‘Apache’ seedling rootstocks in a Teller sandy loam soil (fine-loamy, mixed, active, thermic Udic Argiustoll). Trees were diagonally spaced 24.4 by 24.4 m with Bermudagrass [*Cynodon dactylon* (L.) Pers.] ground cover. A 3 m wide vegetation-free area was maintained the entire row length with herbicides. Natural rainfall of 607 mm during the study period (Apr. through Oct. 2010) was supplemented by traveling gun irrigation. Commercial management for pests and fertilization were used. Diammonium phosphate and urea were each

applied in a band application at rate of 482 kg·ha<sup>-1</sup> of material in March of 2010. Ten trees were randomly selected within the orchard for the SPAD study (Table 8).

Table 8. Cultivar and nitrogen treatments for pecan trees in study.

Cultivar	Number of trees	Baserate (kg·ha <sup>-1</sup> N)	Urea (kg·ha <sup>-1</sup> N)
Pawnee	5	50	0
Pawnee	5	50	56
Pawnee	5	50	112
Pawnee	5	50	224
Pawnee	5	50	448
Kanza	5	0	0
Kanza	5	50	112
Kanza	5	0	'Durana' clover
Maramec	10	87	222

#### Sampling protocol – SPAD meter

Trees were sampled mid-month from May through October (Cleveland orchard) and April through September (Perkins orchard) in 2010. SPAD readings (SPAD 502Plus, Konica Minolta, Osaka, Japan) were taken by a technician standing on the ground from 10 middle leaflet pairs on the middle leaf of current season shoots approximately evenly spaced around the circumference of the tree canopy. Measurements were taken adjacent to the midrib at the middle of the leaflet with the adaxial surface of the leaflet was facing the light source of the SPAD meter. Individual SPAD readings were averaged for each tree. These same 10 leaflet pairs were collected and combined for elemental analysis. Leaves were dried and ground and then N concentration for each tree was determined using a Leco Truspec N analyzer (St. Joseph, MI, USA).

#### Sampling protocol and image processing – Vis-NIR multispectral camera

A multispectral camera (Duncan Tech MS3100, Auburn, CA) was used to obtain images of the same trees that were measured with the SPAD meter in the Cleveland, OK orchard. Images were

acquired on 15 Sept. and 13 Oct. 2010, the same day that the SPAD meter measurements were taken. The camera images were 1392 x 1040 pixels by 8-bits (256 intensity levels) in three optical wavebands centered at 550, 670 and 780 nm ( $\pm 10$  nm) through a 14 mm focal length lens. The camera was mounted on a truck at a height approximately 2.5m above ground level.

A reflectance target containing two panels with diffuse reflectance of 10 and 99% was mounted on a tripod, 1.8 m above ground level, facing the camera to provide a reference of solar irradiance in each image (Labsphere, Inc., Model SRT-SP-050, North Sutton, N.H.). It was located under the drip line of the tree so it was about the same distance from the camera as the near edge of the tree canopy. An image containing a pecan tree and the reflectance target was composed by positioning the truck so that the sun was directly behind the camera (Fig. 37). Distance from the camera to the trunk of each tree was between 6 and 10 m. Rows in the orchard were oriented east to west. Images were taken mid-morning on cloud free days, to insure that the sun directly illuminated a significant portion of the tree and the reflectance target. Images were saved to a portable computer which was also used to set gain and exposure of the camera. Gain and exposure time for each waveband were adjusted such that light from the 10 and 98% reflectance targets resulted in intensities in the linear range of the camera response and did not saturate the camera sensor. Target image intensities were 40 and 220 (out of 255) for the 10 and 99% reflectance targets, respectively. Camera gain and exposure time were set once at the start of each sampling date and remained constant for about 1.5 h while 40 trees in the sample were imaged (Table 9). At these gain and exposure settings, noise from the camera sensor was minimal even at low illumination levels (Weckler et al. 2002).

Table 9. Duncan Tech MS3100 camera gain and exposure settings for collecting pecan images

	Camera Gain setting			Exposure time (ms)		
	IR	Red	Green	IR	Red	Green
September	9.6	13.4	9.0	10.0	10.8	9.0
October	9.6	13.2	8.0	10.0	10.8	8.0

Images were processed using Matlab (MathWorks, Inc., Natick, MA) software (Appendix C). The location of the reflectance target was first selected from the image to obtain a reference intensity of red, green and NIR ambient light. A rectangle was then selected, roughly including the canopy area of each tree and excluding other objects, trees and grass in the background, from the tree image (Fig. 37). Image pixels outside the rectangle were cropped and not included in further analysis. Irradiance for each pixel was then extracted from the red, green and NIR cropped images. The intensity of each pixel in the three cropped images were then linearly normalized to a 0 to 255 scale using intensity values obtained from the 10 and 99% reflectance targets in the same image. This step allowed images of different trees to be compared to each other.



Fig. 37. Representative NIR image composition of pecan tree obtained with multispectral camera. Reflectance standard (a) is in lower left of image. Rectangle represents leaf area selected for analysis. (Image of 'Pawnee', row 2, tree 13, Oct. 2010).

Leaves are highly reflective to NIR radiation while branches, trunks and other materials generally are not. Pixels from the normalized NIR image with intensities within a threshold window were classified as leaf pixels (LP). Various threshold windows, with low NIR intensities ranging from

25 to 200 in increments of 25, were evaluated to classify LP. Threshold window spans were defined in two ways. One method set the high value 50 units above the lower limit and the other used 255 as the high intensity limit for all threshold windows. A vegetative index (VI) was calculated for each LP by using the appropriate individual pixel intensities of the NIR, green and red images for each threshold window. VI for each tree was the mean of the VI calculated for LP classified in each image. The optimum threshold window for classifying LP was determined by regression analysis.

### Statistical analysis

Data were analyzed using SAS MIXED (SAS Institute Inc., Cary, NC) using repeated measures. Regressions using least squares analysis techniques tested for significant main effects and interactions of SPAD, VI, cultivar, and sampling date to foliar N concentration. Linear, quadratic and cubic relationships of SPAD and VI to foliar N were investigated.

## Results and discussion

### Foliar nitrogen

Foliar N concentration ranged from 1.8% to 3.8 % of dry leaf mass across all samples (Fig. 38). Nitrogen levels fell with time ( $P < 0.0001$ ) during this study following expected seasonal variations.

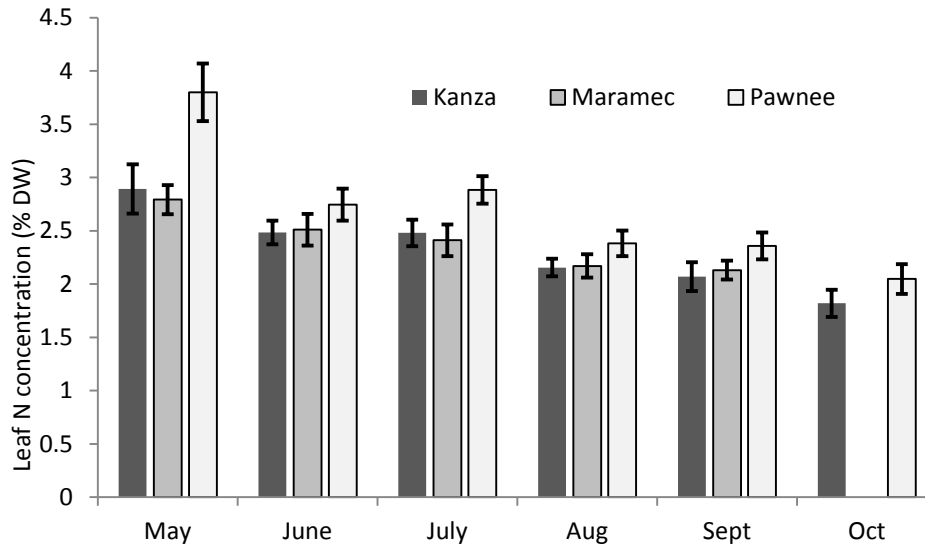


Fig. 38. Mass fraction of nitrogen in dried pecan leaves during 2010 growing season for ‘Kanza’ (n=15), ‘Maramec’ (n=10), and ‘Pawnee’ (n=25) trees. Bars on graph indicate standard deviation.

### SPAD meter

SPAD values varied from 26.2 to 52.3 with the lowest readings occurring in May (Fig. 39). Foliar N was generally positively correlated to SPAD readings but the specific relationships varied across the three cultivars and growing season. There was a significant cultivar by month interaction ( $P < 0.0001$ ) thus equations predicting foliar N from SPAD meter readings are reported for each cultivar by month (Table 10). No cultivar exhibited significant relationships between SPAD and foliar N in May, the first month of the study. Significant linear models were found for ‘Maramec’ and ‘Pawnee’ in all subsequent months. For ‘Kanza’, the only significant models found were in June and October. Correlation analysis shows that from 39% to 87% of the variation of leaf N was predicted by SPAD readings where significant relationships were found (Table 10 and Fig. 39). Higher order models did not result in improved correlations. Slopes of the regression equations generally decreased as the season progressed indicating the SPAD response to foliar N concentration was also declining.

Table 10. Equations for predicting foliar nitrogen concentration from SPAD readings on three cultivars of pecan.

Month	Kanza		Maramec		Pawnee	
	Equation	R <sup>2</sup>	Equation	R <sup>2</sup>	Equation	R <sup>2</sup>
May	--	NS	--	NS	--	NS
June	N= 0.29+0.055S	0.39*	N= -0.46+0.071S	0.75**	N= 0.03+0.060S	0.64***
July	--	NS	N= -0.17+0.056S	0.87***	N= 0.51+0.049S	0.47***
Aug	--	NS	N= 0.95+0.027S	0.58*	N= -0.92+0.067S	0.74***
Sept	--	NS	N= 0.66+0.032S	0.40*	N= -0.47+0.058S	0.67***
Oct	N= 0.32+0.037S	0.72***	---	---	N= 0.34+0.037S	0.66***

NS, \*, \*\*, \*\*\* Not significant (NS) or significant at 5% (\*), 1% (\*\*) or 0.1% (\*\*\*).

N = Leaf nitrogen concentration (% DW) S = Mean of 10 SPAD meter readings.



Researchers evaluating SPAD meters on other plant species have found patterns similar to the present study reflecting seasonal changes in foliar N and leaf optical properties. Chang and Robison (2003) found that SPAD readings on sweetgum (*Liquidambar styraciflura* L.) trees were positively correlated with foliar N, however, the regression relationships varied with sampling date and location in the crown. Seasonal physiological changes and environmental factors resulted in variation of leaf optical properties, which in turn affect response of the SPAD meter. These researchers improved correlation of the regression relationships by adding a term for foliar moisture content or by predicting N content on a leaf area basis instead of concentration by leaf mass. By dividing SPAD response by specific leaf weight (ratio of leaf dry weight to leaf area), Peng et al. (1993) were able to increase the coefficient of determination ( $R^2$ ) of the regression equations from 0.49 to 0.93 on five rice (*Oryza sativa* L.) cultivars. This correction essentially accounts for variation in leaf thickness among samples. Adding these or similar measures to the SPAD sampling protocol increases the duration and effort required to gather data thus negating some of the advantages inherent to the SPAD sampling protocol.

#### Vis-NIR multispectral camera

The distribution of the intensity of NIR leaf pixels (LP), after normalization to a 0 to 255 scale, was approximately lognormal with peak values ranging from 35 to 81 for all trees in the study. The distributions of pixel intensity in the red and green images were both maximum at zero intensity and green images were brighter than red (Fig. 40). The peak of the NIR histogram occurred at higher intensities for 'Kanza' than 'Pawnee' however there was no significant temporal difference (Table 11).

Table 11. Histogram peak intensity (S.E.) of NIR image pixels from images of ‘Pawnee’ and ‘Kanza’ pecan trees taken in 2010.

Month	Pixel intensity	
	Kanza	Pawnee
Sept	68.2 (3.5) a <sup>2</sup>	53.9 (2.5) b
Oct	63.9 (3.3) a	48.1 (2.6) b

<sup>2</sup>Means followed by the same letter are not significantly different by LSD test (P≤0.05).

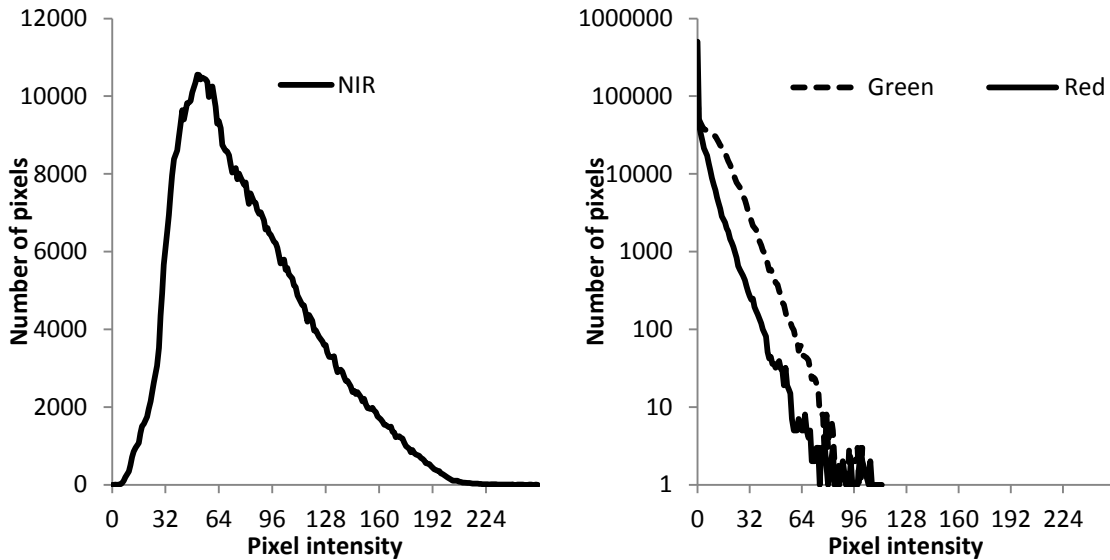


Fig. 40. Intensity distribution (0 to 255) of NIR, green and red pixels in leaf area image of representative pecan tree. (‘Pawnee’, row 2, tree 13, Oct. 2010).

At low NIR intensity thresholds, some of the reflected light was from branches and other non-leaf areas in the images. As the threshold level was raised to 150 (out of 255) most of the non-leaf reflections were removed from the images (Fig. 41). Raising the threshold level reduced the number of pixels remaining in the image for VI calculations. On several images in this study, no NIR pixels had intensity values above 200. Correlation coefficients of foliar N to NDVI and GNDVI obtained from linear regression were maximized when the NIR threshold window for classification of leaf pixels ranged from 150 to 200.

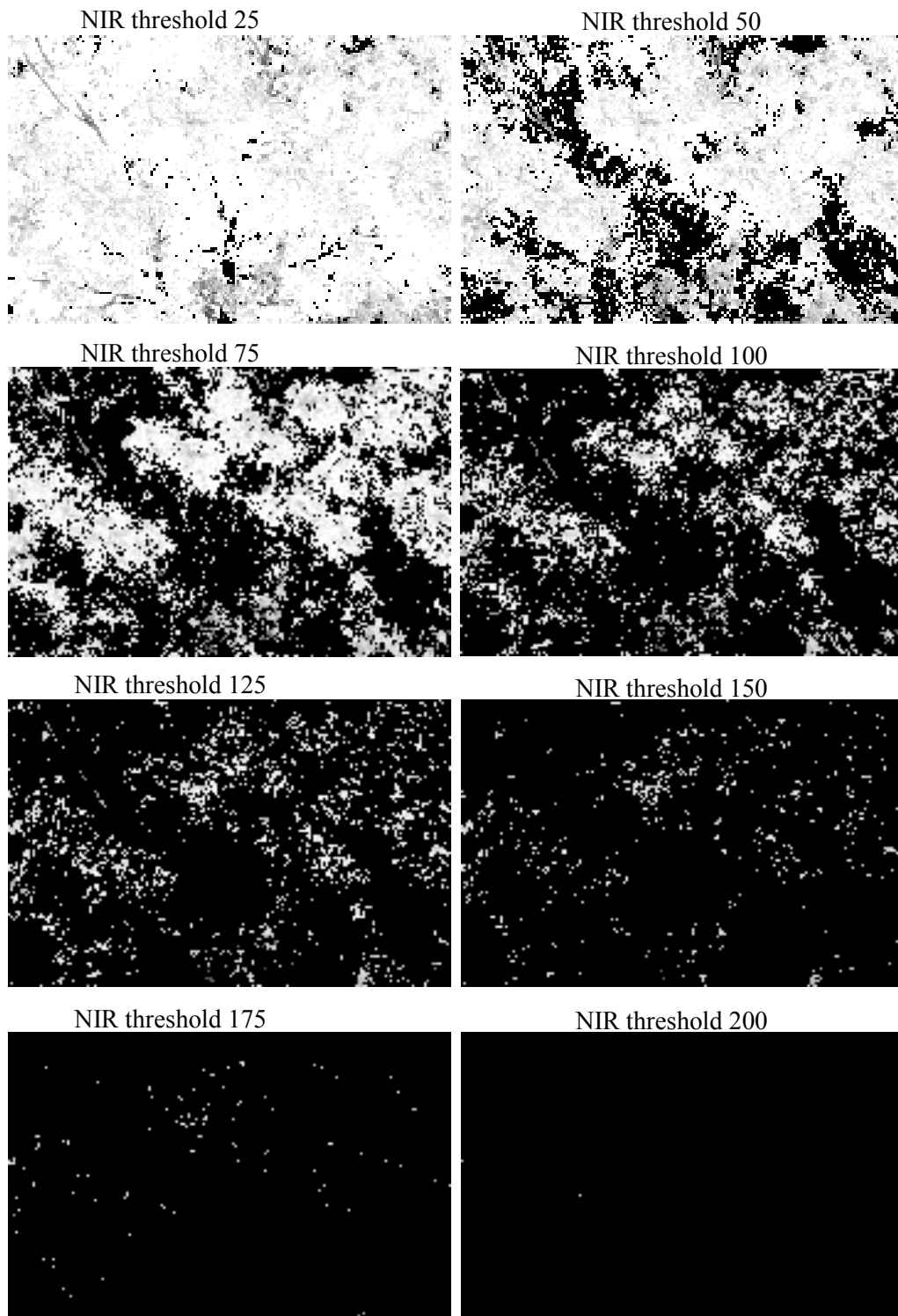


Fig. 41. Effect of NIR pixel threshold (0 to 255 scale) on leaf area image of a representative pecan tree. Black areas indicate pixels below the threshold. (Image of ‘Pawnee’, row 2, tree 13, Oct. 2010).

Linear models relating foliar N to NDVI and GNDVI were found for ‘Pawnee’ trees in both months of the study, although the correlation coefficients were generally low (Table 12). No simple regression models were identified for ‘Kanza’ however. The mean intensity of leaf pixels in the red image when using a threshold window of 150-200 was  $9.9 \pm 0.38$  S.E. This low value suggests that NDVI may be saturating and green reflectivity may provide additional predictive power to the model (Gitelson et al. 1996). The corresponding intensity of green pixels was higher at  $29.8 \pm 0.56$  S.E. Regression models using GNDVI did not have significantly better performance however (Table 12).

Table 12. Regression relationships of leaf N concentration to NDVI, GNDVI and green reflectance from images of ‘Pawnee’ and ‘Kanza’ pecan trees taken in 2010.

Month	Predictor variable(s)	Kanza		Pawnee	
		Equation	R <sup>2</sup>	Equation	R <sup>2</sup>
Sept	NDVI	--	NS	$N=3.122NDVI-0.344$	0.31**
Sept	GNDVI	--	NS	$N=2.157GNDVI+0.893$	0.21*
Sept	NDVI & Green	$N=-9.15NDVI-15.28G+12.77^z$	0.51*	$N=2.799NDVI-0.715G+0.038$	0.31*
Oct	NDVI	--	NS	$N=3.173NDVI-0.786$	0.29**
Oct	GNDVI	--	NS	$N=3.943GNDVI-0.879$	0.48***
Oct	NDVI & Green	--	NS	$N=0.162NDVI-8.279G+2.818$	0.48**

NS, \*, \*\*, \*\*\* Not significant (NS) or significant at 5% (\*), 1% (\*\*) or 0.1% (\*\*\*).

<sup>z</sup> N = leaf nitrogen concentration (% DW), NDVI and GNDVI are mean VI calculated from leaf pixels (LP) of tree images. G = mean intensity of green LP (0 to 1).

Multiple linear regression modeling using NIR, green and red reflected light intensity in addition to NDVI, and GNDVI as predictor variables for foliar N did not produce models superior to simple linear regressions. Relationships that included the mean intensity of reflected green light for LP and NDVI improved performance slightly and produced significant models for ‘Kanza’ in September and ‘Pawnee’ in both months of the study (Table 12). Correlations for these relationships were weak with maximum R<sup>2</sup> of 0.51.

## Conclusion

These experiments indicate that SPAD meters and in-field Vis-NIR cameras have potential to provide useful indications of pecan leaf N concentration for some cultivars of pecan. The change in instrument response due to seasonal and cultivar variation necessitates obtaining calibration equations for each pecan cultivar at selected growth stages. The correlation of SPAD and/or Vis-NIR camera image data to leaf N was generally low. Improvements are needed before the tested protocols can replace traditional foliar N analysis. These protocols may, however, provide a useful alternative to chemical analysis in cases where rapid and/or relative foliar N measurements are needed.

## References

- Chang, S. X., and D. J. Robison. 2003. Nondestructive and rapid estimation of hardwood foliar nitrogen status using the SPAD-502 chlorophyll meter. *Forest Ecology and Management* 181 (3): 331-338.
- Conner, P. J., and R. E. Worley. 2000. Alternate bearing intensity of pecan cultivars. *Hortscience* 35 (6): 1067-1069.
- Diver, S. G., M. W. Smith, and R. W. McNew. 1984. Influence of fruit development on seasonal elemental concentrations and distribution in fruit and leaves of pecan. *Communications in Soil Science and Plant Analysis* 15 (6): 619-637.
- Filella, I., L. Serrano, J. Serra, and J. Peñuelas. 1995. Evaluating wheat nitrogen status with canopy reflectance indices and discriminant analysis. *Crop Sci.* 35 (5): 1400-1405.
- Gianquinto, G., J. Goffart, M. Olivier, G. Guarda, M. Colauzzi, L. Dalla Costa, G. Delle Vedove, J. Vos, and D. Mackerron. 2004. The use of hand-held chlorophyll meters as a tool to assess the nitrogen status and to guide nitrogen fertilization of potato crop. *Potato Research* 47 (1): 35-80.
- Gitelson, A. A., Y. J. Kaufman, and M. N. Merzlyak. 1996. Use of a green channel in remote sensing of global vegetation from EOS-MODIS. *Remote Sensing of Environment* 58 (3): 289-298.
- Hansen, P. M., and J. K. Schjoerring. 2003. Reflectance measurement of canopy biomass and nitrogen status in wheat crops using normalized difference vegetation indices and partial least squares regression. *Remote Sensing of Environment* 86 (4): 542-553.

- Jifon, J. L., J. P. Syvertsen, and E. Whaley. 2005. Growth environment and leaf anatomy affect nondestructive estimates of chlorophyll and nitrogen in citrus sp. leaves. *Journal of the American Society for Horticultural Science* 130 (2): 152-158.
- Jones, C. L., N. O. Maness, M. L. Stone, and R. Jayasekara. 2007. Chlorophyll estimation using multispectral reflectance and height sensing. *Transactions of the ASABE* 50 (5): 1867-1872.
- Ma, B. L., M. J. Morrison, and L. M. Dwyer. 1995. Canopy light reflectance and field greenness to assess nitrogen fertilization and yield of maize. *Agron. J.* 88 (6): 915-920.
- Markwell, J., J. Osterman, and J. Mitchell. 1995. Calibration of the Minolta SPAD-502 leaf chlorophyll meter. *Photosynthesis Research* 46 (3): 467-472.
- McDonald, K. C., M. C. Dobson, and F. T. Ulaby. 1991. Modeling multi-frequency diurnal backscatter from a walnut orchard. *Geoscience and Remote Sensing, IEEE Transactions on* 29 (6): 852-863.
- Neilsen, D., E. J. Hogue, G. H. Neilsen, and P. Parchomchuk. 1995. Using SPAD-502 values to assess the nitrogen status of apple trees. *HortScience* 30 (3): 508-512.
- Peng, S., F. V. García, R. C. Laza, and K. G. Cassman. 1993. Adjustment for specific leaf weight improves chlorophyll meter's estimate of rice leaf nitrogen concentration. *Agron. J.* 85 (5): 987-990.
- Perry, E. M., and J. R. Davenport. 2007. Spectral and spatial differences in response of vegetation indices to nitrogen treatments on apple. *Computers and Electronics in Agriculture* 59 (1-2): 56-65.

- Plant, R. E., D. S. Munk, B. R. Roberts, R. L. Vargas, D. W. Rains, R. L. Travis, and R. B. Hutmacher. 2000. Relationships between remotely sensed reflectance data and cotton growth and yield. *Transactions of the ASAE* 43 (3): 535-546.
- Qi, Y., S. Bai, and G. M. Heisler. 2003. Changes in ultraviolet-B and visible optical properties and absorbing pigment concentrations in pecan leaves during a growing season. *Agricultural and Forest Meteorology* 120 (1-4): 229-240.
- Reyniers, M., and E. Vrindts. 2006. Measuring wheat nitrogen status from space and groundbased platform. *International Journal of Remote Sensing* 27 (3): 549-567.
- Richardson, A. D., S. P. Duigan, and G. P. Berlyn. 2002. An evaluation of noninvasive methods to estimate foliar chlorophyll content. *New Phytologist* 153 (1): 185-194.
- Simorte, V., G. Bertoni, C. Dupraz, and P. Masson. 2001. Assessment of nitrogen nutrition of walnut trees using foliar analysis and chlorophyll measurements. *Journal of Plant Nutrition* 24 (10): 1645-1660.
- Smith, M. W., C. T. Rohla, and N. O. Maness. 2007. Correlations of crop load and return bloom with root and shoot concentrations of potassium, nitrogen, and nonstructural carbohydrates in pecan. *J. Amer. Soc. Hort. Sci.* 132 (1): 44-51.
- Soria-Ruiz, J., H. McNairn, Y. Fernandez-Ordenez, and J. Bugden-Storie. 2007. Corn monitoring and crop yield using optical and RADARSAT-2 images. In *International Geoscience and Remote Sensing Symposium*. Barcelona: IEEE International.
- van den Berg, A. K., and T. D. Perkins. 2004. Evaluation of a portable chlorophyll meter to estimate chlorophyll and nitrogen contents in sugar maple (*Acer saccharum* Marsh.) leaves. *Forest Ecology and Management* 200 (1-3): 113-117.

- Weckler, P. R., J. B. Solie, M. L. Stone, R. S. Jayasekara, and C. N. Washmon. 2002. Airborne Collection of NDVI Data on Winter Wheat in Oklahoma. In *2002 ASAE Annual Meeting*. Chicago: ASAE.
- Wood, B. W., P. J. Conner, and R. E. Worley. 2004. Insight into alternate bearing of pecan. *Acta Hort.* 636: 617-629.
- Wood, C. W., P. W. Tracy, D. W. Reeves, and K. L. Edmisten. 1992. Determination of cotton nitrogen status with a handheld chlorophyll meter. *Journal of plant nutrition* 15 (9): 1435.
- Ye, X., K. Sakai, S.-i. Asada, and A. Sasao. 2008. Application of narrow-band TBVI in estimating fruit yield in citrus. *Biosystems Engineering* 99 (2): 179-189.
- Zarco-Tejada, P. J., S. L. Ustin, and M. L. Whiting. 2005. Temporal and Spatial Relationships between Within-Field Yield Variability in Cotton and High-Spatial Hyperspectral Remote Sensing Imagery. *Agron. J.* 97 (3): 641-653.

## CHAPTER V

### CONCLUSION

This research investigated three sensor technologies for rapid and in situ measurement of plant physical and physiological conditions. Quantification of waxes that occur on all aerial plant surfaces using Fourier transform infrared spectroscopy with attenuated total reflectance (FTIR-ATR) optics is a novel application of this technology that may assist producers, processors and plant breeders investigating the plant cuticle. Research on backscattered microwaves from pecan tree canopy samples is the first step in developing a new method to estimate pecan yield using short-range terrestrial radar systems. The third area of research investigated optical sensor technologies for more efficient measurements of foliar nitrogen concentration in pecan orchards.

Quantification of cuticular wax on spinach leaves empirically determined from Fourier transform infrared spectroscopy with attenuated total reflectance (FTIR-ATR) measurements resulted in predictions that correlated well to results obtained from gas chromatography (GC). This new method is in situ, requires minimal sample preparation, and can measure waxes in a small area defined by the active sensing region of the FTIR-ATR optics. It does not have the ability to provide detailed information about composition of the extracted waxes that GC does however.

Further research on this new method will likely ultimately depend on the application. There are opportunities to improve accuracy and precision, robustness, and to extend the method to other plant organs and species. Contact between the internally reflecting element (IRE) and the leaf

sample are critically important and the current leaf clamping method could be optimized to maintain uniform and repeatable pressure. This would be especially important for fragile specimens where cell disruption causes interference as was observed when testing rehydrated spinach leaves. An important attribute of robust measuring systems is the detection of invalid or suspect sensor readings. In our system, this can be caused by foreign material, poor IRE to leaf contact, cell disruption, and other conditions. Identification of spectral features that indicate sensor faults would enhance the measurement protocol.

These empirical wax prediction models were developed from GC measurements of extracted cuticular wax. Crosschecking our results against other methods of wax measurement would increase confidence in the models. Our attempts to measure cuticle cross section thickness on transmission electron microscope images were not successful. Improvements to the chemical fixation protocols, cryo-fixation, and/or scanning electron microscope imaging, may result in a method to validate FTIR-ATR measurements. It may also allow extension of the FTIR-ATR method to quantify thickness of the entire cuticle membrane, which may be of interest to some researchers.

Precision agriculture applications rely on sensing of crop parameters on a fine scale so that treatments can be applied at the correct amount only where needed. Pecans present an untapped opportunity for application of precision agriculture practices to improve efficiency and production. In situ yield estimates of nuts and quantification of foliar nitrogen concentration were investigated as two enabling technologies for precision agriculture in pecans.

Laboratory experiments indicated that backscattered microwaves from pecan tree canopy components may be useful for measuring biomass with short-range radars located within an orchard. Reflected signal strength across a large portion of the 1 to 18 GHz frequency range tested was positively correlated to water and dry matter mass in the canopy samples ( $R^2 > 0.63$  and

0.78 respectively). More research will be required to extend these initial findings into a method for quantifying nut yield in an orchard. Scenarios for discerning nut yield from canopy reflectance data are undefined but are likely to involve spatial comparisons of canopy biomass throughout the growing season as nuts grow in size and mature. A three dimensional map of canopy biomass in an orchard may be obtained by adding range finding capabilities to the backscattered microwave biomass estimates and incorporating precision global positioning system data. Capabilities of the microwave sensor itself (power, directionality, gain, polarity, bandwidth and frequency) will also need to be optimized for the measurement system.

Current protocols for assessing nitrogen needs in pecan involve laboratory analysis of manually harvested leaves. In addition to being time consuming, these methods are too costly for producers to measure every tree in an orchard. In field tests, a hand-held chlorophyll meter resulted in significant distinct linear relationships predicting leaf nitrogen for various months and cultivars in the study, but the correlations were weak ( $R^2$  ranged from 0.21 to 0.87). Measuring leaf nitrogen with a hand-held meter remains a manual process although it provides immediate results and lab fees are eliminated. In related research, equations predicting leaf nitrogen were computed from pecan tree canopy images obtained with a high resolution, visible and near infrared camera mounted on a vehicle maneuvered through the rows of the orchard. The best nitrogen prediction models used normalized difference vegetative index and green reflectance extracted from the camera image data. Correlations obtained in these experiments were weak ( $R^2$  between 0.21 and 0.51 for months and cultivars with significant linear relationships) and insufficient for replacing traditional manual methods of measuring leaf nitrogen. Additional research to improve the nitrogen prediction models is needed. Important areas of investigation are pecan leaf spectral characteristics throughout ontogeny and changes to how images are acquired. Once an understanding of leaf reflectance is complete, subtle changes to the sensor filters, especially in the red region, can be investigated to improve performance. The experiments

performed here used reflected ambient light. This imposes restrictions on the times and orientations from which camera images can be acquired in an orchard and the illuminating solar spectrum may not be optimal for sensing leaf nitrogen. A sensor with its own light source may be able to overcome these limitations.

Sensor technologies can improve efficiency and enable new capabilities in agriculture production, processing and research. Each of the sensing technologies investigated in this research show promise for rapid in situ measurement of plant physical and physiological conditions. With additional research, they may also have utility on other plants and cropping systems.

## APPENDIX A

### LEAF AND CUTICULAR WAX DATA FROM GC AND FTIR-ATR MODELS

Table A13. Composition of cuticular waxes from fast and slow growth spinach leaves for training, validation and field grown samples. Amounts are determined by gas chromatography from mid-leaf extractions of abaxial and adaxial surfaces.

Sample	Age (d)	Growth type	Leaf side	Leaf area (cm <sup>2</sup> )	GC results (ug/cm <sup>2</sup> )							Total wax
					Alcohols		Alkanes					
					24C	26C	29C	29C	29C	29C	29C	
Train 1	54	Fast	Bot	29.0	0.44	0.50	0.10	0.12	1.00	0.15	0.18	2.49
Train 2	54	Fast	Top	29.0	0.42	0.82	0.08	0.09	0.93	0.15	0.20	2.70
Train 3	54	Fast	Bot	31.5	0.23	0.73	0.15	0.10	2.03	0.14	0.18	3.55
Train 4	54	Fast	Top	31.5	0.20	0.50	0.08	0.05	1.15	0.08	0.19	2.25
Train 5	54	Slow	Bot	37.0	0.96	0.45	0.13	0.13	0.66	0.16	0.13	2.62
Train 6	54	Slow	Top	37.0	0.85	0.62	0.09	0.07	0.53	0.09	0.10	2.36
Train 7	54	Slow	Bot	42.0	0.81	0.24	0.04	0.05	0.21	0.05	0.05	1.46
Train 8	54	Slow	Top	42.0	0.91	0.50	0.09	0.08	0.32	0.09	0.09	2.09
Train 9	48	Fast	Bot	24.7	0.30	0.53	0.05	0.00	1.49	0.00	0.00	2.37
Train 10	48	Fast	Top	24.7	0.41	0.83	0.04	0.00	1.21	0.00	0.00	2.49
Train 11	48	Fast	Bot	27.3	0.27	0.59	0.01	0.00	1.41	0.00	0.00	2.28
Train 12	48	Fast	Top	27.3	0.29	0.52	0.01	0.00	1.05	0.00	0.00	1.86
Train 13	48	Slow	Bot	16.0	0.51	0.33	0.02	0.00	0.42	0.00	0.00	1.28
Train 14	48	Slow	Top	16.0	0.70	0.66	0.08	0.02	0.86	0.00	0.05	2.37
Train 15	48	Slow	Bot	16.4	0.62	0.31	0.00	0.00	0.16	0.00	0.00	1.09
Train 16	48	Slow	Top	16.4	0.73	0.84	0.00	0.00	0.21	0.00	0.00	1.79
Train 17	63	Fast	Bot	23.2	0.38	0.89	0.15	0.08	2.01	0.10	0.12	3.73
Train 18	63	Fast	Top	23.2	0.26	0.59	0.11	0.07	1.19	0.13	0.14	2.48
Train 19	63	Fast	Bot	22.7	0.25	0.77	0.16	0.15	2.27	0.23	0.23	4.07
Train 20	63	Fast	Top	22.7	0.21	0.85	0.21	0.25	2.11	0.40	0.37	4.39
Train 21	42	Fast	Bot	27.4	0.90	0.47	0.06	0.06	0.58	0.06	0.09	2.23
Train 22	42	Fast	Top	27.4	0.88	0.70	0.09	0.09	0.64	0.12	0.14	2.66
Train 23	42	Fast	Bot	32.3	0.74	0.43	0.11	0.12	0.64	0.12	0.13	2.29
Train 24	42	Fast	Top	32.3	0.76	0.41	0.13	0.14	0.77	0.17	0.17	2.55
Train 25	63	Slow	Bot	25.3	1.32	0.46	0.18	0.20	0.80	0.25	0.22	3.43
Train 26	63	Slow	Top	25.3	1.08	0.56	0.09	0.10	0.42	0.12	0.11	2.49
Train 27	63	Slow	Bot	20.6	0.70	0.71	0.14	0.15	1.02	0.21	0.19	3.11
Train 28	63	Slow	Top	20.6	1.33	1.97	0.22	0.19	1.33	0.24	0.25	5.54

Val 1	54	Fast	Bot	38.7	0.37	0.38	0.10	0.10	1.10	0.14	0.19	2.37
Val 2	54	Fast	Top	38.7	0.69	0.82	0.08	0.08	0.71	0.12	0.15	2.65
Val 3	54	Fast	Bot	41.8	0.50	0.63	0.08	0.05	1.19	0.08	0.17	2.70
Val 4	54	Fast	Top	41.8	0.70	0.75	0.08	0.06	0.93	0.10	0.16	2.77
Val 5	54	Slow	Bot	24.5	1.00	0.47	0.11	0.08	0.57	0.09	0.09	2.42
Val 6	54	Slow	Top	24.5	1.12	1.12	0.13	0.12	0.64	0.13	0.13	3.39
Val 7	54	Slow	Bot	15.7	1.03	0.43	0.12	0.13	0.56	0.16	0.15	2.57
Val 8	54	Slow	Top	15.7	1.40	1.39	0.12	0.06	0.71	0.08	0.12	3.88
Val 9	54	Slow	Bot	21.4	0.99	0.44	0.13	0.07	0.63	0.08	0.09	2.42
Val 10	54	Slow	Top	21.4	1.14	0.71	0.16	0.10	0.50	0.10	0.10	2.81
Val 11	61	Fast	Bot	82.4	0.28	0.54	0.05	0.02	1.41	0.09	0.19	2.59
Val 12	61	Fast	Top	82.4	0.20	0.46	0.04	0.02	1.08	0.05	0.13	1.98
Val 13	61	Fast	Bot	90.2	0.33	0.51	0.09	0.03	1.54	0.07	0.12	2.67
Field 1	63	Field	Bot	31.5	0.27	0.51	0.03	0.00	1.54	0.01	0.07	2.43
Field 2	63	Field	Top	31.5	0.42	0.40	0.00	0.00	0.73	0.00	0.03	1.57
Field 3	63	Field	Bot	47.0	0.44	0.98	0.13	0.01	2.25	0.11	0.19	4.12
Field 4	63	Field	Top	47.0	0.45	0.63	0.05	0.00	1.11	0.01	0.06	2.32
Field 5	63	Field	Bot	34.0	0.33	0.75	0.21	0.00	1.53	0.01	0.05	2.87
Field 6	63	Field	Top	34.0	0.56	0.77	0.03	0.00	0.96	0.01	0.05	2.37
Field 7	63	Field	Bot	99.0	0.81	0.83	0.10	0.00	1.43	0.03	0.05	3.26
Field 8	63	Field	Top	99.0	0.54	0.75	0.01	0.00	1.05	0.00	0.00	2.35

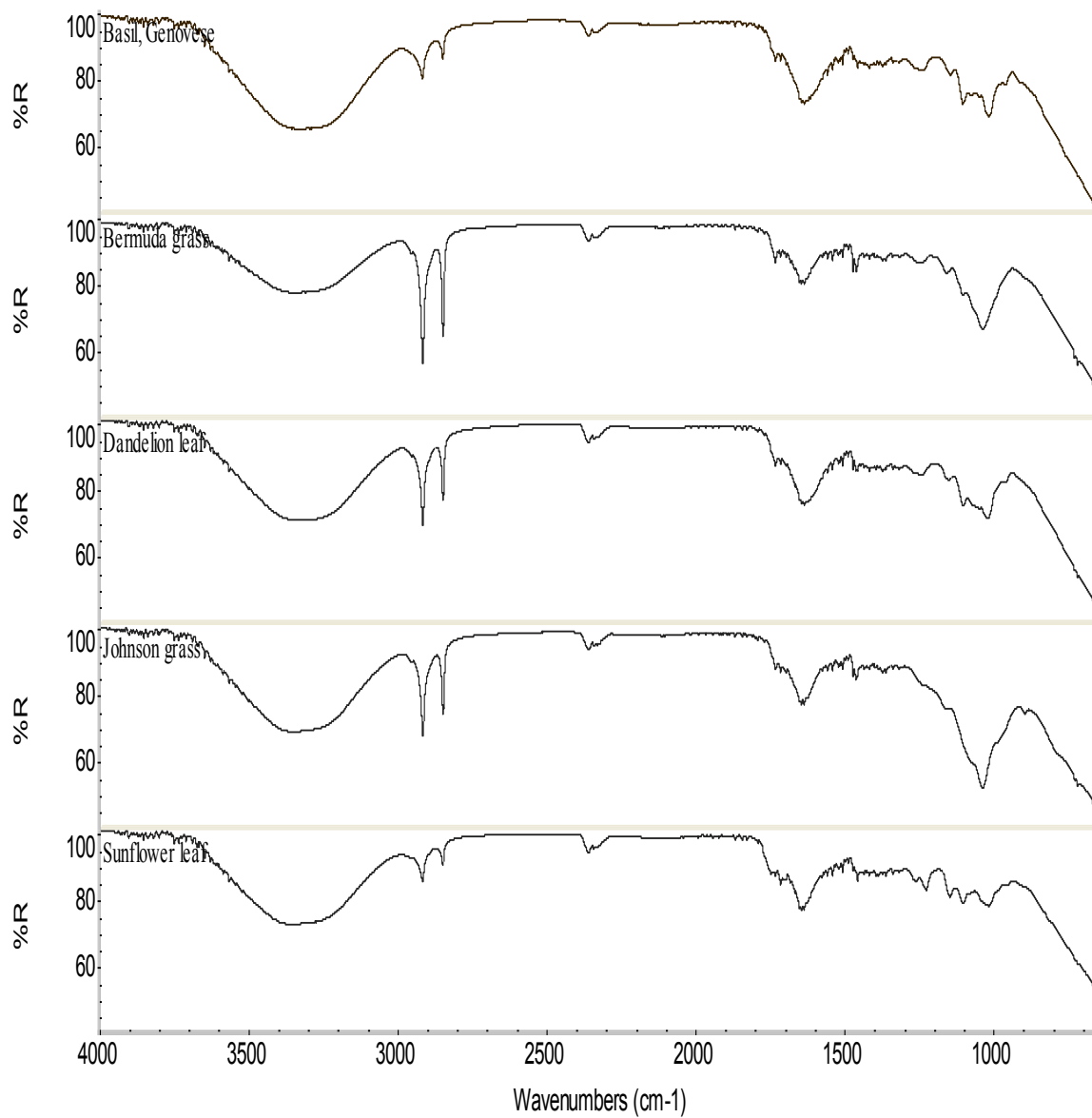
Table A14. Cuticular wax load predicted on spinach leaves for training, validation and field grown samples for each of the 14 best performing models with 4 or 5 predictor frequencies.

Sample	Predicted wax (ug/cm <sup>2</sup> )													
	Model number													
	1	2	3	4	5	6	7	8	9	10	11	12	13	14
Train 1	2.48	2.42	2.53	2.30	2.45	2.42	2.63	2.18	2.15	2.33	2.09	2.32	2.36	2.31
Train 2	2.46	2.16	2.39	2.32	2.31	2.31	2.07	2.29	2.71	2.78	2.43	2.52	2.62	2.56
Train 3	3.57	3.53	3.38	3.45	3.33	3.39	3.40	3.47	3.47	3.59	3.64	3.55	3.56	3.60
Train 4	3.01	2.86	3.27	2.86	3.11	3.14	3.14	2.85	3.05	2.93	2.75	3.03	3.04	3.08
Train 5	2.44	2.48	2.48	2.45	2.39	2.42	2.45	2.42	2.39	2.42	2.56	2.32	2.37	2.40
Train 6	2.22	2.15	2.37	2.11	2.35	2.31	2.32	1.99	2.24	2.10	2.05	2.10	2.24	2.25
Train 7	1.70	1.93	1.64	1.92	1.92	1.81	1.76	1.99	1.85	1.78	1.71	1.74	1.69	1.82
Train 8	2.21	2.41	2.48	2.39	2.64	2.53	2.61	2.21	2.29	2.19	2.01	2.16	2.23	2.28
Train 9	2.14	2.28	2.34	2.16	2.36	2.53	2.56	2.68	1.94	1.91	2.14	2.26	2.02	2.07
Train 10	2.26	2.70	2.42	2.73	2.34	2.39	2.27	2.54	2.44	2.26	2.77	2.48	2.34	2.42
Train 11	2.01	1.76	1.86	1.93	1.98	2.04	1.82	2.21	2.35	2.19	1.96	2.14	2.08	2.19
Train 12	2.50	2.27	2.41	2.26	2.45	2.43	2.29	2.43	2.54	2.57	2.40	2.53	2.57	2.57
Train 13	1.08	0.92	1.12	0.92	0.85	0.98	1.07	0.89	1.12	1.19	1.08	1.12	1.16	1.04

Train 14	1.96	2.06	2.04	2.13	2.05	1.98	2.00	1.81	2.03	1.88	2.07	1.86	1.93	1.93
Train 15	1.31	1.64	1.28	1.60	1.29	1.30	1.44	1.63	1.31	1.26	1.58	1.31	1.22	1.28
Train 16	1.68	1.86	1.64	1.77	1.66	1.58	1.75	1.61	1.55	1.76	1.58	1.62	1.67	1.61
Train 17	3.43	3.43	3.15	4.04	3.55	3.31	3.37	3.55	4.00	3.43	3.51	3.43	3.33	3.37
Train 18	3.04	2.80	2.67	3.02	2.69	2.69	2.72	2.73	3.20	3.11	3.42	3.00	3.08	2.97
Train 19	4.26	4.39	4.17	4.32	4.27	4.33	4.32	4.44	4.13	4.22	3.99	4.31	4.17	4.24
Train 20	4.29	4.27	4.41	4.44	4.31	4.35	4.24	4.25	4.50	4.31	4.33	4.40	4.34	4.37
Train 21	2.50	2.46	2.51	2.41	2.57	2.49	2.60	2.52	2.26	2.39	2.41	2.43	2.41	2.32
Train 22	2.59	2.62	2.34	2.66	2.52	2.38	2.29	2.63	2.62	2.85	2.54	2.62	2.67	2.59
Train 23	2.27	2.09	2.09	2.04	2.07	2.01	2.23	2.09	1.98	2.10	2.09	2.14	2.17	2.05
Train 24	2.25	2.36	2.56	2.42	2.48	2.63	2.42	2.35	2.40	2.25	2.94	2.37	2.33	2.35
Train 25	3.24	3.23	3.27	3.10	3.15	3.17	3.07	3.21	3.14	3.30	3.06	3.22	3.21	3.29
Train 26	2.67	2.40	2.76	2.31	2.57	2.77	2.64	2.77	2.77	2.63	2.75	2.77	2.81	2.84
Train 27	3.63	3.57	3.32	3.26	3.42	3.38	3.51	3.64	3.20	3.53	3.21	3.55	3.58	3.52
Train 28	4.91	5.04	5.10	4.75	4.97	4.97	5.02	4.69	4.44	4.88	5.03	4.78	4.90	4.78
Val 1	2.90	3.55	4.16	3.24	4.37	4.12	4.16	3.07	2.33	2.84	2.14	2.82	2.75	2.68
Val 2	3.29	3.72	4.62	3.54	4.65	4.44	4.23	3.44	3.05	3.52	2.69	3.37	3.35	3.27
Val 3	3.46	4.24	4.77	4.09	5.08	4.89	4.83	3.99	3.04	3.33	3.07	3.49	3.23	3.22
Val 4	3.53	4.14	4.90	3.99	4.90	4.87	4.72	4.19	3.21	3.56	3.20	3.71	3.43	3.38
Val 5	2.33	2.01	2.93	2.18	2.75	2.69	2.60	2.49	2.55	2.22	1.85	2.37	2.28	2.35
Val 6	2.29	1.95	2.84	2.05	2.67	2.58	2.55	1.91	2.42	2.16	1.84	2.24	2.37	2.31
Val 7	3.31	2.95	3.85	2.93	3.61	3.59	3.55	3.42	3.21	3.25	2.77	3.26	3.25	3.24
Val 8	3.12	3.66	4.35	3.54	4.28	4.16	3.98	3.40	3.14	3.15	2.93	3.29	3.20	3.27
Val 9	2.20	3.04	3.77	3.09	3.64	3.80	3.40	2.99	2.58	2.12	3.13	2.54	2.28	2.49
Val 10	2.52	3.08	4.34	3.17	4.03	4.23	3.77	3.17	3.03	2.43	3.08	2.89	2.71	2.90
Val 11	3.02	2.70	2.58	2.64	2.76	2.81	2.71	3.42	2.88	3.28	2.68	3.11	2.95	3.00
Val 12	2.43	1.86	1.71	1.75	1.88	1.84	1.88	2.33	2.10	2.78	2.06	2.33	2.41	2.25
Val 13	3.25	2.46	1.95	2.47	2.72	2.06	2.46	2.87	2.79	3.58	1.27	2.90	3.07	2.87
Field 1	3.04	3.77	3.40	3.33	3.44	3.69	3.59	3.05	2.52	2.84	3.12	3.10	2.98	3.06
Field 2	2.53	3.30	2.56	3.00	2.73	2.95	2.74	2.71	2.24	2.67	2.93	2.72	2.57	2.60
Field 3	3.03	4.37	3.81	4.03	3.75	4.45	3.83	3.34	3.04	2.72	4.05	3.50	3.23	3.50
Field 4	3.47	4.85	3.89	4.65	3.98	4.46	3.81	3.72	3.62	3.48	4.60	3.95	3.71	3.93
Field 5	3.37	4.83	3.09	4.29	3.52	3.74	3.74	3.37	2.62	3.38	3.45	3.38	3.23	3.26
Field 6	3.48	4.96	3.01	4.54	3.43	3.67	3.48	3.30	2.99	3.80	3.80	3.58	3.52	3.52
Field 7	3.15	4.30	3.25	4.08	3.64	3.74	3.44	3.29	2.97	3.10	3.55	3.31	3.16	3.29
Field 8	3.77	4.73	3.63	4.73	3.72	4.00	3.44	3.76	3.90	4.11	4.92	4.05	3.94	4.00

## APPENDIX B

REPRESENTATIVE FTIR-ATR SPECTRAL PROFILES FROM ADAXIAL SURFACE OF GENOVESE BASIL, BERMUDA GRASS, DANDELION LEAF, JOHNSON GRASS AND SUNFLOWER LEAF.



## APPENDIX C

### CUTICULAR WAX PREDICTIONS ON FRESH AND REHYDRATED DRIED LEAVES

Table B15. Cuticular wax predicted on fresh spinach leaves (n=48) by each of the 14 best performing models with 4 or 5 predictor frequencies.

Sample	Predicted wax on fresh leaf by each model ( $\mu\text{g}/\text{cm}^2$ )													
	1	2	3	4	5	6	7	8	9	10	11	12	13	14
1	2.91	3.83	2.42	5.22	3.84	1.92	2.67	2.56	2.85	2.44	2.58	3.15	3.38	3.99
2	3.60	5.76	3.58	7.90	5.54	2.53	3.89	4.16	3.89	3.21	3.71	3.85	4.59	5.87
3	3.54	4.67	3.41	6.50	5.10	2.88	3.73	3.34	3.60	3.20	3.42	3.86	4.03	5.25
4	3.06	4.19	3.42	5.13	4.40	1.61	3.88	3.62	3.16	2.58	2.77	4.22	3.91	3.73
5	3.32	4.98	3.11	7.33	5.04	2.63	3.32	3.88	3.43	2.96	3.26	3.40	3.89	5.64
6	3.09	4.64	3.26	6.33	4.75	1.76	3.77	4.09	3.33	2.62	2.95	3.89	4.18	4.69
7	3.54	4.44	3.14	6.21	4.91	2.83	3.41	2.88	3.60	3.14	3.34	3.66	4.26	5.13
8	3.32	5.38	2.69	6.95	4.48	2.51	2.86	3.45	3.44	2.94	3.33	3.04	4.01	4.90
9	3.04	4.57	3.33	5.60	4.39	2.22	3.76	3.72	3.34	2.76	3.10	3.71	3.95	4.14
10	2.61	4.54	2.91	6.03	4.54	1.76	3.53	3.30	3.16	2.43	2.91	3.32	3.95	4.43
11	3.11	4.42	2.53	6.70	4.53	2.40	2.79	3.17	3.28	2.69	3.01	2.93	4.15	5.37
12	2.39	4.37	2.65	5.56	4.10	1.13	3.16	3.00	2.83	2.03	2.56	3.07	3.70	3.79
13	2.90	3.70	2.59	4.58	3.55	2.05	2.88	3.04	2.82	2.45	2.54	3.30	3.31	3.44
14	3.61	4.93	3.55	6.34	4.96	2.28	4.02	4.08	3.79	3.14	3.44	4.20	4.53	4.86
15	3.32	4.42	3.43	5.70	4.86	2.54	3.75	2.99	3.35	2.98	3.21	3.84	3.64	4.47
16	2.54	3.85	2.64	5.81	4.17	1.63	2.76	2.92	2.43	2.15	2.23	3.23	2.71	4.25
17	3.40	3.98	2.85	5.14	4.08	2.80	3.02	2.75	3.28	2.99	3.06	3.40	3.58	4.22
18	3.32	4.24	2.99	5.36	4.21	2.78	3.26	3.34	3.30	2.99	3.10	3.50	3.59	4.22
19	3.56	4.42	3.40	5.35	4.51	2.72	3.68	3.38	3.50	3.15	3.29	3.92	3.91	4.21
20	4.14	5.44	4.25	7.54	6.08	3.17	4.53	4.09	4.25	3.74	4.05	4.59	4.80	6.16
21	3.21	4.25	3.77	4.83	4.63	2.02	4.21	3.31	3.29	2.83	3.04	4.44	3.70	3.58
22	4.41	5.39	4.46	6.51	5.76	3.25	4.92	4.30	4.53	3.96	4.22	5.09	5.21	5.31
23	3.88	5.10	3.91	6.27	5.34	2.78	4.29	3.67	3.93	3.43	3.66	4.53	4.64	4.82
24	3.61	4.97	3.75	6.16	5.21	2.62	4.29	3.58	3.89	3.26	3.66	4.17	4.50	4.83
25	4.43	5.74	4.17	6.68	5.63	3.81	4.57	3.97	4.63	4.11	4.49	4.53	5.25	5.36
26	4.40	5.93	3.92	7.31	5.88	3.74	4.34	3.70	4.65	4.03	4.49	4.22	5.51	5.82
27	2.23	3.66	2.52	4.23	3.37	0.99	2.66	2.06	2.36	1.90	2.31	2.76	2.52	2.85
28	3.82	4.94	4.20	5.50	5.19	2.76	4.77	3.89	4.08	3.47	3.84	4.68	4.79	4.35

29	4.80	6.73	3.52	9.42	6.29	4.08	3.89	4.55	5.06	4.32	4.78	3.97	6.29	7.50
30	3.76	4.09	3.45	4.41	4.18	2.96	3.84	3.43	3.76	3.34	3.49	4.05	4.35	3.78
31	3.20	4.47	3.39	5.32	4.30	2.43	3.64	3.40	3.39	2.96	3.25	3.63	3.66	4.07
32	3.15	4.55	2.61	5.24	4.07	2.33	2.98	2.49	3.26	2.81	3.17	3.07	3.77	3.83
33	4.04	5.33	4.14	6.84	5.72	2.74	4.73	4.16	4.36	3.57	3.98	4.78	5.36	5.50
34	3.76	5.26	3.66	7.46	5.95	3.07	3.96	3.05	3.83	3.41	3.73	3.99	4.30	5.92
35	3.84	4.68	3.69	6.64	5.45	3.20	3.92	3.22	3.92	3.49	3.72	4.04	4.54	5.70
36	4.33	5.66	4.13	7.33	6.04	3.56	4.52	3.98	4.44	3.93	4.23	4.53	5.11	5.88
37	3.82	4.70	3.23	6.01	4.75	3.32	3.60	3.34	3.97	3.53	3.78	3.70	4.49	5.07
38	4.51	5.47	3.23	7.69	5.48	4.05	3.42	3.58	4.47	4.06	4.26	3.71	5.14	6.49
39	4.34	5.96	3.82	7.67	6.07	3.68	4.04	3.25	4.45	3.94	4.38	3.95	5.11	6.05
40	4.23	5.42	4.15	6.84	5.98	3.35	4.90	4.00	4.58	3.89	4.28	4.76	5.38	5.68
41	3.62	5.76	3.62	6.25	4.68	2.98	4.25	4.89	3.90	3.37	3.75	3.96	4.20	4.19
42	4.11	5.87	3.34	8.07	5.42	3.39	3.65	4.60	4.28	3.62	3.95	3.84	5.30	6.18
43	3.17	5.40	3.26	7.73	5.35	2.38	3.78	4.05	3.70	2.97	3.48	3.61	4.62	5.85
44	2.27	4.33	2.70	4.31	3.52	1.01	3.51	3.52	2.77	2.02	2.59	3.14	3.30	2.54
45	2.97	4.72	3.12	5.16	4.33	1.55	3.60	2.90	3.25	2.57	3.13	3.53	3.85	3.52
46	4.11	4.80	3.99	6.54	5.74	2.79	4.33	3.47	4.02	3.58	3.74	4.78	4.69	5.48
47	3.07	3.76	2.54	4.55	3.89	2.53	2.63	1.95	2.71	2.67	2.70	3.05	2.61	3.44
48	3.77	4.92	3.11	6.53	4.91	3.36	3.54	3.41	4.00	3.47	3.79	3.56	4.76	5.39

Table B16. Cuticular wax predicted on rehydrated spinach leaves (n=48) by each of the 14 best performing models with 4 or 5 predictor frequencies. Rehydrated leaf cuticular wax predictions have been multiplied by 75.4% to account for shrinkage due to drying/rehydration process.

Sample	Predicted wax on rehydrated dried leaf by each model ( $\mu\text{g}/\text{cm}^2$ )													
	1	2	3	4	5	6	7	8	9	10	11	12	13	14
1	3.18	3.93	2.80	2.83	3.31	3.17	3.38	2.24	3.16	3.05	3.12	3.29	3.20	1.90
2	2.77	3.52	2.73	3.13	3.15	2.46	3.16	2.64	2.78	2.61	2.64	3.15	2.79	2.19
3	5.15	6.10	5.06	4.10	5.61	5.14	5.99	3.47	5.37	4.96	5.25	5.63	6.01	3.07
4	4.23	5.52	4.83	5.28	5.40	3.23	5.58	4.88	4.48	3.87	4.08	5.50	5.12	3.79
5	3.03	3.63	2.65	3.10	3.21	2.60	3.09	2.62	2.83	2.63	2.53	3.48	3.11	1.95
6	3.50	4.24	3.62	3.96	4.15	2.79	4.14	3.42	3.52	3.13	3.16	4.30	3.98	2.84
7	3.25	3.71	3.38	3.22	3.74	2.86	3.75	2.63	3.32	3.08	3.16	3.70	3.43	2.60
8	3.47	5.00	3.60	4.17	4.20	3.03	4.35	3.83	3.68	3.22	3.35	4.36	4.28	2.49
9	3.45	4.72	4.08	4.39	4.59	2.67	4.75	3.80	3.78	3.21	3.38	4.72	4.51	3.03
10	2.47	3.36	2.69	2.66	3.29	1.83	3.20	1.77	2.43	2.15	2.16	3.55	2.83	1.42
11	3.82	4.15	4.16	4.08	4.46	3.39	4.55	3.71	4.05	3.71	3.88	4.26	4.15	3.76
12	3.74	4.06	3.99	3.89	4.45	2.95	4.58	3.48	3.85	3.38	3.48	4.62	4.26	3.26
13	4.17	4.79	4.42	3.86	4.77	3.84	5.04	3.41	4.44	4.06	4.27	4.75	4.80	3.25
14	3.69	4.03	3.52	3.63	4.10	3.02	4.06	3.08	3.63	3.36	3.41	4.13	3.80	2.93

15	4.10	4.96	4.81	4.92	5.21	3.29	5.57	4.85	4.54	3.92	4.20	5.17	5.15	4.10
16	3.20	3.84	3.02	3.21	3.52	2.86	3.61	2.95	3.20	3.01	3.06	3.60	3.31	2.35
17	3.15	3.69	2.96	3.36	3.39	2.97	3.48	3.04	3.36	3.09	3.21	3.21	3.45	2.82
18	4.45	4.99	4.21	4.78	4.59	4.23	4.77	4.68	4.71	4.32	4.44	4.48	5.03	4.16
19	3.54	3.97	3.40	3.40	3.85	3.07	4.02	3.16	3.67	3.31	3.46	3.86	4.04	2.83
20	3.73	4.34	4.04	4.30	4.39	2.99	4.61	4.13	3.98	3.50	3.65	4.42	4.46	3.57
21	4.10	5.62	4.57	5.16	5.34	3.05	5.57	4.68	4.47	3.75	4.03	5.47	5.44	3.51
22	4.39	5.66	4.97	5.84	5.56	3.21	5.75	5.35	4.84	4.12	4.42	5.54	5.74	4.55
23	3.81	4.53	3.85	4.27	4.25	3.19	4.48	4.07	4.10	3.65	3.86	4.14	4.42	3.53
24	3.79	4.47	4.11	4.17	4.62	2.99	4.78	3.73	4.02	3.52	3.69	4.67	4.54	3.33
25	4.30	4.08	3.58	3.16	4.23	4.22	4.03	2.24	4.05	4.08	3.97	4.15	3.94	2.92
26	3.75	3.32	2.99	2.28	3.63	3.67	3.44	1.45	3.43	3.53	3.41	3.63	3.25	2.25
27	3.38	4.21	3.33	3.81	3.77	2.98	3.95	3.47	3.65	3.30	3.48	3.63	3.79	3.01
28	4.76	4.43	4.63	3.66	5.18	4.39	5.20	2.92	4.74	4.57	4.64	5.04	4.77	3.73
29	3.50	4.51	3.43	3.96	3.96	3.30	4.10	3.45	3.76	3.45	3.63	3.75	3.98	3.00
30	5.21	5.05	4.53	4.46	5.34	5.25	5.04	3.27	5.11	5.00	5.05	4.91	5.17	4.31
31	4.64	5.53	4.48	5.16	5.28	4.64	5.12	4.09	4.81	4.50	4.62	4.96	5.17	4.14
32	3.84	5.20	3.81	4.47	4.79	3.56	4.60	3.25	3.89	3.58	3.72	4.68	4.49	2.91
33	3.58	3.87	3.56	3.56	4.12	2.81	4.10	2.89	3.60	3.31	3.34	4.17	3.75	2.95
34	5.15	5.66	4.78	3.67	5.57	5.12	5.59	2.88	4.89	4.74	4.83	5.61	5.15	2.64
35	3.65	3.94	3.86	3.84	4.32	3.27	4.27	3.16	3.74	3.49	3.57	4.12	3.80	3.40
36	4.93	5.56	4.54	4.91	5.31	4.87	5.25	4.19	5.03	4.68	4.82	5.08	5.40	4.05
37	2.97	3.68	2.38	2.01	3.01	3.14	3.07	1.41	2.69	2.76	2.71	3.18	2.58	0.90
38	3.08	3.69	2.31	2.15	3.09	3.24	2.84	1.01	2.73	2.84	2.77	3.10	2.63	1.09
39	3.96	4.22	3.61	3.74	4.22	3.76	4.02	2.93	3.85	3.73	3.71	4.07	3.82	3.14
40	3.75	4.15	3.18	3.42	3.89	3.34	3.76	2.86	3.46	3.34	3.23	4.07	3.55	2.40
41	4.20	4.80	3.76	4.21	4.26	4.07	4.28	3.79	4.16	4.05	4.04	4.20	3.99	3.33
42	3.56	3.80	3.15	3.31	3.60	3.27	3.49	2.73	3.40	3.28	3.23	3.67	3.43	2.65
43	3.46	3.63	2.92	3.17	3.42	3.45	3.40	2.66	3.53	3.39	3.39	3.33	3.65	2.85
44	3.63	4.22	3.40	3.60	4.08	3.16	3.98	3.16	3.40	3.25	3.20	4.20	3.43	2.48
45	3.87	4.02	3.72	3.44	4.50	2.93	4.47	2.71	3.84	3.52	3.57	4.60	4.20	2.91
46	4.29	4.47	4.53	4.13	5.13	3.21	5.32	3.72	4.39	3.96	4.06	5.28	4.89	3.64
47	4.36	4.22	3.56	3.50	4.13	4.32	4.02	2.92	4.21	4.19	4.12	4.01	4.13	3.27
48	4.04	3.43	3.10	2.24	3.58	4.42	3.43	1.48	3.84	3.97	3.89	3.38	3.65	2.55

## APPENDIX D

### MATLAB PROGRAM FOR ANALYZING PECAN TREE IMAGES

```
%+++++
%This program reads in images of pecan trees, allows manual selection
%of reflection targets and calculates vegetative indices. Additional %analysis of VI data is also performed
%
%James Hardin
%24Jan2012
%+++++

% Read in image files, select reflection target and tree area.
% List row and tree number in nX2 array
SeptTrees=[2,12;2,13;2,15;2,16;2,17;2,18;2,19;2,20;3,14;3,16;3,18;3,19;3,20;3,21;4,14;4,16;4,17;4,18;4,20
;4,21;5,16;5,19;5,20;5,21;5,22;7,18;7,19;7,22;7,23;8,17;8,18;8,19;8,21;8,22;8,23;11,16;11,17;12,15];
OctTrees=[2,12;2,13;2,15;2,16;2,17;2,19;2,20;3,14;3,16;3,18;3,19;3,20;3,21;4,14;4,16;4,17;4,18;4,20;4,21;
5,16;5,19;5,20;5,21;5,22;7,18;7,19;7,22;7,23;8,17;8,18;8,19;8,21;8,22;8,23;11,16;11,17;12,15;12,16;12,17]
;
RowCount=1; %initialize counter for number of trees
for Mon = 9:10; %9 for Sept, 10 for Oct;
    if Mon==9;
        Month='Sept';
        Trees=SeptTrees;
        [NumTrees, ~]=size(SeptTrees);
    elseif Mon==10;
        Month = 'Oct';
        Trees=OctTrees;
        [NumTrees,~]=size(OctTrees);
    end

    for t=1:NumTrees;
        Row=Trees(t,1);
        SRow=int2str(Row);
        if Row<7
            Cvar=1;
        else Cvar=2;
        end
        Tree=Trees(t,2);
        STree=int2str(Tree);
        % build file names and import
        IR = imread(strcat('I:\Pecans\SPAD meter\',(Month),'2010 images\',r',(SRow),t,(STree),' - IR.tif'));
        Rd = imread(strcat('I:\Pecans\SPAD meter\',(Month),'2010 images\',r',(SRow),t,(STree),' - Rd.tif'));
        Gn = imread(strcat('I:\Pecans\SPAD meter\',(Month),'2010 images\',r',(SRow),t,(STree),' - Gn.tif'));
```

```

figure (1), imshow(IR) %show the IR image for manual selection of target and leaf area
title(['Month ' Row ' SRow ' Tree ' STree ' IR image, Click center of 99% target then select leaf area by
dragging mouse from lower left to upper right, then crop']);

```

```

% FIND INTENSITY FROM REFERENCE STD
% Find reference by clicking center of 99% reflective target.
% "Backspace" to unselect, "enter" to chose selected point
[x,y] = getpts(gcf);
x = round(x);
y = round(y);

```

```

% Find intensity of Rd and IR targets using 3 x 7 pixel region from image
if Mon==9||Row==8||Tree==17;
    IR98Val= 225; % These values for obscure target in Sept 2010 R8T17 image
    IR10Val=51;
    Rd98Val=193;
    Rd10Val=25;
    Gn98Val=229;
    Gn10Val=29;
else
    IR98Val=sum(sum(IR(y-3:1:y+3,x-1:1:x+1)))/21;
    IR10Val=sum(sum(IR(y-3:1:y+3,x+14:1:x+16)))/21;
    Rd98Val=sum(sum(Rd(y-3:1:y+3,x-1:1:x+1)))/21;
    Rd10Val=sum(sum(Rd(y-3:1:y+3,x+14:1:x+16)))/21;
    Gn98Val=sum(sum(Gn(y-3:1:y+3,x-1:1:x+1)))/21;
    Gn10Val=sum(sum(Gn(y-3:1:y+3,x+14:1:x+16)))/21;
end

```

```

% Crop image by dragging from lower left to upper right
% Right click, then select "crop image"
[IRcrop rect] = imcrop(IR);

```

```

% Create cropped red image from coordinates returned from IR crop
Rdcrop = imcrop(Rd, rect);
Gncrop = imcrop(Gn, rect);

```

```

% show cropped images....
% figure, imshow(IRcrop);
% title('Infrared image of analysis area')
% figure, imhist(IRcrop);
% title('IR pixel histogram of analysis area')

```

```

% STRETCH RED AND IR MATRICES TO 10-98% SCALE, DISPLAY IMAGES AND HISTOGRAMS

```

```

%Find slope (M) and intercept (B) of response curve from images using target values.
RdM = (Rd98Val - Rd10Val)/(98-10);
IRM = (IR98Val - IR10Val)/(98-10);
GnM = (Gn98Val - Gn10Val)/(98-10);
RdB = Rd98Val - RdM * 98;
IRB = IR98Val - IRM * 98;
GnB = Gn98Val - GnM * 98;
% Slope adjustment parameter
RdMAdjust = 2.55/RdM;
IRMAAdjust = 2.55/IRM;

```

```

GnMAdjust = 2.55/GnM;
% Create stretched images using intercept and slope adjustment
RdStretch = (Rdcrop - RdB)* RdMAdjust;
IRStretch = (IRcrop - IRB)* IRMAdjust;
GnStretch = (Gncrop - GnB)* GnMAdjust;

%find peak value in IR histogram for later calculations
%figure, imhist(IRStretch);
% title('IR pixel histogram of analysis area')
[Count, Index] = imhist(IRStretch);
[Peak, Index] = max(Count);

% Investigate pixel intensity
for r=1:9;
    IRHistPeak=r*25; %Step through peaks from 25 to 200
    if r==9
        IRHistPeak = Index; %use the peak value found earlier
    end
    % create matrix where leaf pixels are 1 and all else =0
    IRBinHigh = im2bw(IRStretch, (IRHistPeak+50)/255);
    IRBinLow = im2bw(IRStretch, IRHistPeak/255);
    IRBin = IRBinHigh .* IRBinLow; %flag pixels in range
    IRBin = uint8(IRBin); % Change to uint8 for mult later;
        % Discard non-leaf pixels by multiplying red and IR images by "leaf" binary image, these
        are the pixels that will be analyzed
    IRThres = IRStretch .* IRBin;
    RdThres = RdStretch .* IRBin;
    GnThres = GnStretch .* IRBin;
    %Convert IR and Red images to gray scale w/values 0 to 1
    NIR = im2single(IRThres);
    Red = im2single(RdThres);
    Grn = im2single(GnThres);
    % Calculate Index image
    NDVI = (NIR - Red)/(NIR + Red);
    NDVIGn = (NIR - Grn)/(NIR + Grn);
    NRI = (Grn - Red)/(Grn + Red);
    %convert NaN's to 0's
    B=isnan(NDVI);
    NDVI(B)=0;
    C=isnan(NDVIGn);
    NDVIGn(C)=0;
    D=isnan(NRI);
    NRI(D)=0;

    % Compute with lower cutoff only
    IRBinLow = uint8(IRBinLow); % Change to uint8
        % Discard non-leaf pixels by multiplying red and IR images by "leaf" binary image, these
        are the pixels that will be analyzed
    IRThresLow = IRStretch .* IRBinLow;
    RdThresLow = RdStretch .* IRBinLow;
    GnThresLow = GnStretch .* IRBinLow;

    %Convert IR and Red images to gray scale w/ values 0 to 1
    NIRLow = im2single(IRThresLow);
    RedLow = im2single(RdThresLow);

```

```

GrnLow = im2single(GnThresLow);

% Calculate Index image
NDVILow = (NIRLow - RedLow)/(NIRLow + RedLow);
NDVIGnLow = (NIRLow - GrnLow)/(NIRLow + GrnLow);
NRILow = (GrnLow - RedLow)/(GrnLow + RedLow);

%convert NaN's to 0's
B=isnan(NDVILow);
NDVILow(B)=0;
C=isnan(NDVIGnLow);
NDVIGnLow(C)=0;
D=isnan(NRILow);
NRILow(D)=0;

% NDVI Moment calculation
IRBinSum = sum(sum(IRBin));
NDVIMean = sum(sum(NDVI))/IRBinSum;
NDVIGnMean = sum(sum(NDVIGn))/IRBinSum;
NRIMean = sum(sum(NRI))/IRBinSum;
IRRefl = sum(sum(NIR))/IRBinSum;
RedRefl = sum(sum(Red))/IRBinSum;
GrnRefl = sum(sum(Grn))/IRBinSum;
SR=IRRefl/RedRefl;

IRBinSumLow = sum(sum(IRBinLow));
NDVIMeanLow = sum(sum(NDVILow))/IRBinSumLow;
NDVIGnMeanLow = sum(sum(NDVIGnLow))/IRBinSumLow;
NRIMeanLow = sum(sum(NRILow))/IRBinSumLow;
IRReflLow = sum(sum(NIRLow))/IRBinSumLow;
RedReflLow = sum(sum(RedLow))/IRBinSumLow;
GrnReflLow = sum(sum(GrnLow))/IRBinSumLow;
SRLow=IRReflLow/RedReflLow;

SumData(RowCount,:)= [Cvar Mon Row Tree r IRHistPeak NDVIMean NDVIGnMean NRIMean
SR IRRefl RedRefl GrnRefl NDVIMeanLow NDVIGnMeanLow NRIMeanLow SRLow IRReflLow
RedReflLow GrnReflLow IR10Val IR98Val Rd10Val Rd98Val Gn10Val Gn98Val];
RowCount=RowCount+1;
end
%find size of 'out' so new entires are appended
end
end

%% Regression analysis to find the best threshold for leaf pixels
Bass=xlsread('NDVIdata2.xlsx', 'data2');
IndVar=14; %NDVI=7 NDVIGn=8 NRI=9 SR=10 IRRefl=11 RedRefl=12 GrnRefl=13 NDVILow=14
NDVIGnLow=15 NRILow=16 SRLow=17 IRReflLow=18 RedReflLow=19 GrnReflLow=20 IR10Val=21
IR98Val=22 Rd10Val=23 Rd98Val=24 Gn10Val=25 Gn98Val=26
line=1;
% Line numbers in XLSX file....
map=[0,25,50,75,100,125,150,175,200,225,249,273,297,321,345,369,393,417,441,454,467,480,493,506,51
9,532,545,558,573,588,603,618,633,648,663,678,693];
for n=1:36;
top=map(n)+1;

```

```

bot=map(n+1);
Y=Bass(top:bot,6);
X=[Bass(top:bot,IndVar),Bass(top:bot,IndVar+6)];
[r c]=size(X);
Col = ones(r,1); %make a row vector of ones to concatenate to X
X1 = [Col, X];
[b,~,~,~,stats] = regress(Y,X1); %stats (R2 statistic, F statistic, p value, and an estimate of the error
variance)
%load Cvar, month, IRcutoff, b0, b1, R2,pVal into array
SumStats(line,:) = [1, Bass(top,2), Bass(top,1)*25, b(1,1), b(2,1), stats(1), stats(3)]; %first 18 are
Pawnee, next 18 are Kanza
line=line+1;
end

```

APPENDIX E

SPAD READINGS AND NITROGEN ANALYSIS DATA

Table D17. Tree data and associated chlorophyll meter readings and leaf nitrogen analysis results for study samples.

Cultivar	Row	Tree	N (kg/ha)	SPAD reading (mean of 10)						Nitrogen analysis (% dry weight)					
				May	June	July	Aug.	Sep.	Oct.	May	June	July	Aug.	Sep.	Oct.
Kanza	7	18	0	31.6	40.0	41.4	43.7	41.2	41.2	3.20	2.40	2.36	2.05	1.99	1.77
Kanza	7	19	0	30.2	40.3	42.5	45.3	42.3	39.3	2.83	2.43	2.60	2.11	1.99	1.71
Kanza	8	17	0	28.4	38.6	41.8	42.8	40.2	37.3	2.70	2.33	2.22	2.01	1.95	1.66
Kanza	8	18	0	32.1	40.2	43.4	44.7	41.6	37.9	2.88	2.54	2.49	2.12	1.94	1.72
Kanza	8	19	0	28.7	38.1	42.3	41.9	39.4	39.2	2.53	2.30	2.29	2.07	1.93	1.75
Kanza	11	16	162	32.3	40.9	43.6	45.9	47.4	47.8	2.93	2.63	2.42	2.23	2.11	2.04
Kanza	11	17	162	31.2	39.7	43.2	44.7	43.2	43.3	2.90	2.56	2.62	2.30	2.12	1.94
Kanza	12	15	162	30.9	42.2	43.8	46.7	46.4	44.0	2.82	2.60	2.50	2.22	1.97	1.97
Kanza	12	16	162	30.9	38.9	43.4	45.0	43.6	40.4	2.56	2.40	2.39	2.11	1.98	1.97
Kanza	12	17	162	32.0	40.3	45.0	46.1	43.4	43.7	2.58	2.34	2.42	2.12	1.91	1.83
Kanza	7	22	Clover	30.9	41.6	43.4	45.1	43.2	40.7	3.30	2.66	2.65	2.28	2.31	1.81
Kanza	7	23	Clover	30.2	39.3	42.6	45.8	43.4	41.4	3.11	2.50	2.54	2.17	2.13	1.87
Kanza	8	21	Clover	31.5	40.7	42.5	44.3	42.8	41.7	3.01	2.55	2.54	2.20	2.32	1.92
Kanza	8	22	Clover	29.2	37.5	41.1	41.6	40.6	37.6	2.91	2.48	2.56	2.16	2.20	1.74
Kanza	8	23	Clover	30.0	39.0	43.2	44.8	41.7	37.7	3.11	2.55	2.59	2.17	2.19	1.61
Maramec	5	4	309	28.6	40.8	44.5	46.1	46.1	.	2.58	2.43	2.34	2.13	2.02	.
Maramec	6	6	309	29.5	41.2	45.3	46.5	47.2	.	2.74	2.50	2.31	2.17	2.04	.
Maramec	8	6	309	28.1	40.0	44.4	43.6	45.0	.	2.65	2.46	2.42	2.15	2.12	.
Maramec	10	6	309	30.4	38.7	40.3	37.6	44.0	.	3.05	2.24	2.06	2.03	2.07	.
Maramec	12	7	309	30.2	41.7	46.9	42.4	44.2	.	2.70	2.40	2.43	1.94	2.03	.
Maramec	13	7	309	31.5	40.4	46.3	45.1	46.1	.	2.82	2.57	2.43	2.22	2.17	.
Maramec	14	7	309	27.9	43.7	49.5	46.4	47.6	.	2.83	2.69	2.55	2.23	2.28	.
Maramec	15	6	309	29.4	44.0	47.1	48.6	48.6	.	2.87	2.64	2.56	2.27	2.20	.
Maramec	16	6	309	29.2	44.0	47.3	47.6	48.6	.	2.77	2.74	2.49	2.27	2.15	.
Maramec	18	6	309	26.2	41.0	47.4	46.1	48.6	.	2.91	2.44	2.52	2.29	2.22	.
Pawnee	2	12	50	37.6	42.3	47.1	48.8	46.6	45.6	3.55	2.63	2.73	2.35	2.36	.
Pawnee	2	13	50	34.5	43.6	44.8	47.6	46.4	42.5	3.32	2.47	2.54	2.20	2.16	1.84
Pawnee	2	15	50	35.0	45.1	47.8	50.7	46.9	42.9	3.74	2.79	2.90	2.37	2.26	1.84
Pawnee	3	14	50	36.1	43.7	47.0	48.3	47.9	42.0	3.70	2.63	2.71	2.22	2.20	1.94

Pawnee	4	14	50	33.2	45.3	48.2	47.7	46.9	41.3	3.50	2.56	2.78	2.20	2.13	1.94
Pawnee	2	16	106	33.9	43.2	46.3	48.5	45.5	43.5	3.77	2.59	2.86	2.26	2.24	1.87
Pawnee	2	17	106	35.8	48.2	45.6	48.3	47.5	44.1	3.92	2.84	2.91	2.40	2.39	1.87
Pawnee	2	18	106	32.5	44.0	46.4	48.5	47.8	46.8	3.80	2.69	2.81	2.23	2.30	1.97
Pawnee	2	19	106	35.4	44.2	47.3	48.6	47.7	46.0	3.72	2.70	2.74	2.34	2.28	1.95
Pawnee	2	20	106	36.4	41.0	46.7	46.9	45.9	41.5	3.81	2.44	2.81	2.27	2.21	2.09
Pawnee	3	16	162	33.6	43.5	47.2	47.7	47.2	44.1	3.27	2.58	2.87	2.28	2.27	1.97
Pawnee	3	18	162	34.7	42.7	47.8	48.6	48.1	43.5	3.59	2.74	2.95	2.34	2.32	1.96
Pawnee	3	19	162	37.0	45.8	48.7	49.3	49.6	46.2	3.37	2.91	2.88	2.39	2.41	2.10
Pawnee	3	20	162	34.8	45.1	47.6	50.8	49.5	46.7	3.67	2.87	2.83	2.54	2.48	2.13
Pawnee	3	21	162	37.8	45.3	50.6	48.6	50.4	47.1	4.18	2.75	2.95	2.41	2.42	2.12
Pawnee	4	16	274	36.3	44.8	48.9	50.0	46.8	43.3	3.70	2.76	2.90	2.36	2.34	2.01
Pawnee	4	17	274	35.8	45.6	49.0	52.1	50.3	49.0	3.97	2.82	2.92	2.46	2.46	2.24
Pawnee	4	18	274	35.0	47.8	50.9	49.1	50.1	47.3	4.08	2.80	2.93	2.34	2.33	2.03
Pawnee	4	20	274	35.5	47.8	49.8	50.1	49.5	47.8	4.03	2.85	2.96	2.39	2.47	2.13
Pawnee	4	21	274	34.9	47.7	48.0	50.6	50.1	50.9	3.98	3.00	3.14	2.57	2.61	2.25
Pawnee	5	16	498	36.2	46.9	51.8	52.3	49.6	48.7	4.04	2.86	3.08	2.56	2.42	2.10
Pawnee	5	19	498	37.3	47.5	48.7	51.4	52.1	48.3	4.23	2.90	2.83	2.54	2.59	2.23
Pawnee	5	20	498	38.3	46.3	49.7	51.0	49.2	46.3	3.76	2.71	3.04	2.44	2.37	2.09
Pawnee	5	21	498	37.4	47.9	49.3	51.7	51.1	50.4	4.22	2.99	2.92	2.58	2.52	2.29
Pawnee	5	22	498	36.7	46.1	51.4	51.6	50.0	50.7	4.02	2.77	3.04	2.55	2.40	2.19

## VITA

James Albert Hardin

Candidate for the Degree of

Doctor of Philosophy

Thesis: IN SITU SENSING OF LEAF CUTICULAR WAX, PECAN YIELD AND  
PECAN LEAF NITROGEN CONCENTRATION

Major Field: Biosystems Engineering

Biographical:

### Education:

Completed the requirements for the Bachelor of Science in Mechanical Engineering at Michigan Technological University, Houghton, Michigan in 1984.

Completed the requirements for the Doctor of Philosophy in Biosystems Engineering at Oklahoma State University, Stillwater, Oklahoma in July, 2012.

### Experience:

Product Development and Industrial Engineer, IBM Corporation, 1984–2000

Principal Hardware Development Engineer, LVL7 Systems, 2000-2002

Principal Software Project Manager, LVL7 Systems, 2002-2004

Adjunct Instructor, Dept. of Mathematics and Computer Science, Lake Superior State University, 2006

Adjunct Instructor, Division of Science, Math and Engineering, Northern Oklahoma College, 2006-2007

Graduate Research Associate, Biosystems and Agricultural Engineering, Oklahoma State University, 2007-2010

Research Engineer, Biosystems and Agricultural Engineering, Oklahoma State University, 2010-2012

### Professional Memberships:

American Society of Agricultural and Biological

American Society for Engineering Education

Name: James A. Hardin

Date of Degree: July, 2012

Institution: Oklahoma State University

Location: Stillwater, Oklahoma

Title of Study: IN SITU SENSING OF LEAF CUTICULAR WAX, PECAN YIELD  
AND PECAN LEAF NITROGEN CONCENTRATION

Pages in Study: 128

Candidate for the Degree of Doctor of Philosophy

Major Field: Biosystems Engineering

Scope and Method of Study:

The objectives of this study were to develop technologies to enable in situ sensing of plant physiological conditions.

Cuticular wax on spinach leaves was quantified by applying an empirically developed regression relationship to Fourier transform infrared attenuated total reflectance (FTIR-ATR) spectra of fresh plant material.

In the second study, the backscatter response of microwaves from pecan tree canopy samples was investigated to assess the ability of short range radar to estimate nut yield in pecan orchards prior to harvest.

Finally, two methods to assess concentration of nitrogen in pecan leaves were developed. The first method extracted data from high resolution camera images in the green, red and near-infrared bands to calculate foliar nitrogen levels. In the second investigation, regression analysis was used to find relationships between chlorophyll meter measurements and chemical nitrogen analysis.

Findings and Conclusions:

Linear regression models derived from FTIR-ATR spectra were able to predict greater than 86% of wax variation on leaves using 4 or 5 frequencies. DSC did not provide reliable predictions of cuticular wax.

Measurements of short range microwave radiation from 1 to 18 GHz reflected from pecan tree canopy samples resulted in linear regression models that predicted total water and dry mass of the samples over a wide range of frequencies with  $R^2 > 0.63$  and  $0.78$  respectively.

Normalized difference vegetative index (NDVI) and reflectance data extracted from the camera images were significantly correlated to foliar N in both months of the study on 'Pawnee' pecans but only in one month 'Kanza'. The various relationships had  $R^2$  between 0.21 and 0.51. Correlation of foliar N to chlorophyll meter readings was poor in May for all cultivars but distinct significant linear relationships were found for 'Maramec' and 'Pawnee' for each of the other months tested with  $R^2$  ranging from 0.40 to 0.87. Data from 'Kanza' had significant relationships in June and October with  $R^2$  of 0.39 and 0.72, respectively.

ADVISER'S APPROVAL: Dr. Carol L. Jones

---